Fall 12-2021

Design, Quantification, and Strengthening of Interface Interaction Between Aramid Fibers and Polymer Matrix

Karrar Al-Quraishi
University of Maine, Karrar.khlaif@maine.edu

DESIGN, QUANTIFICATION, AND STRENGTHENING OF INTERFACE INTERACTION BETWEEN ARAMID FIBERS AND POLYMER MATRIX

By

Karrar Al-Quraishi

B.S. University of Technology, 2012

M.S. University of Maine, 2017

A DISSERTATION

Submitted in Partial Fulfillment of the

Requirements for the Degree of

Doctor of Philosophy

(in Mechanical Engineering)

The Graduate School

The University of Maine

December 2021

Advisory Committee:

Yingchao Yang, Assistant Professor of Mechanical Engineering, Advisor

Zhihe Jin, Professor of Mechanical Engineering

Vincent Caccese, Professor of Mechanical Engineering

Ling Li, Assistant Professor of Sustainable Bioenergy Systems

Bo Li, Assistant Professor of Mechanical Engineering

DESIGN, QUANTIFICATION, AND STRENGTHENING OF INTERFACE INTERACTION BETWEEN ARAMID FIBERS AND POLYMER MATRIX

By
Karrar Al-Quraishi

Dissertation Advisor: Dr. Yingchao Yang

An Abstract of the Dissertation Presented
in Partial Fulfillment of the Requirements for the
Degree of Doctor of Philosophy
(in Mechanical Engineering)
December 2021

Composites reinforced by aramid fibers may suffer poor interface interactions during mechanical loading due to the smooth and chemically inert surface of the fibers. Three main strategies have been used to improve the interface shear strength (IFSS) including increasing surface roughness, enriching fiber surface with functional groups, and surface coating with ceramic particles. Plasma treatment is usually employed to functionalize and roughen surface of the fibers, leading to strengthening of the interface between the fibers and polymer matrix. A concern for fibers reinforced polymers is that the IFSS would significantly decrease once the composite is exposed to elevated temperatures. To maintain the mechanical performance of the composite at elevated temperatures, a polymer-derived-ceramics (PDC) precursor additive is used to stabilize the interface of the fabricated composite. Testing has shown that the IFSS of composites reinforced by untreated fibers is 29.32 ± 1.00 MPa and 26.10 ± 5.23 MPa at 50 °C and 100 °C, respectively, which surpasses 23.46 ± 2.32 MPa, the IFSS without PDC stabilization at room temperature. Regarding the functional groups, they have been created on the surface of the fibers through plasma or chemical treatments to improve the mechanical performance of aramid fiber reinforced composites. Unfortunately, these functional groups may reorient toward the fiber and be passivated by polar molecules in air over time and then become inactive and unable to bond to the matrix. The active period of the functional groups after a plasma treatment has been carefully evaluated. It is

found that the fiber surface can be reactivated by drying with and without water molecule pretreatment. With drying at 100 °C for 10 hours, the IFSS can be restored from ~23 MPa to ~30 MPa. Regarding the last method to enhance the IFSS, chemical vaper deposition (CVD) and physical vaper deposition (PVD) have been used as an alternative methods to improve the IFSS by synthesizing ceramic nanoparticles MoO_3 on the aramid fibers. A few advantages include no damage to aramid fibers which will help preserve mechanical properties of the aramid fibers and no concern on passivation as ceramic nanoparticles are stable compared to functional groups. Contrast to the bare improvement on IFSS from the MoO_3 grown with PVD, the IFSS reaches 31 MPa from the nanoparticles fabricated with CVD, which suggests CVD would deliver a better interface interaction between MoO_3 and fibers. These projects will benefit the engineering of aramid fibers into composites by largely taking advantage of their superior mechanical properties. Further research into interactions between heat treatment and strengthening additives would help us fundamentally understand the interface of advanced composite materials, as well as provide theoretical guidance for designing the interface between reinforcement and matrix.

DEDICATION

I dedicate my dissertation work to my family and my friends. A special feeling of gratitude to my loving parents who have provided invaluable support. I dedicate this work to my wife, I am grateful for her love, endless support, and encouragement. I dedicate this work and give special thanks to my sisters and brothers; they have never left my side and are very special. I will always appreciate all of you for what you have done. All of you have been my best cheerleaders.

ACKNOWLEDGEMENTS

I would like to thank Dr. Yingchao Yang for giving me the opportunity to work with him and for advising me throughout these projects. His guidance and mentorship have helped me to grow as a person and as a scientist. Many thanks also go to my advisory committee, Drs. Zhihe Jin, Vincent Caccese, Ling Li at UMaine and Dr. Bo Li at Villanova University, for their invaluable participation. I would also like to thank my colleagues in Dr. Yang's group and collaborators at UMaine and other Universities for their help in all phases of the projects. Finally, I am grateful to my family and friends who provided invaluable support whenever I needed.

TABLE OF CONTENTS

LIST OF TABLES

LIST OF FIGURES

LIST OF EQUATIONS

CHAPTER 1

1 INTRODUCTION

A composite material is the combination of two or more substance with different properties, such as, mud bricks, plywood, fiberglass, concrete, carbon fibers, and rubber tires. Combing dissimilar mechanical, chemical, or physical properties of original elements is to create a unique material with advanced properties. Composite materials have two components: matrix and reinforcement. The reinforcement has unique mechanical and physical properties to improve the certain performance of the composite. According to matrix component, composites can be classified into polymer matrix composite, metal matrix composite, and ceramic matrix composite. In addition, according to the matrix ingredient forms, composites can be categorized as particulate-reinforced composite, flake-reinforced composite, fiber-reinforced composite, and laminated composite.[12] The matrix is response for holding the structure together and transferring the load to fibers and providing basic physical and chemical properties. For example, embedding aramid fibers into a polymer matrix, which can give a high impact resistance, excellent strength and toughness, low density, and impressive corrosion resistance, makes it to be an ideal candidate for reinforcement material in the manufacture of body armor, aerospace components, marine hulls, and automotive components.[3456] Figure 1.1 shows a wide range of applications that use the composite materials. For example, the composite materials occupy ~52% of the total structure of some airplanes, where they contribute to the nose section, rear fuselage, fuselage section, fin, and etc, as demonstrated in the Figure 1.2.

Figure 1.1 Composite materials have a wide range the applications.[7]

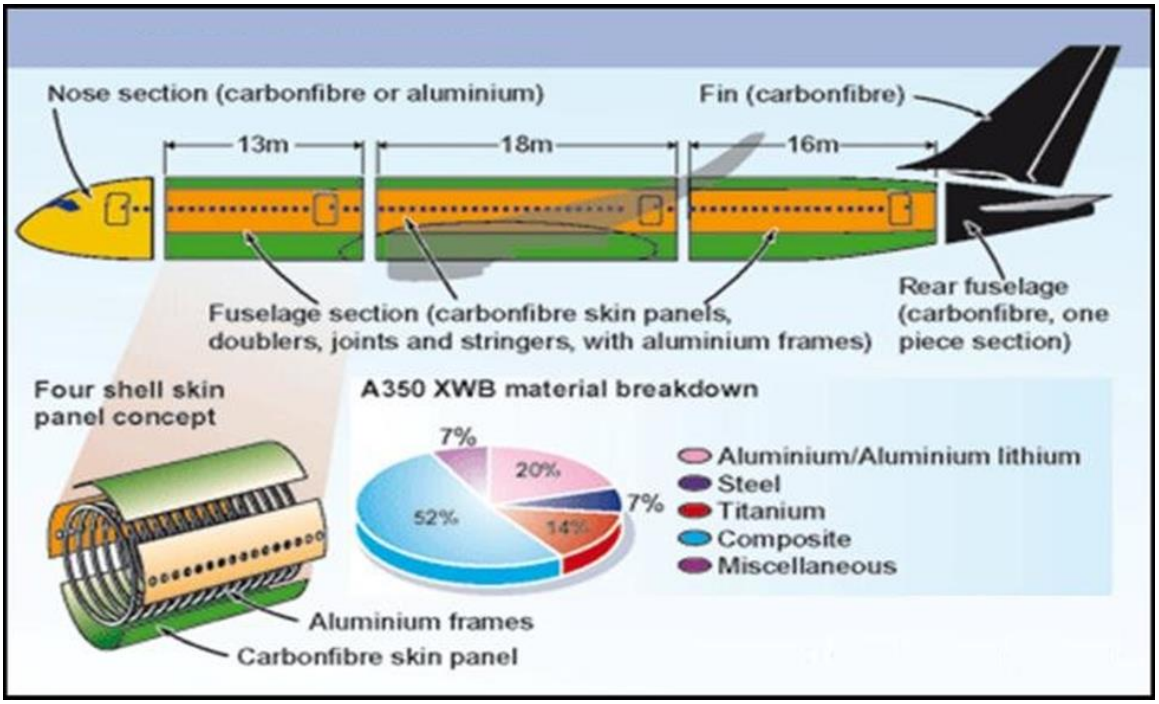

Figure 1.2 The composite materials represent ~52% of the total structure.[8]

1.1 Nano/micro composite

Nano/micro composite has received a wide intention due to their mechanical properties, thermal conductivities, and electrical properties.[359] For example, mixing layered fillers of the nano-silicate metal and unlayered micro-scale silica fillers and then sputtering them in epoxy resin, would help increase the electrical isolation strength by 7% and the insulation time by ~24 times, comparing to the pure epoxy.[10] Goulouti K, *et al*. successfully got an excellent thermal isolation (thermal transmittance values of below 0.15 W/m K) be replacing the thermal breaks stainless steel bars that has a low insulation layer by another thermal break composed of a great insulating aramid and glass fiber-reinforced polymer.[5] Peng L, *et al*. employed the injection chemical vapor deposition (ICVD) method to graft the multi-walled carbon nanotubes (MWCNTs) on the carbon fiber (CF) surface to get high fracture strength of the composite at lighter weight.[11] Figure 1.3a and b show as received CFs (with IFSS value 17.4 MPa) and coated by Silicon dioxide (SiO_2), respectively, to enable the MWCNTs to be firmly connected with the CF. Also, Figure 1.3c shows a high intensity of the entangled MWCNTs coating the CF with IFSS value 22.3MPa. Moreover, the CFs were immersing in toluene with 5 vol.% from each of tetraethoxysilane and silicon tetrachloride for getting aligned MWCNT as shown in the Figure 1.3d where the IFSS was improved to 25.2MPa. [11]

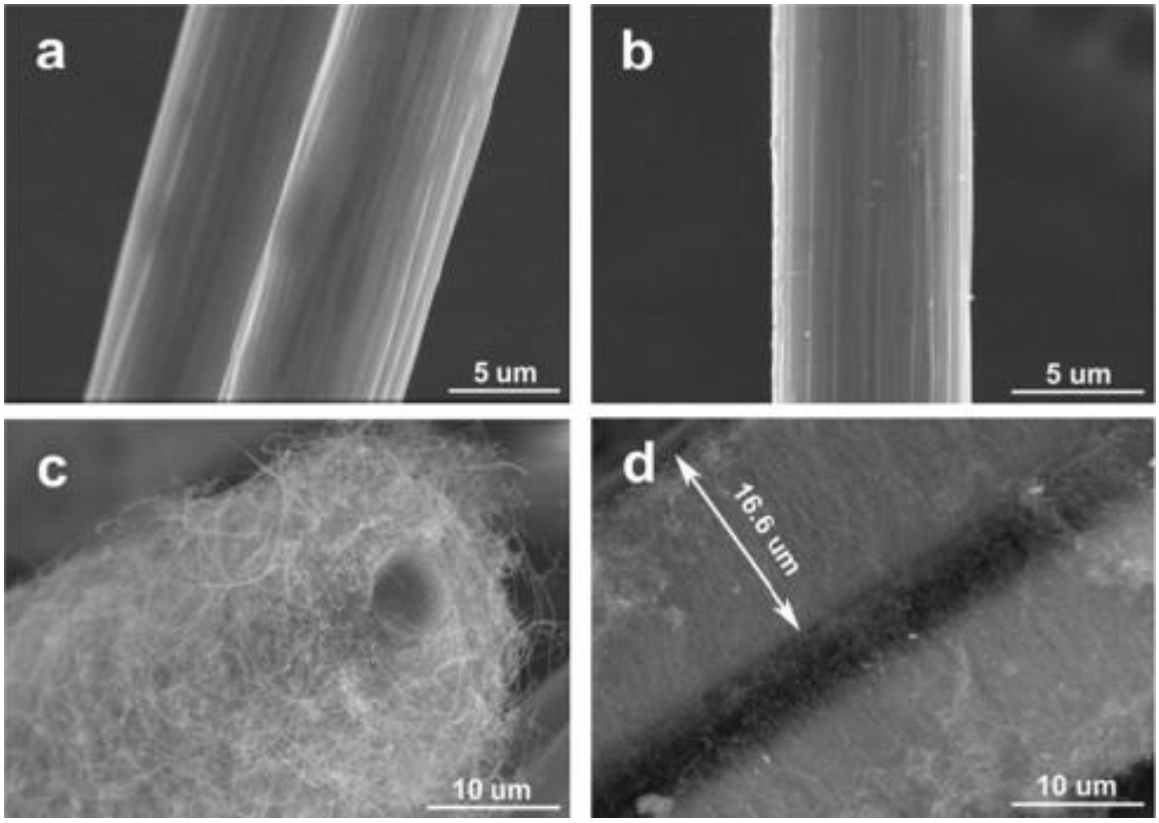

Figure 1.3 SEM images of (a) untreated CFs (b) coated CFs by SiO2 (c) grafted CF with entangled MWCNTs (d) grafted CF with aligned MWCNTs.[11]

1.2 Interface shearing strength (IFSS) between the fibers and the matrix

The mechanical performance of all fiber-reinforced composites depending not only on one element properties such as the fibers but also the reinforcement/matrix interface.[1213] A weak interface bond between the fiber and its matrix suggests incomplete load transfer which may pull-out the fibers from the matrix at low mechanical strength. In opposite, a strong interaction between reinforcement and its matrix leads to an efficient load transfer and build composites with higher strength. For example, composites reinforced by aramid fibers may suffer poor interface interactions during mechanical loading due to the smooth and passivated surface of the fibers.[1415] Figure 1.4a,b and c show a high magnification of the SEM images of the carbon fibers reinforced maleic anhydride-grafted-polypropylene, the interaction is low

between the fibers and the matrix and the separation between them already occurred.[16] In addition, Figure 1.4c shows low magnification of the of SiC fibers reinforced ceramic matrix, all the fibers pulled-out for the same reason and the composite structure were collapsed. For the ideal composite, the fiber (or the nanotubes) should fracture and pull-out partially on the same time.[17] Three existing strategies to improve interface bonding mainly consist of increasing roughness of the fiber surface, creating functional groups and fabricating particles on fiber surface.

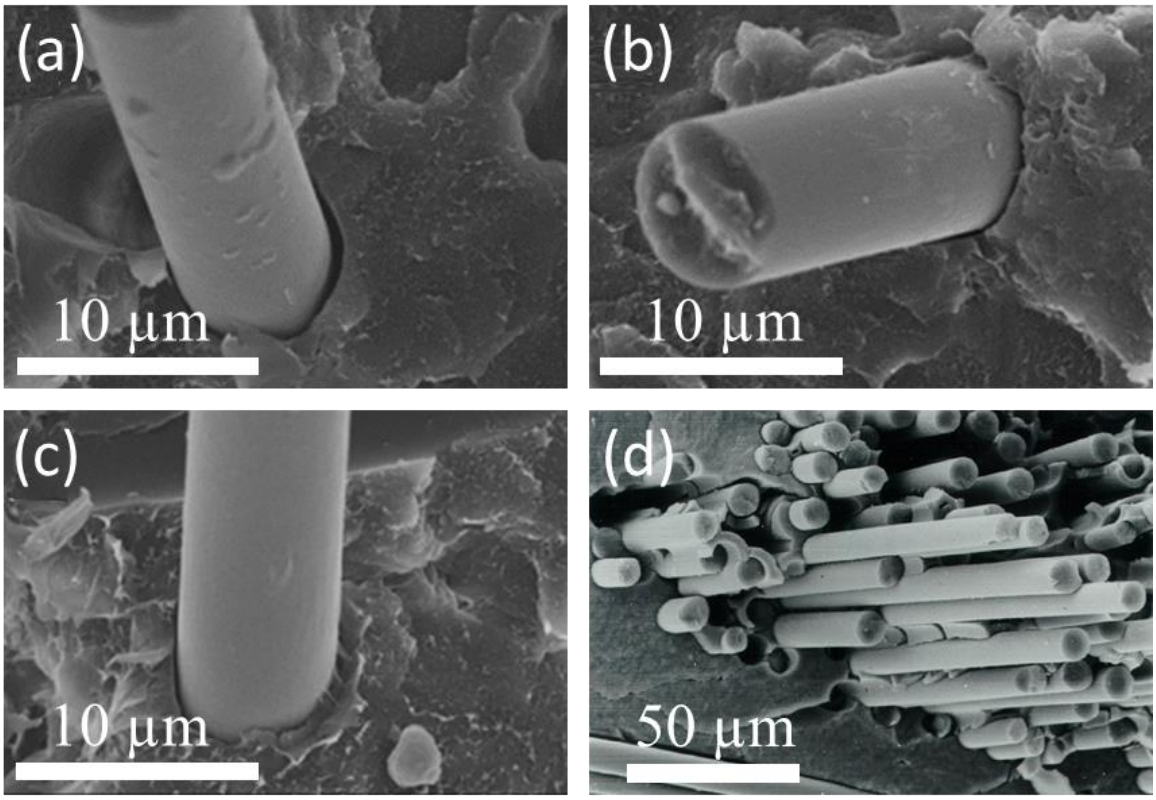

Figure 1.4 SEM images of (a), (b) and (c) High magnification of the carbon fibers reinforced maleic anhydride-grafted-polypropylene matrix (d) Low magnification of SiC fibers reinforced a ceramic matrix .[1618]

1.2.1 Surface roughness

1.2.1.1 Plasma or chemical treatment

To increase the IFSS between the fibers and polymer matrix, plasma treatment can be employed to increase the surface roughness of the fibers by melting the most outer layer of the fiber surface due to the high localized temperatures.[1920] Mechanical interlocking resulting from increased surface roughness leads to increase the sliding resistance and subsequently allows an efficient load transfer from the matrix to fibers.[21] Although the surface with a higher roughness has a better efficiency in load transfer, the fracture strength of the fibers will be weakened by the generated surface defects. As a result, the mechanical performance of the fabricated composites cannot be significantly improved. Therefore, the degree of surface treatment is critical for optimal balance of surface defects and fiber strength. Controversially, several investigations have showed that the tensile strength of the fibers is independent of the plasma treatment while others demonstrated it could increase or decrease depending on the period of the plasma treatment. For example, Sinha E, *et al.* applied the argon gas to treat the jute fibers with three different periods of treatment 5, 10, and 15 min. These fibers were used in jutepolyester composites to perform flexural tests. The flexural strength decreased to 153 MPa in the composites reinforced with 5 min treated fibers. With increasing the treatment period to 10 min and 15 min, the flexural strength of the composite first reached 181 MPa and then decreased to 144 MPa.[22] Another study demonstrated that the composites have better mechanical performance with fibers were treated by plasma for 3−10 min.[23] The surface roughness increases by increasing the power of the oxygen plasma.[24] Figure 1.5a-f show SEM images of the untreated and treated surfaces of the Kevlar fibers using oxygen plasma treatment where the surface roughness is dramatically increased. As example of the chemical surface treatment, the IFSS between the Jute fibers and polymeric matrices was increase to 67.22 % and 112.3 % after immersing the fibers in the NaOH and NaOH + Silanem, respectively. NaOH can remove the residual layers on fiber

surface such as the oils and wax and enhances functionality of the fiber surface. Also, NaOH + Silanem will improve fiber surface properties.[25]

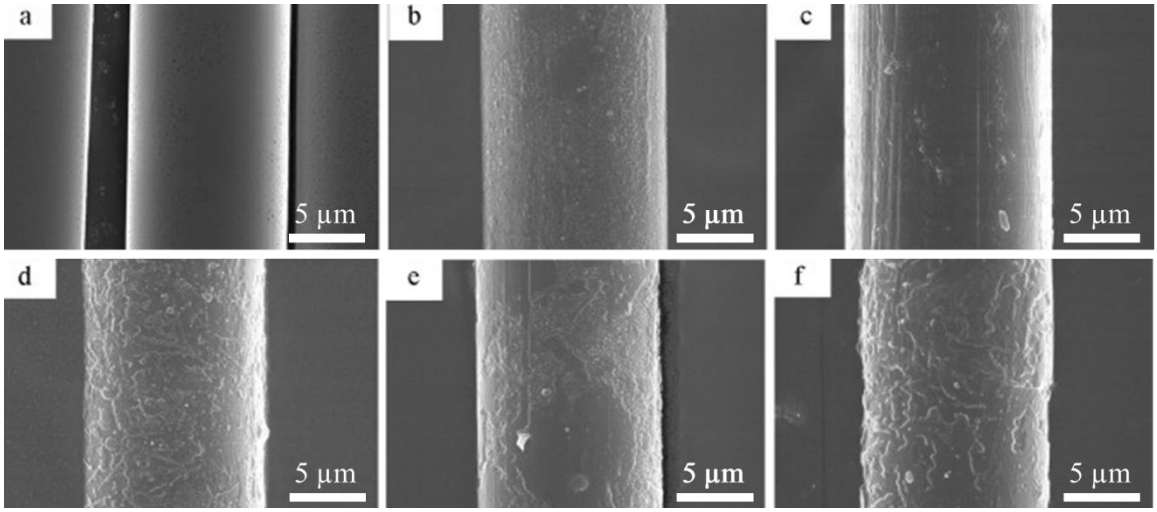

Figure 1.5 SEM images of the surfaces of Kevlar Fibers (a), untreated Kevlar Fibers (b-f) treated Kevlar fibers by oxygen plasma treatment for period of 5 min at different powers (b) 50W (c) 70W, (d) 100W, (e) 120W, and (f) 150W.[24]

1.2.1.2 Chemical vapor deposition (CVD)

CVD method can be used to synthesize selected nanoparticles, nanowires, and nanotubes on the surface of the fiber including ceramic particles, aluminums particles, and carbon nanotubes (CNTs) or even organic chemicals such as $(CH_3)_2Cl_2Si$. Grafting nanoparticles on the fiber surface may help in increasing the IFSS between the fiber and its matrix without sacrificing the tensile strength and other mechanical properties.[11] For the fibers with high melting temperature, such as carbon fibers, CVD method has been widely to carry out growth of ceramic particles and CNTs. Figure 6 shows the carbon fibers before and after growth of CNTs. Figure 1.6a show pristine carbon fiber, where it has a very smooth surface. At 800 °C and 700 °C, the CNTs intensively grew shown in the SEM images of the Figure 1.6b and c, respectively.

Decreasing the growth temperature from 800 °C to 700 °C will increase the homogeneity of CNTs on the surface of the carbon fibers.[26] In addition, the carbon fibers will be with less degree of catalyst accumulation.[26] For the fibers with low melting temperature, such as aramid fibers with glass transition temperature of 510 °C – 560 °C.[27], one of the biggest challenges is the required high temperature (~800°C) to grow nanoparticles on aramid fibers using CVD method. The high temperature may heavily damage the aramid fibers during nanostructure growth.

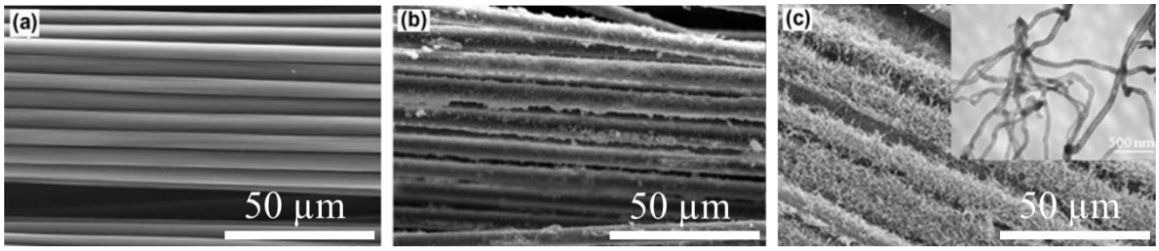

Figure 1.6 SEM images (a) pristine carbon fibers, (b) and (c) show carbon nanotubes coat the carbon fibers at temperatures 800 °C and 700 °C, respectively. inset of the figure (c) TEM image shows the dimensions of carbon nanotubes that coat the fibers surface.[26]

1.2.1.3 Physical vapor deposition (PVD)

In some cases, the composites material will collapse suddenly once reaching the maximum load without noticed warning if plasma or chemical surface treatment are used, due to the complex interfacial structure and the growth of microcracks and generating the new flaws.[28,29,30] Using the PVD is an alternative method to overcome these problems and improve the IFSS.[31] Also, the PVD method can be used to dimmish the ozone concentrate by modifying activated carbon fibers and coating them with an uniform thin layer of the gold or manganese .[32] Yang B, *et al.* use this method to coat the glass fibers with MWCNTs, where the IFSS is successfully improved from 30.23 MPa of the pristine fiber to 34.95 MPa after immersing CFs in the MWCNT solution for 4 times and then MWCNTs were deposited on GF surface

by physical vapor deposition (PVD).[31] The intensity of the MWCNTs on the fiber surface depends on several factors such as the concentration of the solution of the nanoparticles or the nanotubes, the period time of dispersion, and immersion cycles.[31] The Figure 1.1a-h show SEM images of the glass fibers before and after immersing them in a MWNTS solution, where the MWCNTs on the surface of the glass fibers are dramatically increased after immersing these fibers in a higher concentration of MWCNTs solution.

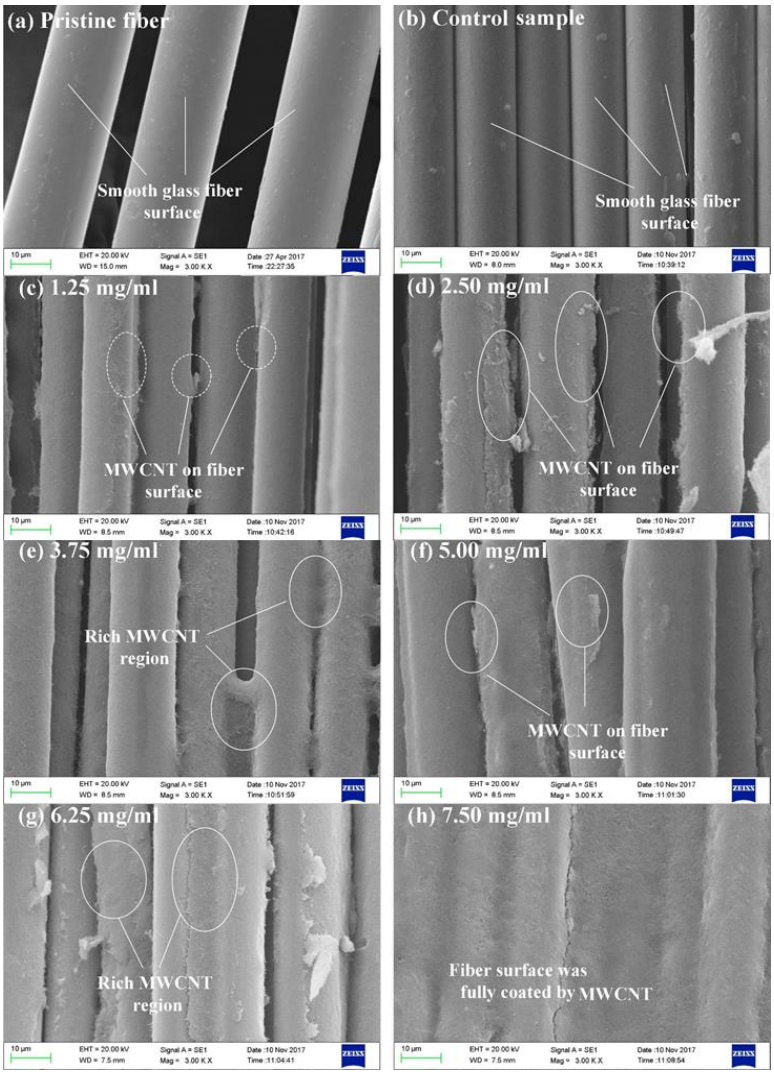

Figure 1.7 SEM Images glass fibers before and after coated with of MWCNT: (a) and (b) are glass fibers before the coating process, (c–h) the density of the MWCNTs on the glass fibers are increasing after immersing these fibers in higher concentration of MWCNT solution.

1.2.2 Functional groups

Enriching the fiber surface with the functional groups is another method to improve the IFSS. Generating functional groups rather than increasing the surface roughness would enable solid connection between fibers and matrix. Specific functional groups including hydroxyl, amino, and carboxylic acid can greatly enhance the wettability and allow to covalently bond to matrix, leading to improve the IFSS.[33] The balance between generating functional groups and surface roughness during treatment is critical. Keeping the fiber surface smooth will help maintain tensile strength of the fibers, while the increased surface roughness resulting from generated defects will facilitate the IFSS improvement. Figure 1.8 shows a new generated functional groups such as carboxyl (R–COOH) and hydroxyl (R-OH) after using the oxygen plasma treatment where R is a carbon or hydrogen atom.[33]

The aging of treated polymer surface is undesired phenomenon because it will make the surface lose its hydrophilic property with time elapsing and negatively affect the IFSS.[34] Several researches have been done to understand the aging behavior of the treated polymer surfaces.[353637] Ren Y *et al*. employed the atmospheric pressure plasma treatment to investigate the aging of aramid fiber's surface (The aging occurs due to the absorbed moisture by the surface of the fiber).[35] The results showed the fibers are not fully passivated after 30 days treatment, and the IFSS maintained ~75% of the improved value.[35]

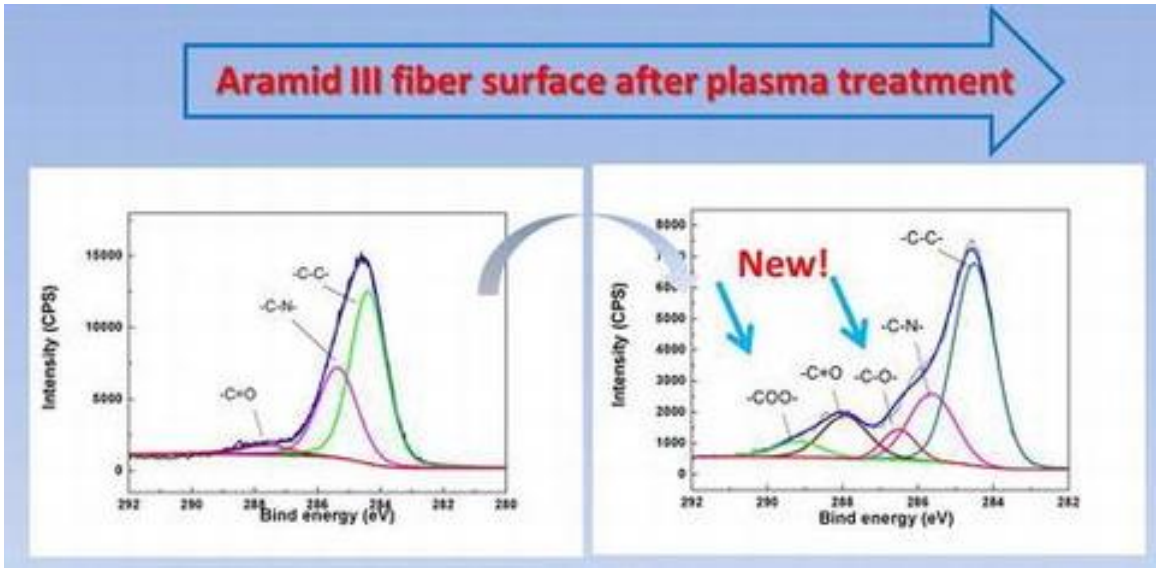

Figure 1.8 New generated functional groups such as carboxyl and hydroxyl after using the oxygen plasma treatment.[33]

1.3 The mechanic testing for interface shearing strength

As increasing surface roughness and creating functional groups through various methods can help improve the interface interaction, it is critical to understand how to quantify the IFSS. To date, several test methods have been adopted by both universities and industries to investigate the IFSS of the microfibers such as the push-out test,[38] the pull-out test,[3940]the microbond test,[41] and the fragmentation test,[12] by embedding the microfibers in the matrixes.

1.3.1 The push-out test

This method is to apply compression load on the fiber from one side to debond it from the other side, which considers a direct method. Several requirements should be met to use the push-out method. (I) the required diameter of the indenter tool for pushing the fiber out of the fiber should be equal to the diameter of the fiber. (II) the embedded length of the fiber equals to the matrix's thickness. (III) depending on the interaction between the fiber and its matrix and the magnitude of the applied load, the embedded length should be very short to prevent the damaging of the fiber rather than the push-out. For the push-

out method, some fibers cannot be probed due to their small diameters and their stiffness. If all requirements are met simultaneously, a huge disparity would be found in the tests result,.[42] Figure 1.9 shows a schematic demonstration for the push-out procedure. In the Figure 1.9a, the diameter of the load cell and fiber are same. Also, the thickness of the matrix is equal to the embedded length of the fiber. Figure 1.9b and c show the sample during and after the push-out test, respectively, where the load should be applied from the top side to push the fiber out of the matrix toward the bottom side. Rebillat F, *et al.* is an example for characteristic the IFSS of microfibers by using the push-out method.[13] In this work the Eq. 1.1 was used to calculate the IFSS, where F, r, l represents the applied load, fiber diameter, embedded length and cross section area of the fiber.

$$\tau = \frac{F}{2\pi r l} \qquad \text{Equation 1.1}$$

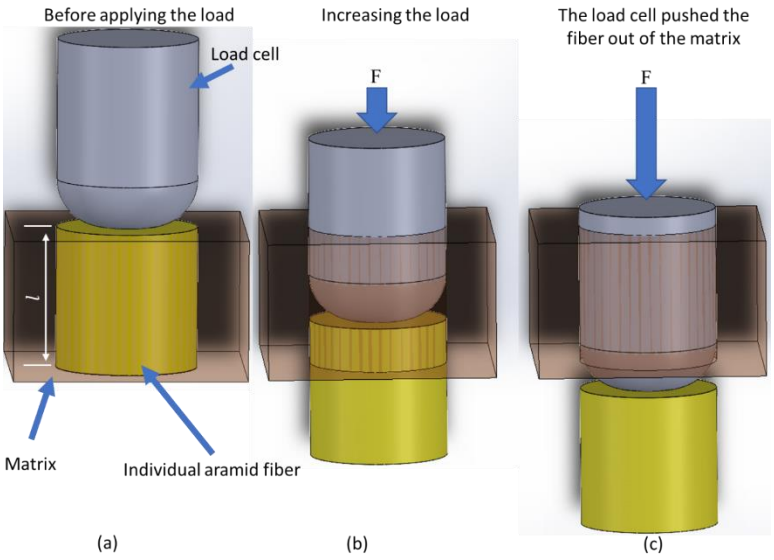

Figure 1.9 A schematic demonstration of the push-out test (a) Before applying the load, (b) During the increasing the load, and (c) After the separation between the fiber and the matrix due to the applied critical load.

1.3.2 The microbond test.

In 1987, Miller B, *et al.*[43] employed the microbond method to characteristic the IFSS. The procedure included carrying a small droplet of a resin by an applicator (with diameter ~30 µm) and placing it on the fiber surface. A microscope was used to measure the size of the droplet. Also, after the droplets were cured, the diameter and the embedded length can be measured with aid of the microscope. One end of the fiber should be glued to a metal tape to manipulate the sample and connect it to the load cell. The sample can be placed between two sharp edges and then apply a normal force from the other side to pull the fiber out of the droplet as shown in the Figure 1.10a. The reason of using the two sharp edges is to prevent the droplet from moving to the other side during the increasing of the applied load as shown in the Figure 1.10b. Also, Figure 1.10c shows the sample after the debonding test, where the debonding should occur between the fiber and the droplet rather than the droplet itself. The microbond test is an optimal choice for investigating the IFSS where the test can be started once the droplet of the matrix was cured. Several advantages of using the microbond method. It is easy to control the embedded length and several fibers can be placed on the same substrate and two droplets can be dropped in each fiber which can increase and accelerate the test's number and minimize the required storage space. Also, by using the microbond method, the formed meniscus around the fiber will be around 1% of the total embedded length which can be neglected.[43] Finally, The practical embedded length is usually greater than 40µm.

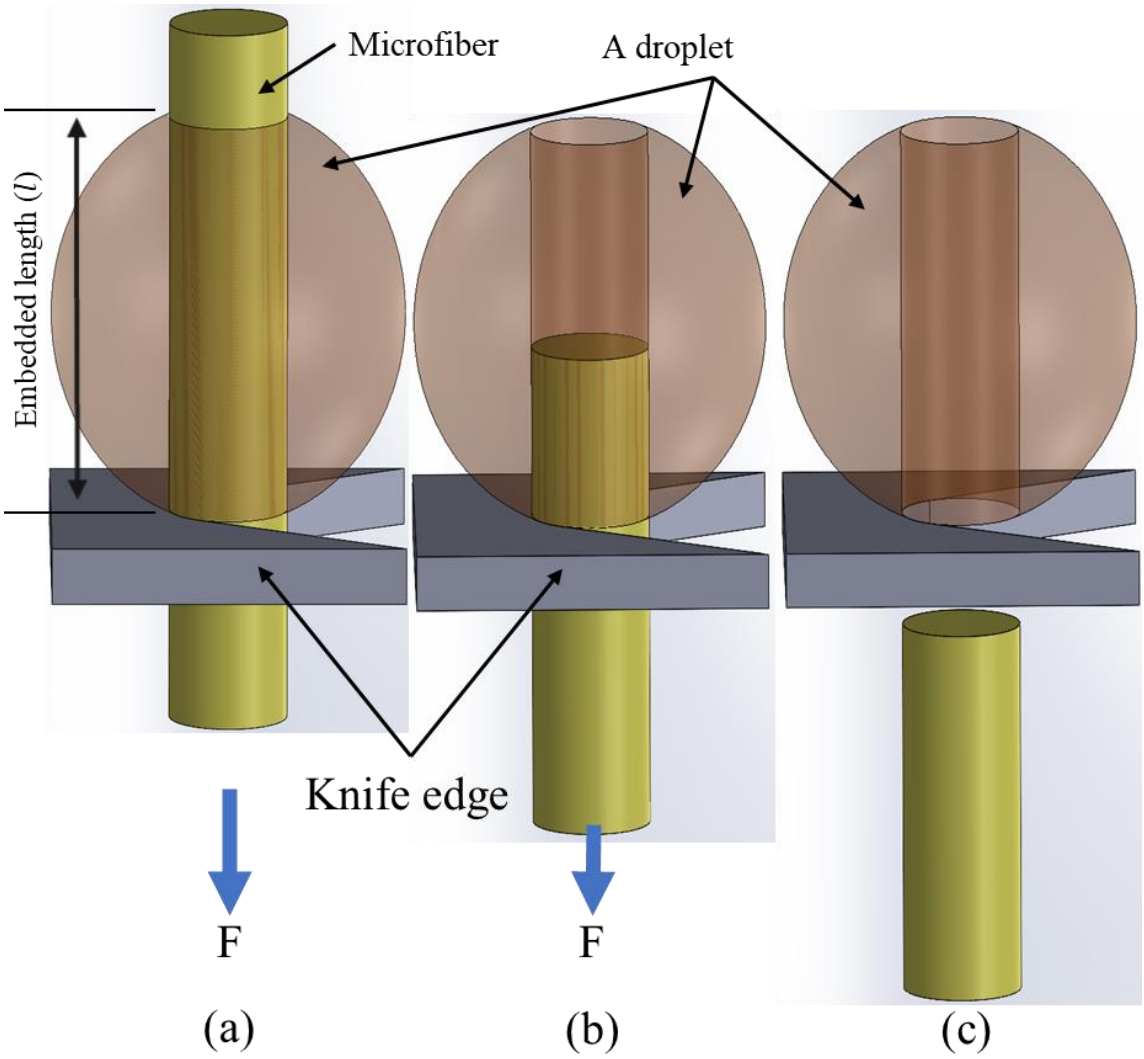

Figure 1.10 A schematic demonstration of the microbond sample (a) before applying the load, where the fiber is embedded in the droplet of the matrix and placed between two sharp edges, (b) during increasing the load to separate the fiber from the matrix, and (c) after the separation between the fiber and the matrix was occurred due to applying the maximum load.

1.3.3 The fragmentation tests.

Fragmentation test is another method which can be used to study the IFSS by applying tensile force on the matrix. It is considered un indirect method compared to the push-out test and microbond tests because the load will not be applied on the fiber directly. The matrix should cover the entire fiber as shown in the Figure 1.11a. The theory of the fragmentation test can be summarized by increasing the applied load on the matrix and transfer it to the fiber through the bonding between the matrix and the fiber surface. The increase of the force will break-up the fiber to shorter fragments until reaching the critical length and then IFSS can be calculated by using the Equation 1.5. According to the Kelly-Tyson model, the shear yield strength of the matrix should be high enough to transfer the load to the fiber otherwise the matrix will yield before reaching the maximum load.[44] The fragments length was suggested to be $\frac{3lc}{4}$ due to the existing of flaws where the $\frac{3lc}{4}$ represent the peak of the histogram for the collected data of fragment lengths after applying the maximum load,[4445] where d is the fiber diameter, σ is the fiber fracture strength at the critical length (Equation1.2), and Lc represents the critical fragment length of the fiber (Equation 1.4), F is the maximum load at the critical length and τ represents IFSS between the fiber and the matrix.

Using the fragmentation method required a special devices and complex extruder. This extruder should be provided with heaters, having several rooms with different temperatures and cooling system to prepare the sample. The extrusion process could generate a premature failure in the fiber due to the applied axial load on the matrix. In short, the sample preparation is a complex procedure. Figure 1.11 b shows the sample during the load increasing. where the fiber has a symmetric shape during break-up to shorter fragments, indicating the load is equally distributed on both sides and there are no flaws on the fiber's surface.[46] Also, Figure 1.11 c shows a schematic demonstration of the sample after the

fragmentation test where the lengths of the fragments are equal. Generally, it is not easy to get identical fragments because preexist the flaws. For this reason, the average length should be calculated by using Equation 1.3. The critical length can be plugged in the Equation 1.2 to find the IFSS.

$$\tau = \frac{F}{\pi * d * Lc/2} \qquad \text{Equation 1.2}$$

$$Lc = \frac{4l_{ave}}{3} \qquad \text{Equation 1.3}$$

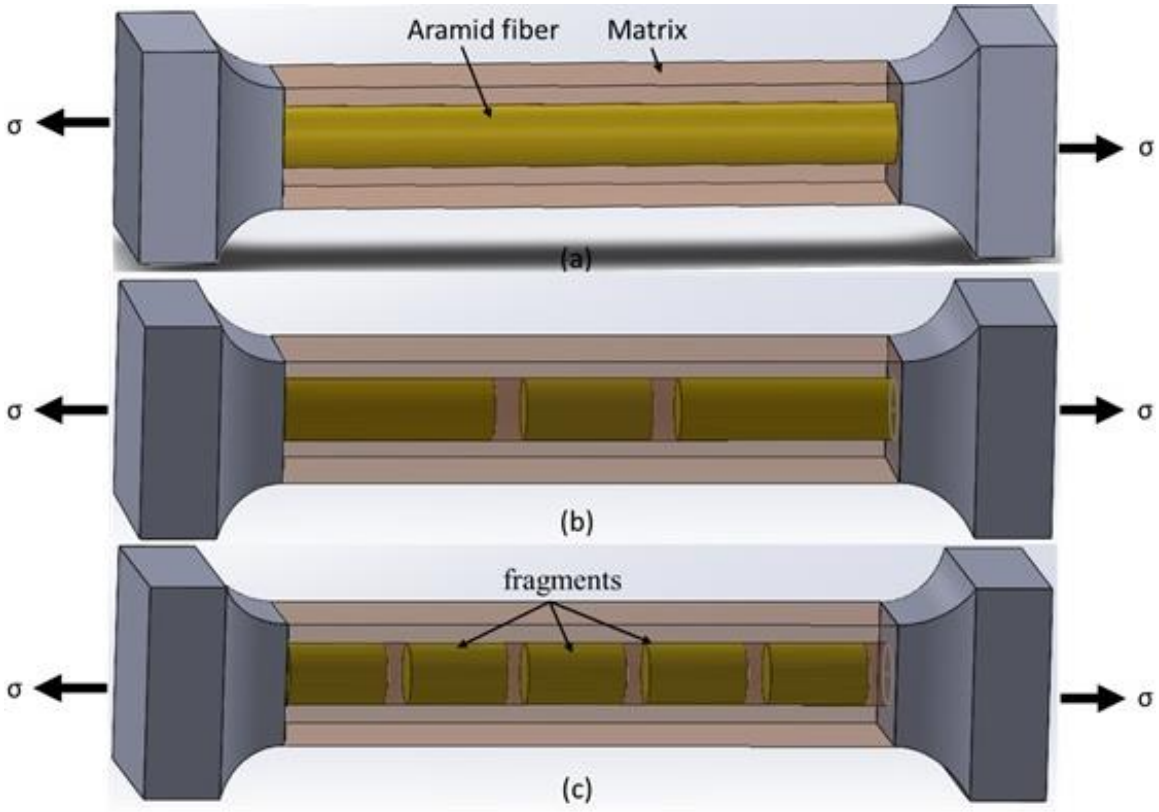

Figure 1.11 shows the fragmentation sample (a) before applying the load where the fiber is entirely embedded in the matrix, (b) during the increasing the load to break the fiber to smaller segments, and (c) after breaking the fiber to short and equal segments after applying the maximum load.

1.3.4 The pull-out test

Pull-out test is another common method to characterize the IFSS.[4739] Figure 1.12 shows a schematic demonstration of the sample before, during and after the pull-out test. On the Figure 1.13a, the fiber is partially embedded in the matrix where the embedded length should be chosen carefully to pull-out the fiber rather than it fractures. Figure 1.12b represents another schematic demonstration, where the fiber is partially pulled-out from the right side after applying the force, while the left side should be clamped to the fixed chew of the micro tester devise. After the poll-out test, should be no missing matrix pieces or severe cracks, otherwise the sample will be neglected and the hole in the matrix should be clear as shown in the Figure 1.12c. Several great features of using the pull-out test, such as, easy to fabricate the sample, well-defined geometry, results with low standard deviation, ease to clamp the fiber to the micro-tester for conducting the pull-out test, and it could be used for a wide range of fiber diameters, making it the best candidate for characterizing the IFSS.

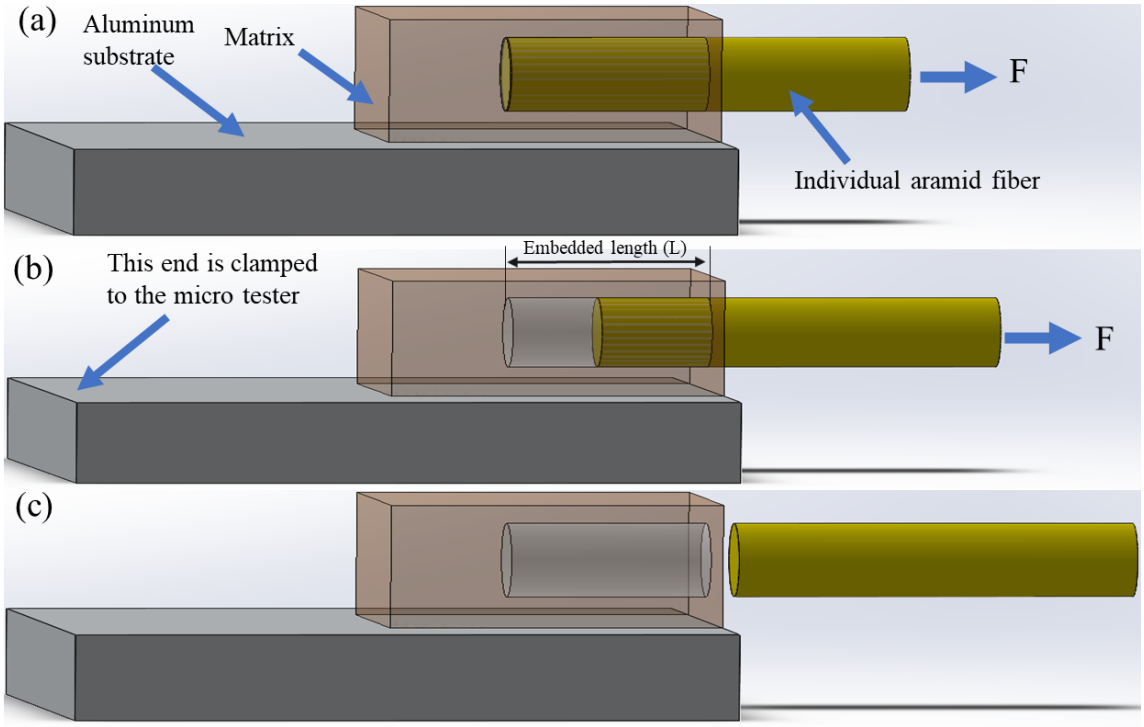

Figure 1.12 a schematic demonstration of the pull-out sample (a) before applying the load, where one end of the fiber is embedded in the matrix, (b) during the load increasing to debond the fiber from the matrix, and (c) the fiber is fully separated from the matrix at the maximum load after pull-out test.

1.4 Research scope

Composites reinforced by aramid fibers may suffer poor interface interactions due to their smooth and chemically inert surface. Addressing this scientific issue is important to advance the application of aramid fibers. In this thesis, the interface interaction between the aramid fibers and the polymer matrix has been improved by three different approaches. These approaches are increasing surface roughness, creating new functional groups, and synthesizing the ceramic nanoparticles on aramid fibers. Also, the interfacial interactions between the carbon fiber and different kinds of substrates will be investigated by identifying hydrogen bonding and van der Waals forces.

The effect of treatment on the mechanical properties is still debatable. Park J*, et al*. used the oxygen-plasma to treat the poly(p-phenylene-2,6-benzobisoxazole (PBO, Zylon) and poly(p-phenylene terephthalamide) (PPTA, Kevlar) fibers .[19] The results shows the IFSS increased for both of the fibers.[19] Another study showed the IFSS decreases if the applied heat treatment on the matrix is increased from 4 minutes to 6 minutes.[48] Sinha E*, et al.* suggested the mechanical properties could decrease or increase depending on the type of treatment and the period of that treatment.[22] Regarding the increasing of the surface roughness by using the plasma treatment, in our work, the optimal period of plasma treatment is carefully chosen. At this optimal period of plasma treatment, the IFSS should be successfully improved without deteriorating the fracture strength. Several topics will be discussed: including the effect of plasma treatment on the fracture strength, IFSS at the room and the elevated temperature.

As a part of improving the IFSS of the aramid fibers, the IFSS at the elevated temperature will be investigated to identify the optimal solution to maintain a high IFSS. Because the micro-tensile tester works at temperature between 5 °C and 40 °C, it is covered with a thermal isolation material to make it works at the temperature ~100 °C as shown in the Figure 1.14a. To increase the temperature of the sample, a heater was connected to the heating aluminum element, and the surface of this element is kept in contact with a thermometer to measure the temperature as demonstrated in the Figure 1.14b. In addition, the heating element is fabricated with dimensions of 10mm X 10mm to fit well on the left jaw of the micro-tester as presented in the Figure 1.14c. Figure 1.14d shows the whole assembly including the micro tester, thermometer, heating element and the isolation materials, where it is clear the required temperature was reached.

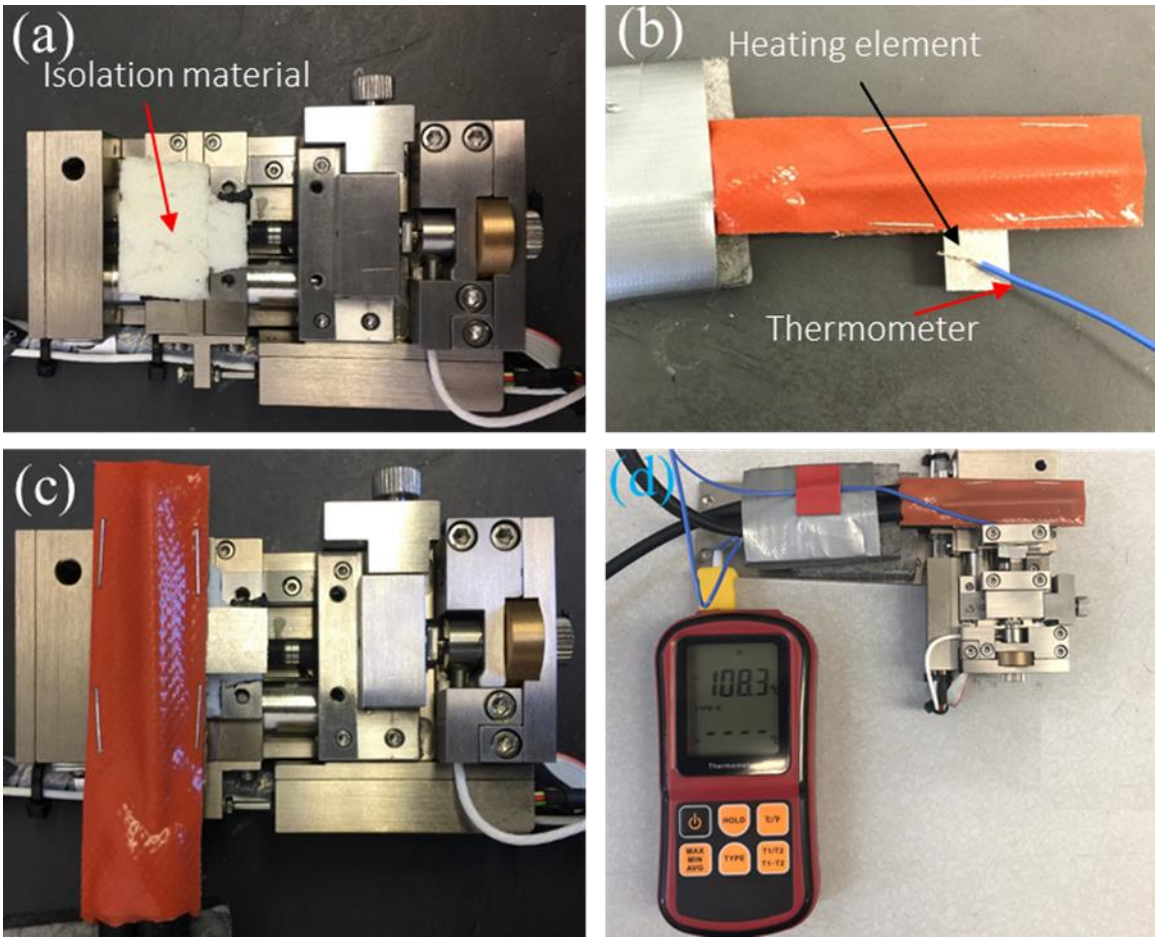

Figure 1.13 The modified micro-tensile tester to make it suitable for the elevated temperature (a) Insulation material is coating the movable jaw, (b) Heating element is connected with a thermometer to provide the accurate temperature, (c) Connecting the heating element with micro-tensile tester by the isolation material to force the heating element heats the sample only (d) All the parts are connected with each other as a one assembly to provide the controlled elevated temperature to the sample without affecting the micro-tensile tester.

The second project focuses on solving the problem of an undesirable phenomenon named the aging of fiber's surface. In this phenomenon, the fiber's surface losses its hydrophilicity with time elapsing, resulting a low interaction between the fiber and the matrix and deteriorated IFSS.[34] The degree of hydrophilic or hydrophobic behaviors of the fiber's surface can be investigated by using contact-angle

measurement and then use it as reference for the surface aging. For example, treating the cellulosic fabrics by a low-pressure of the oxygen plasma decreases the water contact angle from 66° to ~15° and no aging was found for up to 4 days.[49] Also, treating the polyethylene terephthalate fabric by atmospheric pressure air plasma improves the wettability of the fabric and there is no aging during the first 30 days.[50] Also, treating the nylon fabric with different gases including oxygen, argon, air, and helium will improve the wettability of the fabric.[51] In all the mentioned researches, it not clear what is the optimal period of treatment that will activate the fiber's surface and improve IFSS without deteriorate the fracture strength. Also, there is no method for reactivate the inert surface. In this part of the research, the focus will be on choosing the optimal period of plasma treatment that will improve the IFSS without affecting the fracture strength. On the other word, the surface will be dominated through the functional groups rather than the surface roughness. Also, investigating the aging period that makes the fiber loses the IFSS's improvement. Furthermore, using a new technic to activate the fiber's surface again.

In the third project, the IFSS will be improved by using the CVD method to coat the aramid fiber surface with ceramic nanoparticles instead of using the plasma treatment to increase the surface roughness or activate the surface by the functional groups. Using the CVD method means no new generated flaws or concerns regarding the surface passivation. Due to the low decomposition temperatures (T_d) of the aramid fiber (510 °C – 560 °C) and the high required temperature for melting the ceramic particles (700°C), the CVD method would heavily damage the fibers.[27] However, the CVD is the optimal method for improve the mechanical properties of the carbon only due to its high T_d (700 °C - 1200°C).[52] For example, CVD method is great choice for getting 3D dimensions hybridized structure that consists of CNTs and the 2D carbon sheets.[5354] Also, the CVD is used to graft the CNTs on the surface carbon fibers to increase the interface force resistance against the applied load to improve IFSS between the fiber and its matrix.[11] To make it possible to use the CVD method for coating the aramid

fiber surface with ceramic nanoparticles, new technic will be used. One of the most important advantages of this method, The IFSS and the fracture strength will be in high performance.

In the last project, as strong force originated from breaking covalent bonds can be easily quantified throughout various testing platforms, while weak interfacial sliding resistance (ISR) originating from hydrogen bonding or van der Waals (vdW) force is very challenging to measure. Facilitated by the in-house nanomechanical testing system, we are able to precisely quantify and clearly distinguish the interfacial interaction between individual carbon fibers and several substrates governed by either hydrogen bonding or vdW force. The *ad hoc* studies demonstrate that hydrogen bonding rather than vdW force has a great potential in sewing the interface if both surfaces are supportive to form hydrogen bonds.

CHAPTER 2

2 IMPROVING THE IFSS OF THE ARAMID FIBERS AT THE ROOM AND ELEVATED TEMPERATURE BY INCREASING THE SURFACE ROUGHNESS.

2.1 Introduction

The mechanical properties of the intrinsic properties of the fibers and the reinforcement/matrix interface are important for high-performance of composites materials.[55565758] A weak interface bond has incomplete load transfer, which may result in the reinforcements being pulled out thus resulting in composites with low mechanical strength. In contrast, a strong interface bond yields composites with higher strength but lower toughness. Generally, in order to have both high strength and high toughness, the ideal fracture for fiber-reinforced composites should be a combination of partial fibers pulled out of the matrix and partial fibers fractured after mechanical failure.[17] Therefore, microscale tuning of interface bonding may greatly impact both fundamental research and engineering applications of the composites.

As one of the most common reinforcements, aramid fibers have been widely used as reinforcement material in the manufacture of body armor, aerospace components, marine hulls, and automotive components due to their high impact resistance, excellent strength and toughness, low density, and impressive corrosion resistance.[3456] Regarding their smooth and chemically-inert surfaces, the fabricated composites suffer from poor interface interaction between the fibers and matrix during mechanical loading.[141529] Existing strategies to improve interface bonding mainly consist of creating functional groups and increasing roughness on fiber surface. For functionalization, either strong acid reaction or plasma bombardment has been used to create active functional groups such as carboxyl and hydroxyl.[33] In addition to the generated functional groups, plasma treatment can also induce a rougher surface by melting fibers due to localized high temperatures.[192059] Mechanical interlocking from increased

surface roughness leads to high sliding resistance and subsequently allows efficient load transfer from matrix to fibers.[21]

Although the interface has higher efficiency in load transfer, the fibers are weakened by the generated surface defects. As a result, the mechanical performance of the fabricated composites cannot be significantly improved. Therefore, the degree of surface treatment is critical for optimal balancing of surface defects and fiber strength. Controversially, several studies have demonstrated that the tensile strength of fabricated composites may stay the same, increase or decrease as a result of the strengthening process. For example, Sinha E, *et al.* performed flexural tests using jute-polyester composites with jute fibers treated by argon cold plasma for 5, 10, and 15 min. The flexural strength decreased to 153 MPa in the composites reinforced with 5 min treated fibers. With treatment period increasing to 10 min and 15 min, the flexural strength of the composite first reached 181 MPa and then decreased to 144 MPa.[22] Another study demonstrated that the composites with fibers treated by plasma for 3.10 min have better mechanical performance.[23]

To comprehensively understand how plasma treatment affects the interface interaction between the polymer matrix and aramid fibers, more detailed studies are required. Specifically, how plasma treatment can enrich functional groups and increase surface roughness as well as which one holds greater potential for improving interface interaction needs to be clarified. Additional topics of interest for aramid fiber reinforced composites include interface mechanics at room temperature and mechanical stability in harsh environments such as elevated temperatures. To untangle these inscrutable relationships and address associated concerns, the interface interaction between individual aramid fibers and polymer at room and elevated temperatures has been carefully investigated in this study.

2.2 Experimental

2.2.1 Aramid fibers and plasma treatment

Aramid fibers (DAF III, polyheteroarylene-co-p-phenyleneterephthalamide) were purchased from Bluestar Chengrand Chemical Co. Ltd. The diameter of the fibers is ~17 μm. The pristine fibers were washed carefully with acetone and dried for 3 h at 100 °C. Plasma-treated fibers were prepared by an inductive coupling radio frequency generator (13.56 MHz). Oxygen was kept at a flow rate of about 20-30 cubic centimeters per minute (sccm). The operation pressure was ~30 Pa. The fiber samples were treated for 5 min, 10 min, 15 min and 20 min, with plasma treatment power of 100 W. The treated fibers were kept in a vacuumed container.

2.2.2 Matrix preparation

The epoxy precursor is composed of EMbed 812, Dodecenylsuccinic anhydride (DDSA), N-Methylaniline (NMA), and 2,4,6-Tris (dimethylaminomethyl) phenol (DMP-30) with a volume ratio of 20:16:12:0.7.[60] All components were bought from Electron Microscopy Sciences, Hatfield, PA. The EMbed 812, DDSA, and NMA, was stirred for 15 min and then the DMP-30 was added to the solution and stirred for another 15 min with aid of the magnetic stirrer device. The solution then was placed in the ultrasonic device for ~5 min for degassing. In order to improve the IFSS at elevated temperature, another epoxy precursor was prepared as well. A liquid polymer (CSO-230) (Extreme Environment Materials Solutions, LLC, New York) was mixed with the epoxy precursor with a weight ratio of 1:20. The CSO-230 polymer is based on silicon alkoxide chemistry ($Si(OR)_4$) with some OR sites substituted by hydride and vinyl groups.[61]

2.2.3 Sample preparation for debonding tests

For preparing the sample, aluminum substrate with a smooth and sharp surface with approximate dimensions of 10 mm × 10 mm × 2 mm was used. A small amount of the prepared resin is carried with aid of a fine needle and dropped on the smooth face and close to the sharp edge of the substrate. After placing the sample under the microscope, the fiber can be manipulated by using a sharp tweezer. The microscopy is connected to a monitor to collect the fiber dimensions and control the embedded length as shown in the Figure 2.1a. The objective lens of the microscopy considers a good reference for getting the required embedded length. For example, the size 20 objective lens can cover ~450 µm from the fiber's length. After getting the right embedded length, the sample can be placed in the drying oven at 60 °C for 24 hours until the matrix is formed Finally, the fabricated samples were cured at 60 °C for 24 h in a drying furnace as shown in Figure 2.1b. Deben Micro Tensile Tester (Gatan Inc.) is the optimal device for conducting the pull-out testing and measuring the IFSS is shown in the Figure 2.1c. The tester was installed with a 200 N load cell. The force resolution is 0.001 N. The loading speed was controlled with 0.2 mm/min. The embedding length is less than 1 mm to ensure that the fiber will be pulled out rather than fracture during the debonding test.[62] To prevent the fiber falling off the substrate, another piece of aluminum substrate was used to support the other end of the fiber.

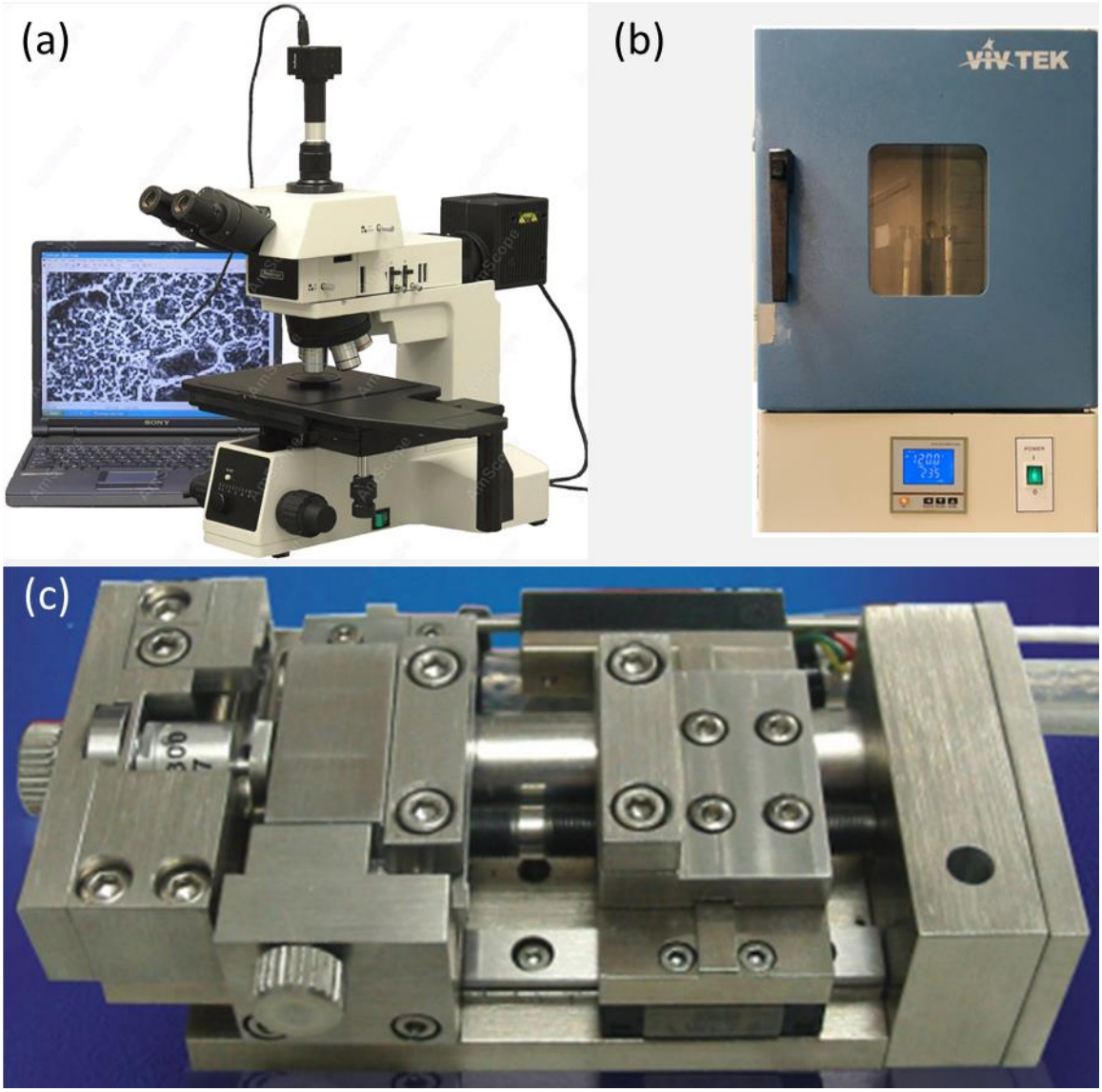

Figure 2.1 The required equipment and devices for preparing the samples and conducting the pull-out tests (a) the optical microscope is connected the monitor (b) the furnace that used for curing the resin, and (c) Deben micro tensile tester (Gatan Inc.)

2.2.4 Debonding tests

To date, several methods have been widely developed to characterize the IFSS including the microbond test[43] , the micro-indentation test[6364] , the fragmentation test [1265], the pull-out test[394766] and the push-out test.[38] Among these methods, the pull-out test holds advantages on well-defined geometry, highly reproducible results, and no limitation in reinforcement size. In this study, the pull-out test was employed to measure the IFSS. Before debonding tests, the diameter and embedded length of the aramid fiber were measured using an optical microscope. The diameter for most fibers is ~17 μm. The Deben Microtest device (Gatan Inc.) installed with a 200 N load cell was used to conduct pull-out tests. The loading speed was controlled at 0.2 mm/min.

2.2.5 Debonding tests at elevated temperatures

The microtensile tester is designed to work at temperatures ranging between 5 °C and 40 °C. To evaluate the interface stability at elevated temperatures, a home-made heating and thermal insulation accessory was assembled using a heating element, control system, and four pieces of thermal insulation material as explained in the chapter one. The temperatures of 50 °C and 100 °C were selected to investigate the interface stability. For debonding testing at elevated temperatures, all parameters were kept the same as those at room temperature.

2.3 Results and Discussion

Before precisely quantifying the interface interaction between aramid fibers and polymer matrix, it is necessary to understand how surface treatment affects mechanical performance of the aramid fibers. Fibers with various periods of plasma treatment including pristine, 5 min, 10 min, 15 min, and 20 min were tested. During tensile test, the loading rate was set as 1.2 mm/s. Figure 2.1 shows the representative stress-strain curves of all tested fibers. Table 2.1 summarizes mechanical properties of the aramid fibers with and without plasma treatment.

Table 2.1 Mechanical properties of aramid fibers with and without plasma treatment.

Sample	Fiber Diameter μm	Tensile Strength GPa	Elastic Modulus GPa
Untreated	16.81±0.66	2.99±0.51	72.76±8.74
5 min treatment	16.66±0.40	2.08±0.48	55.77±13.74
10 min treatment	16.36±0.50	2.27±0.51	71.99±6.65
15 min treatment	16.44±0.52	2.56±0.78	69.78±8.21
20 min treatment	16.70±0.45	2.63±0.80	67.29±7.47

For the untreated fibers, the average tensile strength is 2.99 ± 0.51 GPa. Seven fibers were fractured for getting the average of the tensile strength, and elastic modulus as shown in the Table 2.2. With plasma treatments, the tensile strength decreases. Specially, the fibers with 5 min plasma treatment have the lowest tensile strength of 2.08 ± 0.48 GPa. The reduction in tensile strength reaches ~30%. The degraded tensile strength results from surface damage which is evidenced by morphology difference between the fibers without treatment and with 5 min treatment shown in Figure. 2.2a and 2.2b. Apparently, severe damage is found in Figure 2.1b. Seven individual fibers were fractured to characteristic the average of the tensile strength, and elastic modulus as shown in the Table 2.3. Interestingly, with extension of plasma treatment, the tensile strength significantly rebounds. For example, the tensile strengths for the tested fibers with 10 min, 15 min and 20 min plasma treatment reach 2.27±0.51, 2.56 ± 0.78 GPa and, 2.63±0.80 GPa, respectively which is close to the value of untreated fibers. As the period of plasma treatment increases, the plasma starts to etch away the bumps created earlier, making the fibers smooth again. Figure 2.2a-1d show the surface morphologies of the aramid fibers during different periods of plasma treatment. Once the major surface defects are removed, the stress concentration around the original defects will be eliminated, enabling the stress to be uniformly distributed in the fibers. Therefore, the fibers with extended plasma treatment have tensile strength close to those of pristine fibers. Seven

individual aramid fibers of the 10 min, 15 min and 20 min plasma treatment were fractured to characteristic their average of the tensile strength, and elastic modulus as shown in the Table 2.4 and Table 2.6, respectively.

Table 2.2 Mechanical properties of aramid microfibers without plasma treatment

Sample	Test #	Fiber Diameter μm	Tensile Strength GPa	Elastic Modulus of GPa
Untreated	Test 1	16.71	3.68	65.10
	Test 2	17.86	2.91	72.95
	Test 3	16.71	2.96	60.91
	Test 4	16.28	2.98	87.44
	Test 5	16.71	3.42	71.99
	Test 6	16.86	2.98	71.65
	Test 7	15.86	2.04	79.28
Average± Standard deviation		16.71±0.61	2.99±0.51	72.76±8.74

Table 2.3 Mechanical properties of aramid microfibers with 5 min plasma treatment.

Sample	Test #	Fiber Diameter μm	Tensile Strength GPa	Elastic Modulus of GPa
5 min treated	Test 1	16.86	2.05	51.99
	Test 2	17.43	2.14	32.395
	Test 3	17.14	1.92	68.90
	Test 4	16.42	1.14	64.55
	Test 5	16.86	2.51	54.92
	Test 6	16.86	2.61	46.55
	Test 7	16.00	2.23	71.13
Average± Standard deviation			2.08 ± 0.48	55.77±13.74

Table 2.4 Mechanical properties of aramid microfibers with 10 min plasma treatment.

Sample	Test #	Fiber Diameter µm	Tensile Strength GPa	Elastic Modulus of GPa
10 min treated	Test 1	17.14	2.43	66.85
	Test 2	16.71	1.82	70.18
	Test 3	16.71	1.49	76.99
	Test 4	16.86	2.57	65.62
	Test 5	17.00	2.99	66.59
	Test 6	15.43	2.55	83.70
	Test 7	16.57	2.06	74.00
Average± Standard deviation				71.99±6.65

Table 2.5 Mechanical properties of aramid microfibers with 15 min plasma treatment.

Sample	Test #	Fiber Diameter µm	Tensile Strength GPa	Elastic Modulus of GPa
15 min treated	Test 1	16.36	3.27	77.94
	Test 2	16.29	2.55	62.29
	Test 3	16.14	4.05	80.62
	Test 4	16.71	1.71	72.47
	Test 5	16.57	2.16	74.99
	Test 6	17.00	2.48	57.87
	Test 7	17.71	1.73	62.32
Average± Standard deviation				69.78±8.21

Table 2.6 Mechanical properties of aramid microfibers with 20 min plasma treatment.

Sample	Test #	Fiber Diameter µm	Tensile Strength GPa	Elastic Modulus of GPa
20 min treated	Test 1	16.71	1.10	55.23
	Test 2	16.43	2.62	70.56
	Test 3	16.71	2.91	64.97
	Test 4	16.14	3.47	76.88
	Test 5	16.71	2.91	61.03
	Test 6	16.71	2.18	73.58
	Test 7	17.86	3.25	68.81
Average± Standard deviation				67.29±7.47

Although the elastic modulus of fibers has similar trend to tensile strength, it has large standard deviation. The elastic modulus of polymers depends on the stiffness of polymer chains, which would be affected by their crystallinity, defects, orientation, grafted functional groups, etc. The stress-strain curve of polymers, generally, does not have “perfect” linear region for calculation of elastic modulus, which accounts for the large variation in elastic modulus. The decreased elastic modulus in fibers with 5 min plasma treatment would originate from damages to polymer chains and crystallinity rather than from surface roughness.

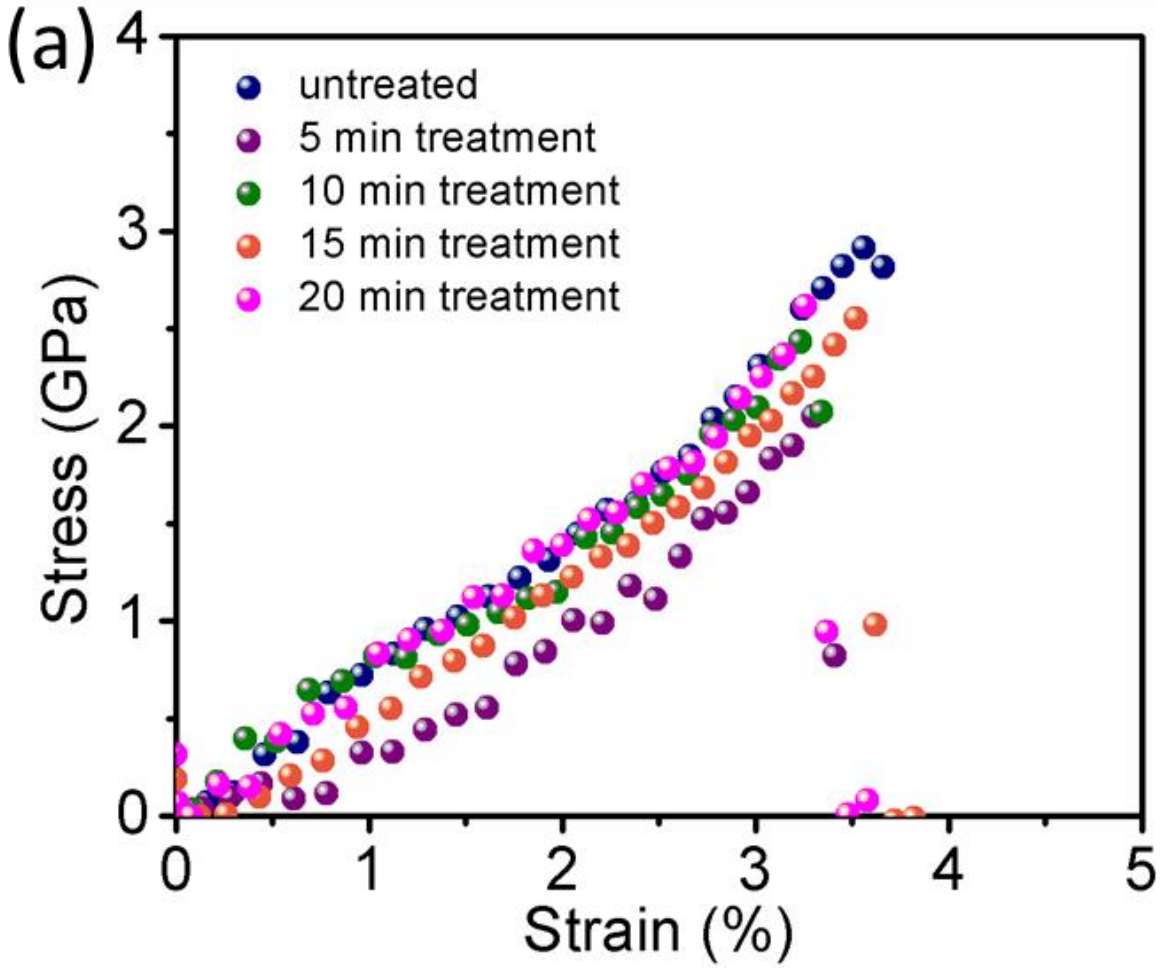

Figure 2.2 Tensile tests of aramid fibers without and with plasma treatments.

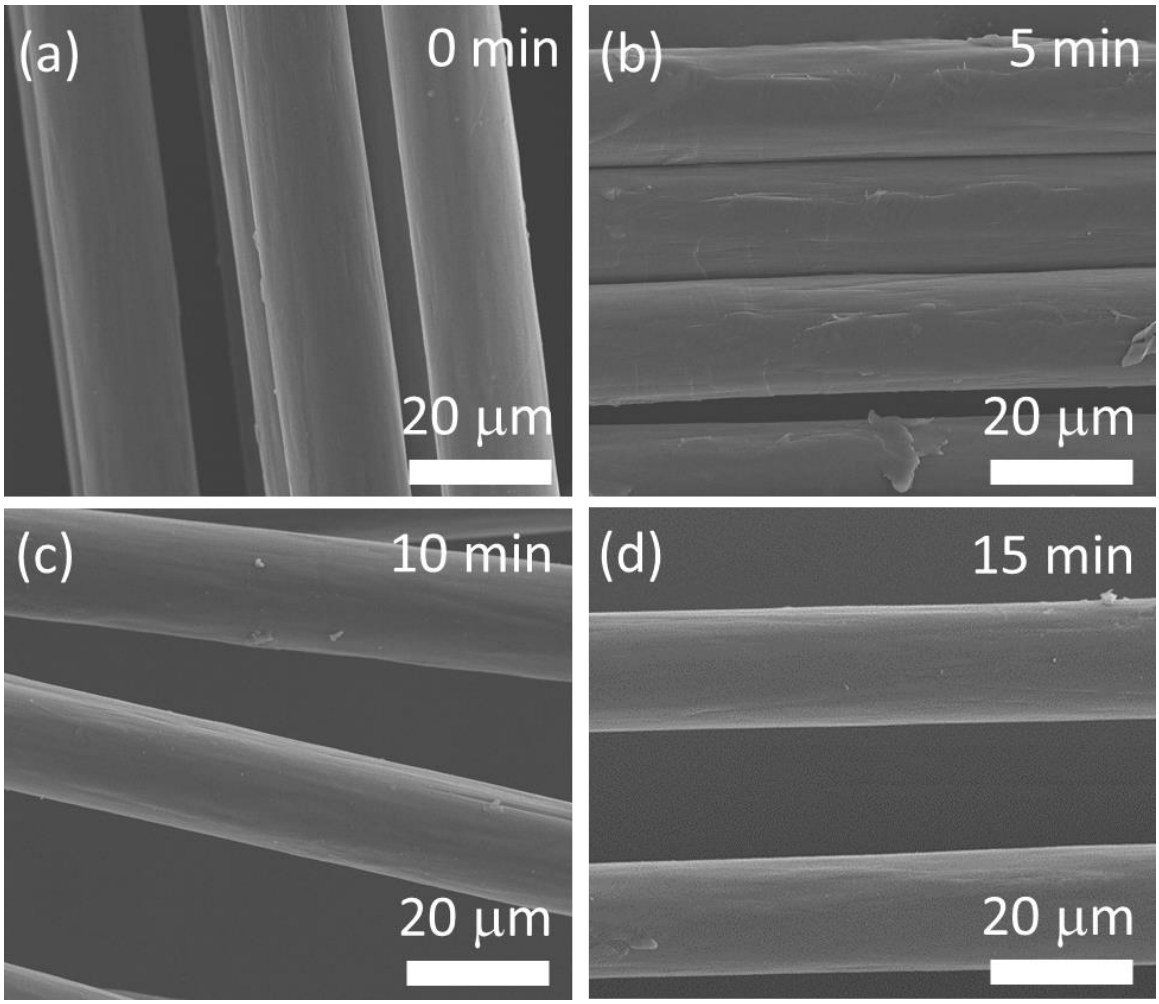

Figure 2.3 SEM images of the aramid fibers' morphologies without and with plasma treatments. Aramid microfibers without plasma treatment (a) and with plasma treatments (b-d): (b) 5 min, (c) 10 min, (d) and 15 min.

As aforementioned, the 5 min plasma treatment creates surface defects which are expected to significantly improve the interaction between the fibers and matrix due to mechanical interlocking.[67686970]

The fibers without surface treatment and with 5 min and 15 min plasma treatments were embedded into the matrix and subsequently pulled out. To prevent the fiber from fracturing rather than pulling out, the embedded length of the aramid fiber in the polymer, *L*, is limited to less than 1.0 mm. The maximum load, *F*, is used to calculate the IFSS with the following equation:

$$\tau = \frac{F}{\pi D L} \qquad \text{Equation 2.1}$$

Where τ is the IFSS and *D* is the diameter of the aramid fibers. Figure 2.3 and Figure 2.4 show the IFSS of the composites and morphology before and after pull-out of the fibers, respectively. The IFSS of the composite reinforced by untreated fibers is 23.46 ± 2.32 MPa (Figure 2.3). This value is slightly higher than 19.2 ± 6.6 MPa, the IFSS between pristine carbon nanotubes (CNTs) and the matrix.[16] It is believed that the surface of CNTs is even more inert, resulting in low possibility of bonding to the matrix while there are several types of functional groups on the aramid fibers, such as -C=O and -C-N- , as demonstrated in X-ray photoelectron spectrum (XPS) in Figure 2.5, which would bridge to the matrix resulting in a stronger interface interaction and higher IFSS. Eight of the untreated individual aramid fibers at the room temperature were embedded in the matrix pulled-out to characteristic their average IFSS as shown in the Table 2.7.

Table 2.7 Interface mechanical properties of aramid microfibers without plasma treatment at room temperature.

Sample	Test #	Fiber Diameter µm	Embedded Length µm	IFSS MPa
Untreated	Test 1	17.24	191.67	22.11
	Test 2	17.91	170.00	23.54
	Test 3	19.60	246.67	25.71
	Test 4	18.59	146.33	20.15
	Test 5	18.59	204.67	20.78
	Test 6	18.25	222.67	23.62
	Test 7	18.93	145.00	26.55
	Test 8	17.57	183.67	25.21
Average± Standard deviation				23.46±2.32

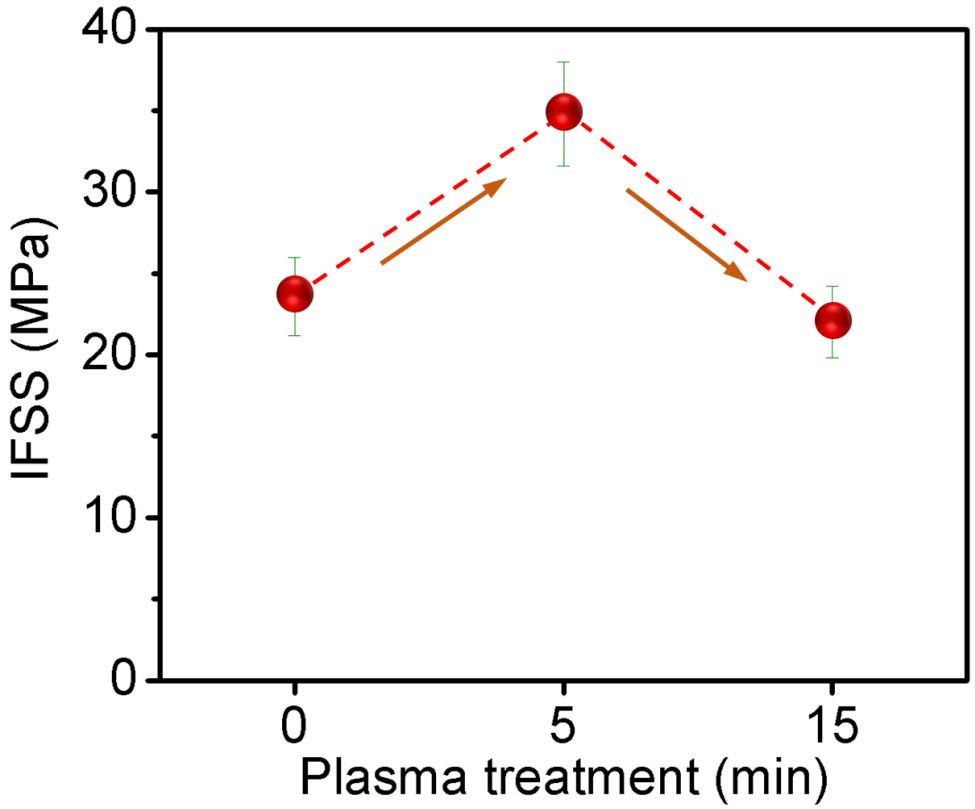

Figure 2.4 Composites reinforced by individual aramid fibers with and without plasma treatment at ambient conditions.

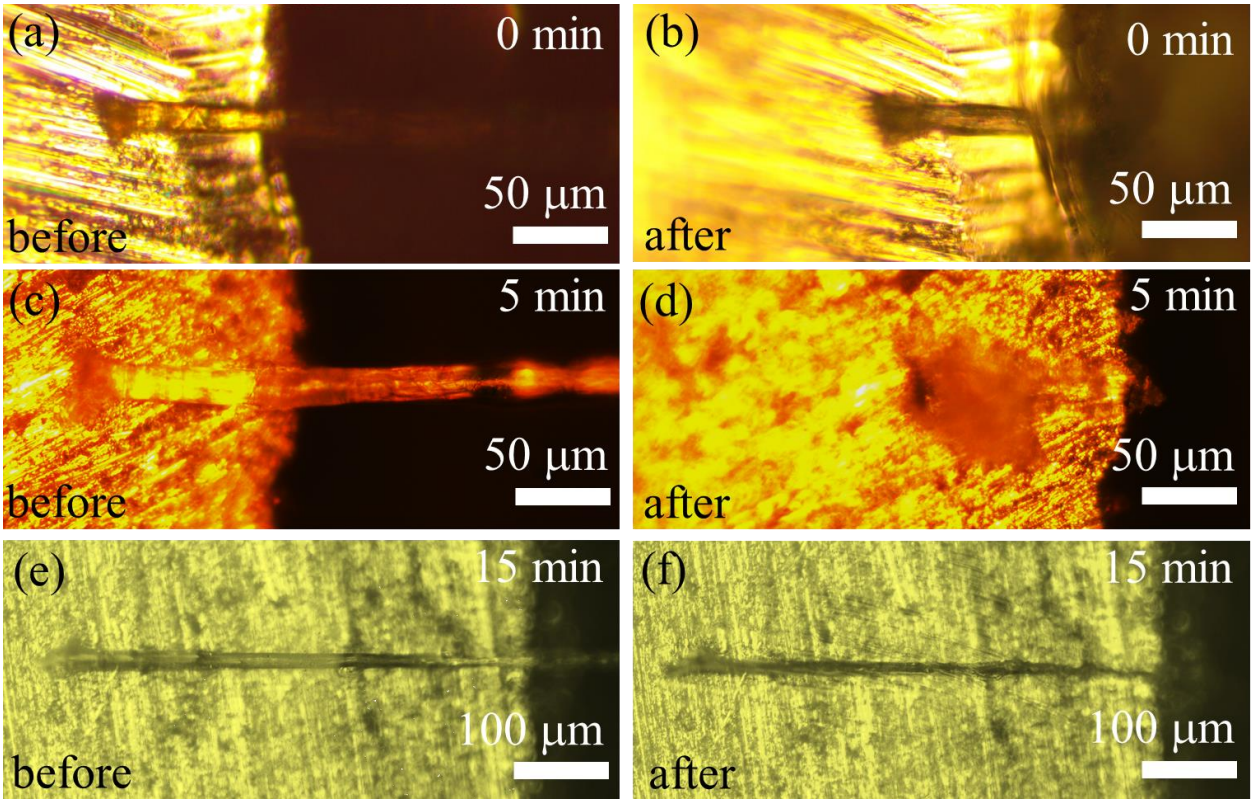

Figure 2.5 Morphology of the composite before and after pull-out of an untreated fiber: (a) and (b); a fiber with 5 min plasma treatment: (c) and (d); a fiber with 15 min plasma treatment: (e) and (f).

Though 5 min plasma treatment evidently "deteriorates" the surface, the pull-out tests show that the IFSS reaches 34.91 ± 3.01 MPa (Table 2.8**)**, demonstrating a 47.5% improvement compared to that of untreated fibers. The high IFSS results from higher surface roughness, shown in Figure 2.2b, newly generated functional groups such as -C-O- and -COO-, demonstrated in Figure 2.5b and Table 2.10, and an increased number of -C=O groups. The surface roughness can result in interface interlocking during mechanical loading and the surface functional groups can enhance the interface interaction. Six of the 5 min treated individual aramid fibers at the room temperature were embedded in the polymers matrix and pulled-out to characteristic their average IFSS as shown in the Table 2.8. To confirm whether surface roughness or surface functional groups dominate the improvement of interface interaction, another

individual aramid fiber with 15 min plasma treatment was first embedded into the matrix, cured, and pulled out using the micro tensile tester. With the same plasma treatment, the category of surface functional groups shown in Figure 2.5b and 2.5c is the same. All those found in the fibers with 5 min treatment can be found in those with 15 min treatment. Therefore, the contribution from the functional groups to IFSS should be similar. However, Figure 2.3 shows that the IFSS of the fibers with 15 min plasma treatment drops down to 22.00 ± 2.22 MPa. Six of the 15 min treated individual aramid fibers at the room temperature were embedded in the polymers matrix and pulled-out to characteristic their average IFSS as shown in the Table 2.9.

Table 2.8 Interface mechanical properties of aramid microfibers with 5 min plasma treatment.

Sample	Test #	Fiber Diameter µm	Embedded Length µm	IFSS MPa
5 min treated	Test 1	16.67	261.00	36.62
	Test 2	17.00	161.00	37.26
	Test 3	17.00	219.33	37.78
	Test 4	17.33	358.67	35.16
	Test 5	17.33	200.00	30.15
	Test 6	17.00	69.67	32.47
Average± Standard deviation				34.91±3.01

Table 2.9 Interface mechanical properties of aramid microfibers with 15 plasma treatment at the room temperature.

Sample	Test #	Fiber Diameter µm	Embedded Length µm	IFSS MPa
15 min treated	Test 1	16.90	193.67	22.14
	Test 2	17.91	132.67	22.81
	Test 3	17.57	368.00	20.82
	Test 4	17.57	282.00	19.16
	Test 5	17.91	100.26	25.087
Average± Standard deviation				22.00±2.22

As Figure 2.2 demonstrates, the surface roughness significantly increases after 5 min treatment and then decreases with increased plasma treatment period. The original surface defects are even etched away after extended plasma treatment, offering a smooth surface. Therefore, the IFSS of the fibers with 15 min treatment is similar to that of untreated fibers. The morphologies of the fibers with and without plasma treatment before and after pull-out tests are shown in Figure 2.4 a-f. Due to the strong interface interaction between the fiber with 5 min plasma treatment and the matrix, the embedded length must be limited to less than 200 µm, otherwise, the fiber will fracture during the pull-out test. The fiber in Figure 2.4 c and Figure 2.4 d has an embedded length of 111.1 µm. In Figure 2.4 d, the dark area results from severe damage to the matrix, suggesting that there is a strong fiber-matrix interaction during mechanical failure. Such observation confirms high IFSS in the composite reinforced by the fiber with 5 min plasma treatment. In contrast, the morphologies of the composites reinforced with untreated fibers and the fibers with 15 min plasma treatment are similar. No severe damage is found along the inner surface of the groove in the matrix.

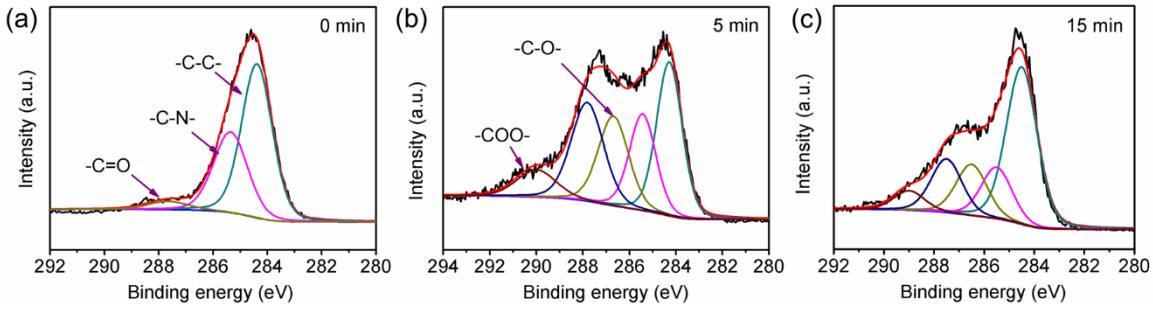

Figure 2.6 XPS analysis of pristine and plasma treated aramid fibers. (a) Untreated fibers. (b) 5 min treatment. (c) 15 min treatment.

Table 2.10 Bonds and their percentages in the fibers without and with plasma treatments.

Bond	-C-C-	-C-N-	-C-O-	-C=O	-COO-
Peak location (eV)	284.4	285.4	286.7	287.6	290.0
Untreated fibers	60.4 %	35.1 %	-	4.5 %	-
5 min treated fibers	29.0 %	18.9 %	20.1 %	23.9 %	8.1 %
15 min treated fibers	47.3 %	15.5 %	15.3 %	16.1 %	5.8 %

Once aramid fiber-reinforced composites are used in a harsh environment, their mechanical stability will be critical. Here, the interface bonding between the aramid fiber and the polymer at elevated temperatures is evaluated. Considering that the polymer used has a glass transition temperature of 175 °C, the debonding tests were carried out at 50 °C and 100 °C in this study. Figure 2.6 show the IFSS of the composites at elevated temperatures. As the temperature increases to 50 °C, the IFSS of the composite decreases to 19.29 ± 1.80 MPa, which is lower than 23.46 ± 2.32 MPa, the IFSS between the untreated fibers and the matrix at 25 °C. With temperature increasing to 100 °C, the IFSS dramatically drops down to 12.4 ± 5.4 MPa, demonstrating a 47.5% decrease compared to that obtained at 25 °C. Apparently, the IFSS is heavily affected at higher temperature.[7172] Five samples of each of the untreated individual aramid fibers at the 50 °C and 100 °C that were embedded in the polymers matrix and pulled-out to characteristic their average IFSS as shown in the Table 2.11 and Table 2.12, respectively.

Table 2.11 Interface mechanical properties of aramid microfibers without plasma treatment at temperature 50 °C.

Sample	Test #	Fiber Diameter µm	Embedded Length µm	IFSS MPa
Untreated	Test 1	17.00	251.33	21.43
	Test 2	17.00	241.67	18.83
	Test 3	17.00	177.00	17.81
	Test 4	17.00	320.33	20.90
	Test 5	17.67	219.33	17.46
Average± Standard deviation				19.29±1.80

Table 2. 12 Interface mechanical properties of aramid microfibers without plasma treatment at temperature 100 °C.

Sample	Test #	Fiber Diameter µm	Embedded Length µm	IFSS MPa
Untreated	Test 1	17.33	225.00	12.85
	Test 2	17.00	152.33	19.11
	Test 3	17.33	189.00	10.26
	Test 4	16.67	134.33	15.11
	Test 5	16.67	380.00	4.69
Average± Standard deviation				12.40±5.40

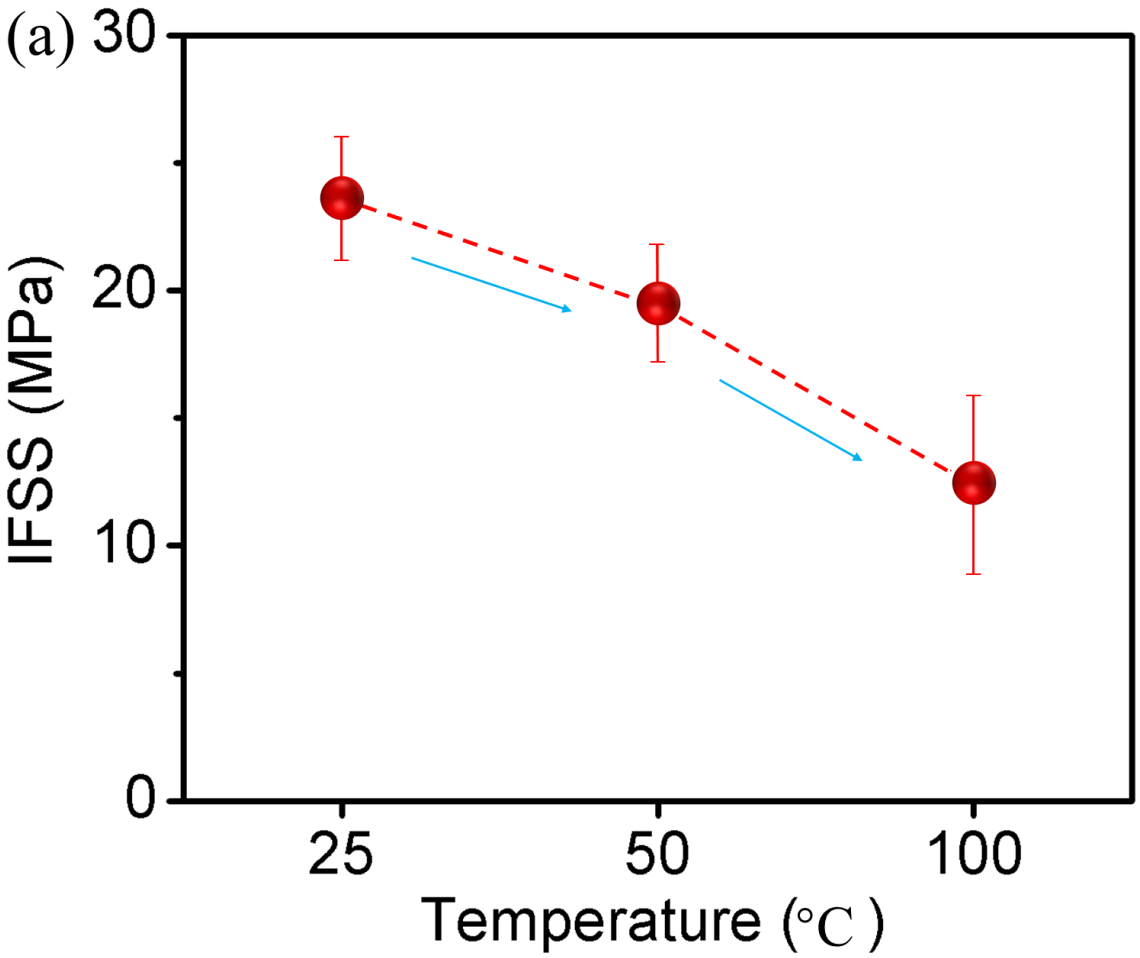

Figure 2.7 Measurement of IFSS for the composites reinforced by individual untreated aramid fibers at elevated temperatures.

At 25 °C, the affected zone after pull-out is just around the embedded area of the fiber, indicated by the residual small and smooth groove in the matrix (Figure 2.7b). As the temperature increases to 100 °C, a piece of the matrix is missing, suggesting that mechanical performance of the matrix deteriorates at high temperatures and the interaction between the fiber and the matrix is not enough to keep the composite in a high performance (Figure 2.7d).

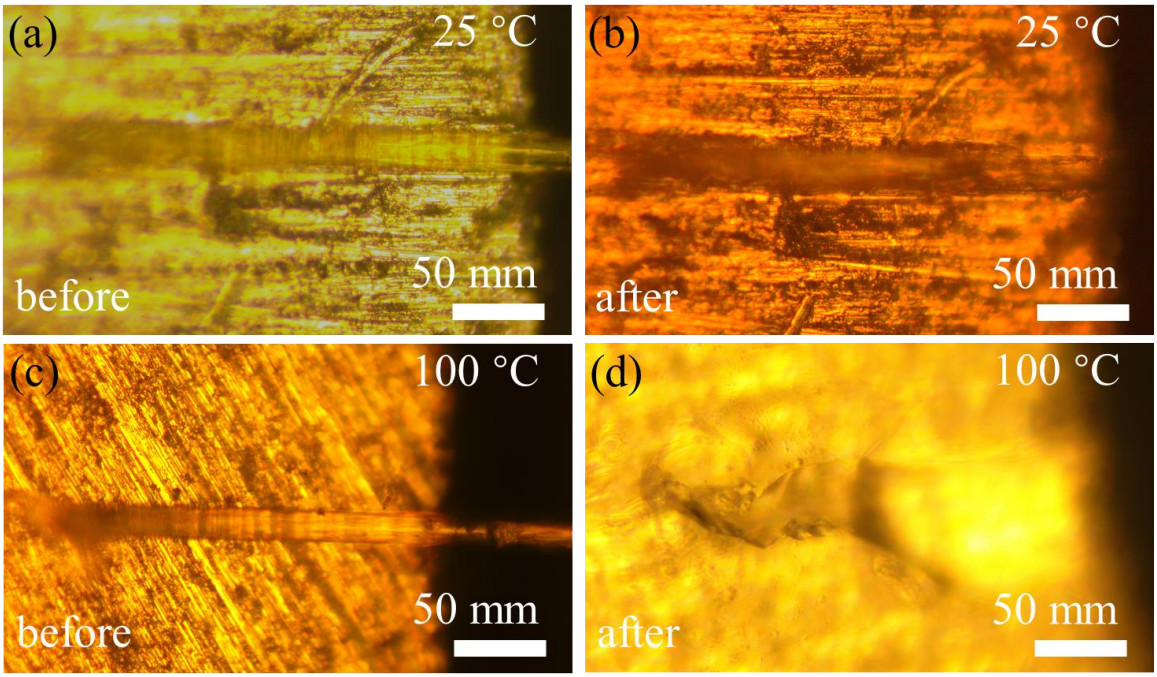

Figure 2.8 Morphology of the composites reinforced by individual aramid fibers at elevated temperatures before and after pull-out at 25 °C: (a) and (b); at 100 °C: (c) and (d).

To improve mechanical stability of the interface between the fiber and the matrix, a polymer-derived ceramic (PDC) precursor is used. The PDC is based on silicon alkoxide chemistry ($Si(OH)_4$) with some OR sites substituted by hydride and vinyl groups. Generally, the PDC precursor crosslinks at 100 °C, and can be converted into ceramics at 1,000 °C. As stated in the experimental section, 5.0 wt.% PDC was mixed with the polymer. Figure 2.8 shows the IFSS of the composite stabilized with 5% PDC at elevated temperatures. With PDC stabilization, the IFSS reaches 30.87 ± 2.92 MPa, demonstrating a 30.5% increase compared to that of pristine fibers pulled out from the polymer. Unlike other fibers which have poor interface interaction with the matrix upon heating, the added PDC significantly stabilizes the interface. Eight individual untreated aramid fibers at the room temperature were embedded in polymer matrix after adding 5% percent of PDC and then pulled-out to characteristic their average IFSS as shown in the Table

2.13. The IFSS of the composites reinforced by aramid fibers surprisingly remains at 29.32 ± 1.0 MPa and 26.10± 5.23 MPa at 50 °C and 100 °C, respectively. Table 2.14 and Table 2.15 show all data including the IFSS, diameter, and embedded length individual untreated aramid fibers at the 50 °C and 100 °C, respectively, after adding 5% percent of PDC and then pulled-out to characteristic their average.

Table 2.13 Interface mechanical properties of aramid microfibers without plasma treatment at 25 °C with PDC.

Sample	Test #	Fiber Diameter µm	Embedded Length µm	IFSS MPa
Untreated	Test 1	17.67	61.00	30.60
	Test 2	17.00	581.33	30.84
	Test 3	17.00	801.32	26.27
	Test 4	17.00	187.00	28.94
	Test 5	17.00	604.67	29.45
	Test 6	18.33	342.67	33.68
	Test 7	17.00	574.67	31.33
	Test 8	18.33	174.00	35.81
Average± Standard deviation				30.87±2.92

Table 2.14 Interface mechanical properties of aramid microfibers without plasma treatment at 50 °C with pdc.

Sample	Test #	Fiber Diameter µm	Embedded Length µm	IFSS MPa
Untreated	Test 1	17.00	207.33	29.08
	Test 2	17.00	295.33	28.13
	Test 3	17.67	207.33	30.52
	Test 4	17.67	100.33	29.56
Average± Standard deviation				29.32±1.00

Table 2.15 Interface mechanical properties of aramid microfibers without plasma treatment at 100 °C with pdc.

Sample	Test #	Fiber Diameter μm	Embedded Length μm	IFSS MPa
	Test 1	17.00	156.00	25.66
	Test 2	17.33	183.67	30.07
	Test 3	17.33	113.67	20.21
	Test 4	17.00	120.00	21.99
	Test 5	17.00	78.33	32.58
Average± Standard deviation				26.10±5.23

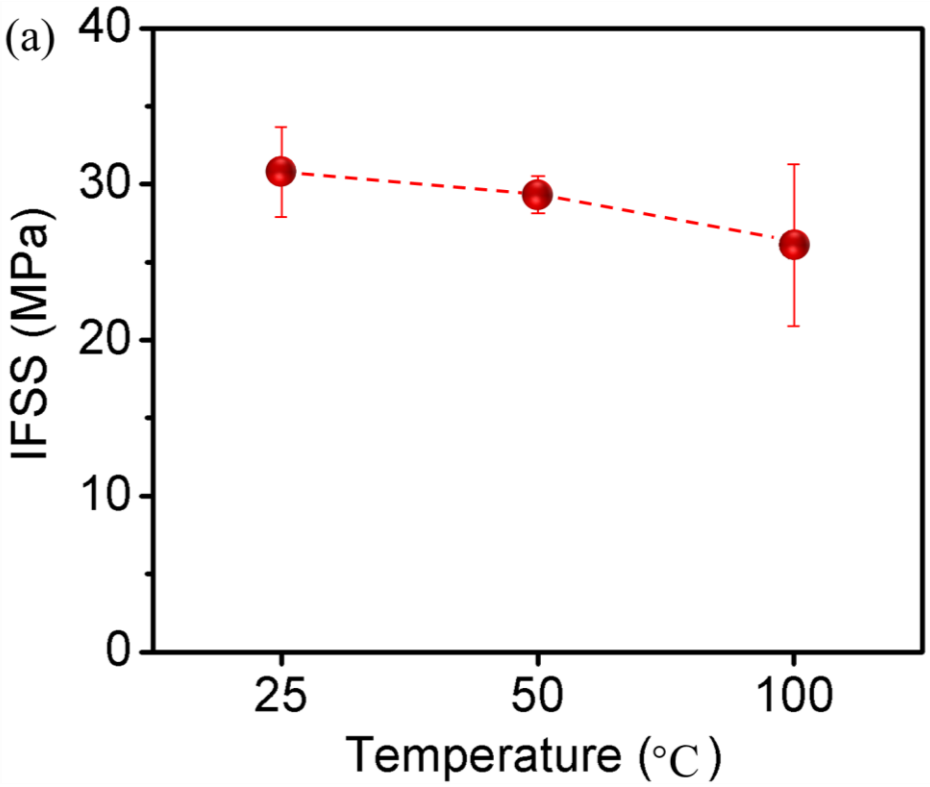

Figure 2.9 Measurement of IFSS for composites reinforced by individual aramid fibers stabilized with 5% PDC at elevated temperatures.

Figure 2.9 shows the morphology after adding with 5% PDC to the composites reinforced by individual aramid fibers before and after pull-out at the room and the elevated temperature. The Figure

2.9b and 2.9d demonstrate morphologies of the embedded areas after fiber pullout at 50 °C and 100 °C, respectively. These embedded areas are not deteriorated like those in Figure 2.7d. As the temperature increases to 100 °C, a saw-tooth fracture surface is observed and included in Figure 2.9d, where there are no missing pieces in the matrix. The rough surface shows the strong interface interaction during mechanical loading as well as indicates that both interface and matrix have been strengthened by the added PDC.

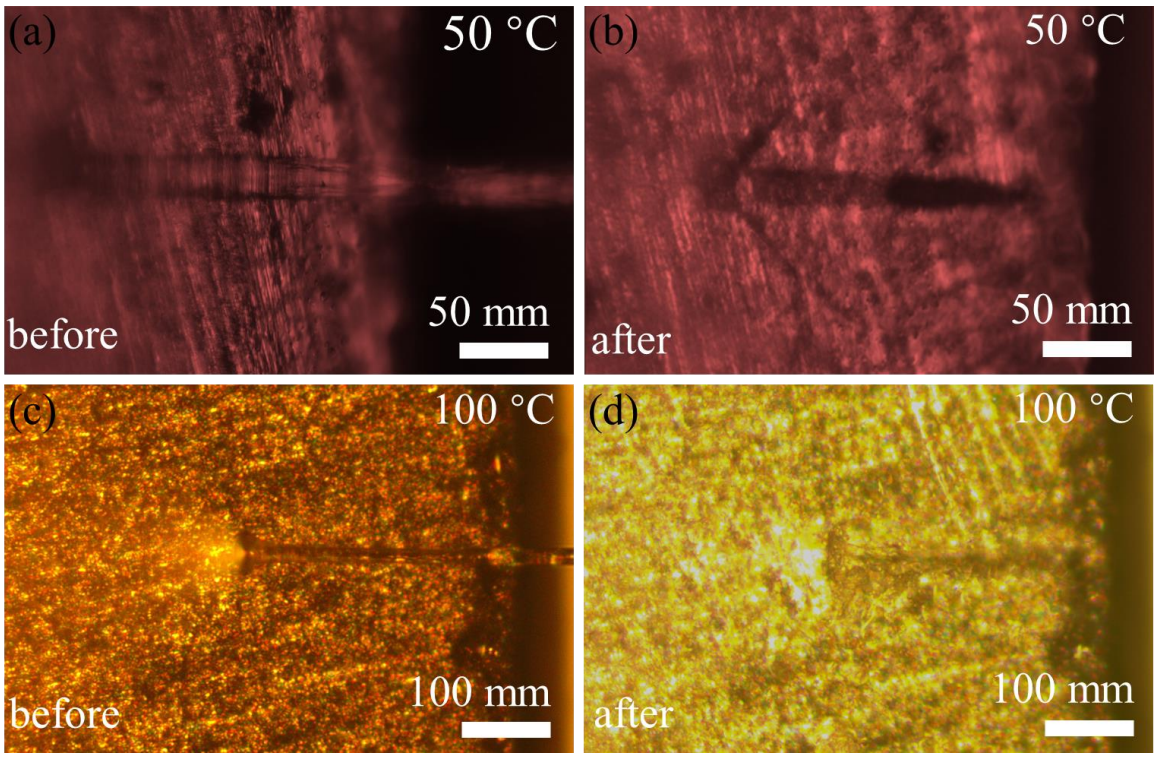

Figure 2.10 Morphology after adding with 5% PDC to the composites reinforced by individual aramid fibers before and after pull-out at 50 °C: (a) and (b); at 100 °C: (c) and (d).

To understand the role of PDC in enhancing the interface interaction between individual fibers and the matrix, FTIR was used to investigate whether there was a reaction between the PDC and the epoxy. Figure 2.10 shows FTIR spectra of PDC only, epoxy only, and a mixture of PDC and epoxy after cure

at 100 °C. The bond of C-H can be found in both PDC and epoxy. Si-H, Si-O-Si, and Si-O-H are characteristic bonds of PDC only, which are not shown in the epoxy spectrum as expected. Importantly, these bonds do not disappear in the mixture of PDC and epoxy, suggesting that there is no reaction between the two components.

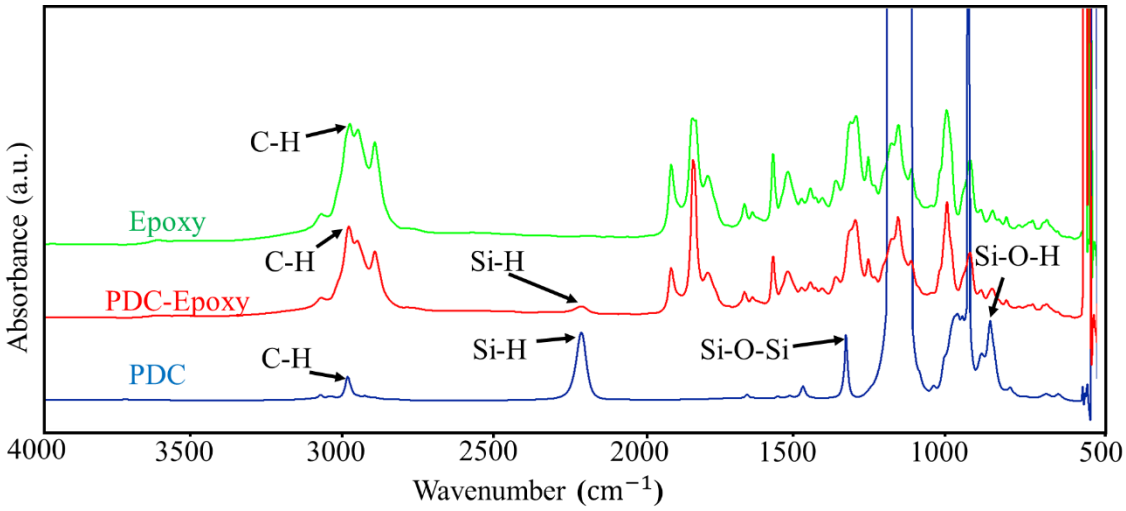

Figure 2.11 FTIR spectra of PDC only, epoxy only, and mixture of PDC and epoxy at 100 °C.

During polymer-ceramic conversion in PDC, generally, there is a large volume shrinkage. In fact, a visible volume shrinkage was also observed in the PDC after crosslinking at 100 °C (Figure 2.11a). There is no doubt that the volume shrinkage would introduce internal stress to the matrix. Figure 2.11b-2.11d schematically demonstrate the molecular status of pure epoxy and the mixture of epoxy and PDC after cure at 100 °C. If there is no PDC, the cured epoxy will be in a "loose" form (**Figure2.11**b) and the required load to pull out the fiber will be low. Considering that there is no reaction between the PDC and the epoxy, the mixed PDC will form a network throughout the epoxy and divide it into many regions. In an individual region (Figure 2.11d), the crosslinked PDC will squeeze the epoxy molecules together, leading to the increase of internal stress and the high interface interaction between the fiber and the matrix. Therefore, the IFSS can be improved at both room and elevated temperatures with the presence of PDC.

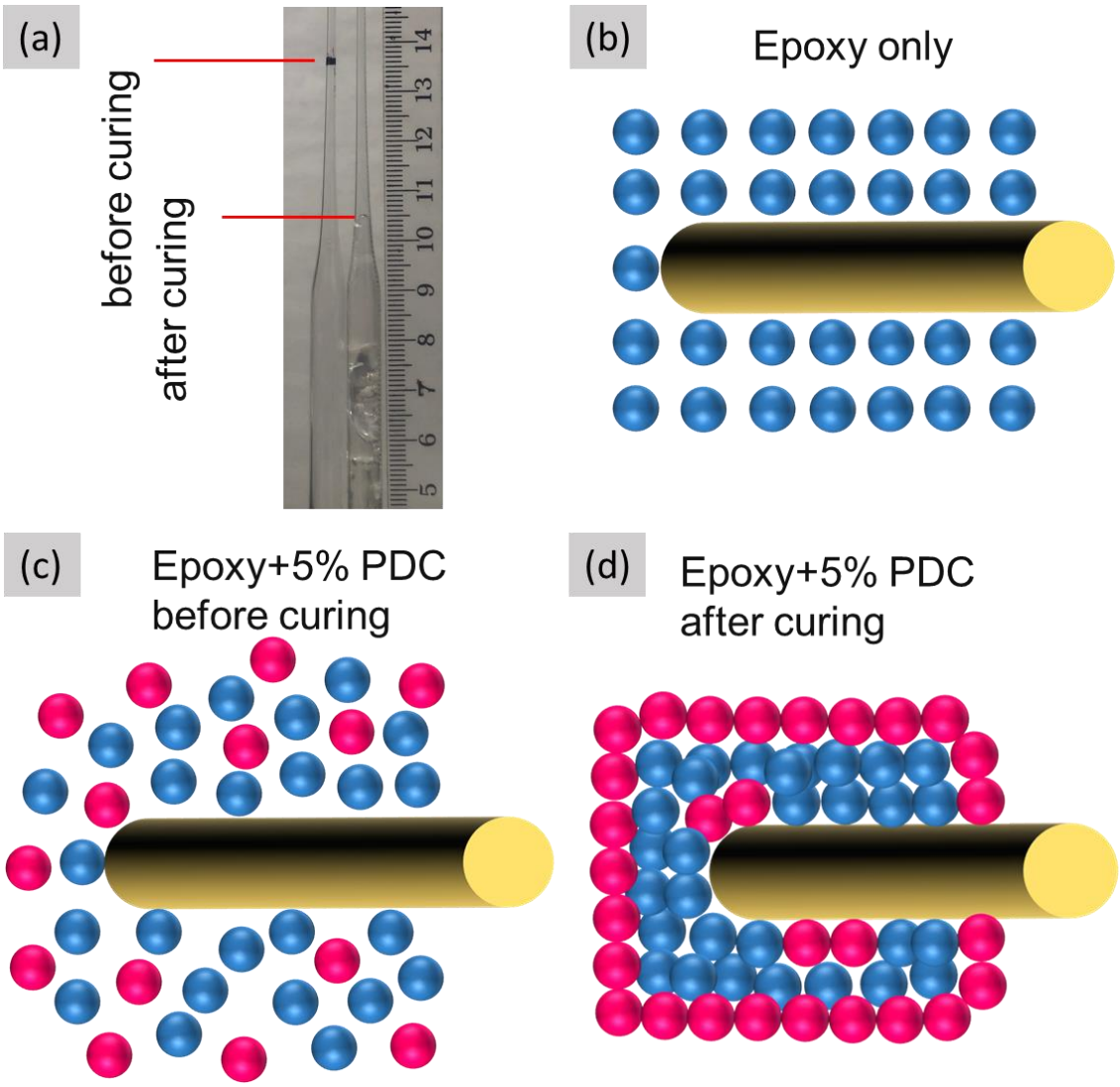

Figure 2.12 Internal stress induced interface strengthening. (a) Volume shrinkage of PDC before and after cure at 100 °C. (b)-(d) Schematic demonstration of internal stress induced by PDC crosslinking.

CHAPTER 3

3 REACTIVATION OF AGED ARAMID FIBERS FOR STRONG INTERFACIAL INTERACTION WITH POLYMER MATRIX

3.1 Introduction

Aramid fibers have dense hydrogen bonding and high crystallinity, which account for their outstanding fracture toughness, high tensile strength, and remarkable thermal and chemical stability.[345673] Among these characteristics, the specific tensile strength of aramid fibers (tensile strength: ~3 GPa; density: ~1.47 g/cm^3) is over 20 times higher than that of 1045 steel (tensile strength: 570~700 MPa; density: ~8.03 g/cm^3).[7475] Benefiting from their exceptional mechanical properties, aramid fibers have been regarded as one of the ideal candidates to reinforce composites. In the fiber reinforced composites, the load is expected to be effectively transferred from a matrix to the fibers in order to inherit their outstanding mechanical performance.[21]The high crystallinity of aramid fibers, reflected as their physically smooth and chemically inert surface, leads to poor interfacial bonding to matrix.[141529] To address this issue, increasing surface roughness and generating functional groups on aramid fibers have typically been adopted to improve the interfacial load transfer in the composites. A rough surface would enable interface interlocking during mechanical loading and the functional groups on aramid fibers would form covalent bonding to matrix. Among all surface treatments, plasma treatment can yield a rough surface and various functional groups depending on the power of plasma, distance between fibers and the plasma gun surface, as well as the period of plasma treatment, and gas being used. [192059] The generated functional groups, such as hydroxyl, amino, and carboxylic acid, greatly enhance the wettability and allow to covalently bond to matrix.[33]

A troublesome phenomenon of the plasma-treated aramid fibers is surface aging: loss of the hydrophilic characteristics after a period of time.[34] Aging can result from a combination of unsaturated

and high-energy functional groups with polar molecules in the air, reorientation of the functional groups toward the fiber to minimize surface energy, or diffusion of polar chemical groups into the fiber.[16] Recently, some research efforts have been devoted to understand aging behavior of physically or chemically treated polymer.[353637] Contact angle measurement has been widely adopted to visualize the degree of hydrophilic or hydrophobic polymers over a period of storage time. For example, Zemljic L, *et al.* demonstrated low-pressure oxygen plasma treatment on cellulosic fabrics. The water contact angle decreased from ~66° to ~15° and no aging was found in the fabrics placed in the air up to 4 days.[49] Similarly, Takke V, *et al.* carried out air plasma treatment under atmospheric pressure on polyethylene terephthalate fabric. The wettability of the fabric was remarkedly improved. Interestingly, the water contact angle over 30 days had little change when the fabric was absent from light.[50] Samantha K, *et al.* performed plasma treatments on nylon fabric with gases including oxygen, argon, air, and helium and had the same conclusion that the surface of polymer would be more hydrophilic after plasma treatment. The plasma-treated surface remained active even after 25 days.[51] In addition to contact angle measurement, Yu Y, *et al.*[35] performed mechanical tests to quantify the IFSS for understanding the aging in aramid fibers. As the fibers were placed in the air for one month, only 30% of the improved IFSS remained. Therefore, the active period of the plasma-treated surface remains a question as to whether it is a few days or weeks.

How fast the aging of aramid fibers occurs is critical to achieving high mechanical performance in the fabricated composites. Compared to freshly functionalized aramid fibers, the aged fibers have poor interfacial bonding to matrix, which leads to inferior mechanical performance of the composites. Therefore, the aging in aramid fibers after plasma treatment should be carefully evaluated. From the point of practical application, if aging has already occurred, how to reactivate the aged surface simply and quickly without further damage to the fibers is worth more research effort. In this study, aramid fibers were treated by oxygen plasma to generate active functional groups. Interfacial shearing testing was carried out to understand the impact of aging on the IFSS. The finding indicates that polar water molecules

dominate passivation of the active surface and then weaken the interfacial load transfer. As water molecules are removed at 100 °C for a few hours, the IFSS can be restored to ~30 MPa, which is similar to that obtained by deboning freshly plasma-treated fibers out of the polymer.

3.2 Experimental Section

3.2.1 Plasma treatment for aramid fibers

Aramid fibers (DAF III, polyheteroarylene-co-p-phenyleneterephthalamide) were purchased from Bluestar Chengrand Chemical Co. Ltd. The diameter of the fibers used is ~17 μm. The pristine fibers were cleaned with ethanol and dried at 100 °C for 3 hours before being embedded into epoxy. A radiofrequency (RF) reactor was used to activate oxygen into plasma to functionalize the fibers. The distance between the plasma gun and the fibers was 35 mm. The treatment periods included 0 minutes, 30 sec, 1 minute, 5 minutes, and 10 minutes.

3.2.2 Matrix preparation

The epoxy consists of four parts which are 44.7 % Embed 812, 35.8 % Dodecenylsuccinic anhydride (DDSA), 17.9 % N-Methylaniline (NMA), and 1.6 % 2,4,6-Tris (dimethylaminomethyl) phenol (DMP-30). All parts were purchased from the Electron Microscopy Sciences, Hatfield, PA. The EMbed 812, DDSA, and NMA were stirred together for 10 - 15 min. Subsequently, the DMP-30 was added to the mixture and stirred for another 10 - 15 min, which was followed by ultrasonic degas.

3.2.3 Preparation for debonding tests

An aluminum plate with a dimension of 10 mm x 10 mm x 2 mm (length x width x height) was used as a substrate to hold the epoxy. The substrate was carefully polished to have sharp and smooth edges. A small droplet of the prepared epoxy was loaded at the edge of the substrate. Facilitated by a

microscope (AmScope ME600TZ), an aramid fiber, either pristine or plasma treated, was loaded into the epoxy embedded to a length of less than 1 mm. The aramid fiber together with the aluminum plate was then placed into a drying oven to cure at 60 °C for 24 h.

3.2.4 Debonding tests

For conduction the pull-out tests, A Deben Micro Tensile Tester (Gatan Inc.) was used. The tester was installed with a 200 N load cell with a force resolution of 0.001 N. The loading speed was maintained to be 0.5 mm/min.

3.2.5 Other characterizations

The aramid fibers with and without plasma treatment, along with the pulled-out fibers were analyzed by an optical microscope, scanning electron microscope (SEM, Zeiss NVision 40), energy dispersive spectrum (EDS), and Fourier transform infrared spectroscopy (FTIR).

3.3 Results and Discussion

To study aging and reactivation of aramid fibers, large surface roughness averaged from peaks and valleys of the fiber surface should be avoided. If this is the case, the interfacial load transfer will be dominated by the interface interlocking rather than functional groups. An optimal period of plasma treatment should initially be identified to ensure that the surface of fibers is not heavily damaged. Here, four periods of plasma treatment were selected, including 30 sec, 1 min, 5 min, and 10 min. All other factors were kept the same, including distance between plasma gun surface and aramid fibers, oxygen flow rate, power of plasma, etc. The pristine fiber was used as a benchmark to compare whether there was any severe damage to the fibers. Figure 3.1a-f show SEM images of the fibers with and without plasma treatment. The untreated fibers and those having 0.5min sec have a very smooth surface as shown in the Figure. 3.1a, 3.1b and the high magnification of the Figure 3.1c that represent the 0.5 min treatments. In

contrast, the fibers with 1 min, 5 min and 10 min plasma treatment experience severe surface damage as shown in Figure 3.1d-f respectively, which is not good for differentiating the aging resulting from passivation of functional groups.

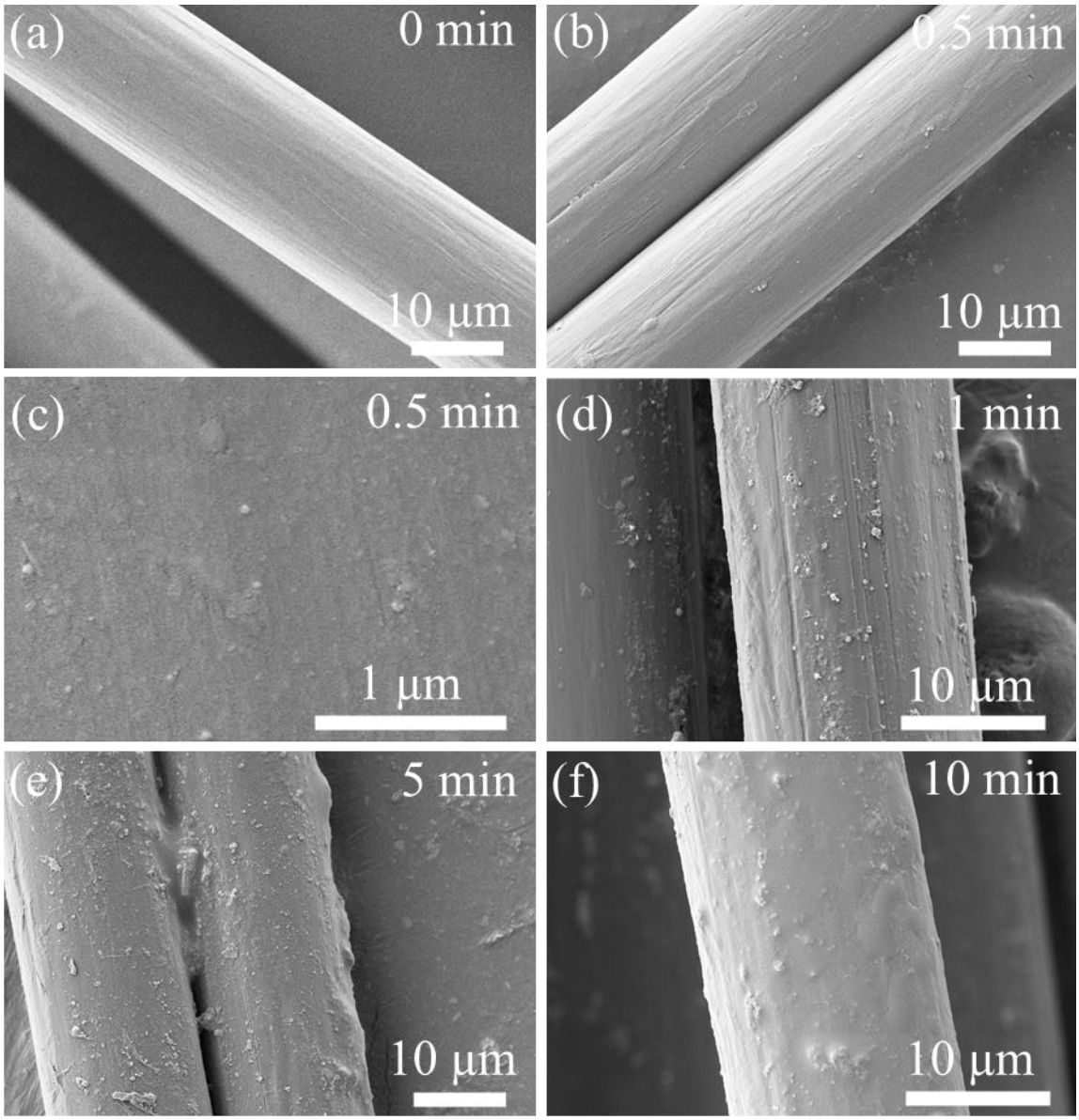

Figure 3.1 Morphology aramid fibers with and without plasma treatment. SEM images of aramid fibers without plasma treatment (a) and with plasma treatment (b-e): (b) low magnification 0.5 min second, (c) high magnification 0.5 min second, (d) 1 min, (e) 5 min, (f) 10 min.

To understand the impact of plasma treatment on mechanical property of aramid fibers, Figure 3.2 presents the representative stress-strain curves of untreated and plasma-treated aramid fibers. The untreated fibers have a tensile strength of 2.87 ± 0.23 GPa as show in the Table 3.1, where five individual aramid fibers were fractured at constant assumed diameter. With a 30 sec plasma treatment, the tensile strength of the aramid fibers slightly decreased to 2.58 ± 0.53 GPa Plasma treatments of 5 min and 10 min results in the tensile strength quickly drops to 1.55 ± 0.99 GPa and 1.68 ± 0.85 GPa, having 45.99 % and 41.46 % decreases, respectively. Table 3.2 summarizes the average of tensile strengths and elastic modulus of the fibers with and without plasma treatment. Individual tests for all fibers with plasma treatment including 0.5 min,1 min, 5 min, and 10 min are presented in the Table 3.3. Table 3.6, where the date of the fracture strength and the elastic modulus with their average and standard deviation are presented. The fibers with 30 sec plasma treatment, which largely preserve their intrinsic mechanical performance and have functional groups on the surface, would be ideal to study aging and reactivation.

Table 3.1 Mechanical properties of aramid microfibers without plasma treatment

Sample	Test #	Tensile Strength GPa	Elastic Modulus of GPa
Untreated	Test 1	3.07	76.83
	Test 2	2.73	76.92
	Test 3	2.61	76.60
	Test 4	3.15	66.43
	Test 5	2.79	67.25
Average± Standard deviation		2.87±0.23	72.81±5.46

Table 3.2 Mechanical properties of aramid fibers with and without plasma treatment.

Sample	**Tensile Strength GPa**	**Elastic Modulus GPa**
Untreated	2.87±0.23	72.81±5.46
30 sec treatment	2.58±0.53	75.33±4.53
1 min treatment	2.37±1.20	74.95±19.87
5 min treatment	1.55±0.99	73.40±10.47
10 min treatment	1.68±0.85	75.07±19.26

Table 3.3 Mechanical properties of aramid microfibers with 30 sec plasma treatment.

Sample	Test #	Tensile Strength GPa	Elastic Modulus of GPa
30 sec treated	Test 1	2.80	71.88
	Test 2	2.17	81.62
	Test 3	3.08	78.63
	Test 4	2.52	72.74
	Test 5	1.78	71.75
Average± Standard deviation		2.47±0.51	75.32±4.53

Table 3.4 Mechanical properties of aramid microfibers with 1 min plasma treatment.

Sample	Test #	Tensile Strength GPa	Elastic Modulus of GPa
1 min treated	Test 1	2.83	81.63
	Test 2	0.86	46.43
	Test 3	2.31	66.67
	Test 4	1.77	80.00
	Test 5	4.08	100.00
Average± Standard deviation		2.37±1.20	74.95±19.87

Table 3.5 Mechanical properties of aramid microfibers with 5 min plasma treatment.

Sample	Test #	Tensile Strength GPa	Elastic Modulus of GPa
5 min treated	Test 1	1.30	81.41
	Test 2	1.30	60.57
	Test 3	1.80	64.52
	Test 4	0.32	84.53
	Test 5	3.05	75.99
Average± Standard deviation		1.55±0.99	73.40±10.47

Table 3.6 Mechanical properties of aramid microfibers with 10 min plasma treatment.

Sample	Test #	Tensile Strength GPa	Elastic Modulus of GPa
10 min treated	Test 1	1.46	81.30
	Test 2	1.44	57.87
	Test 3	1.46	81.99
	Test 4	0.91	53.70
	Test 5	3.14	100.46
Average± Standard deviation		1.68±0.85	19.26±75.06

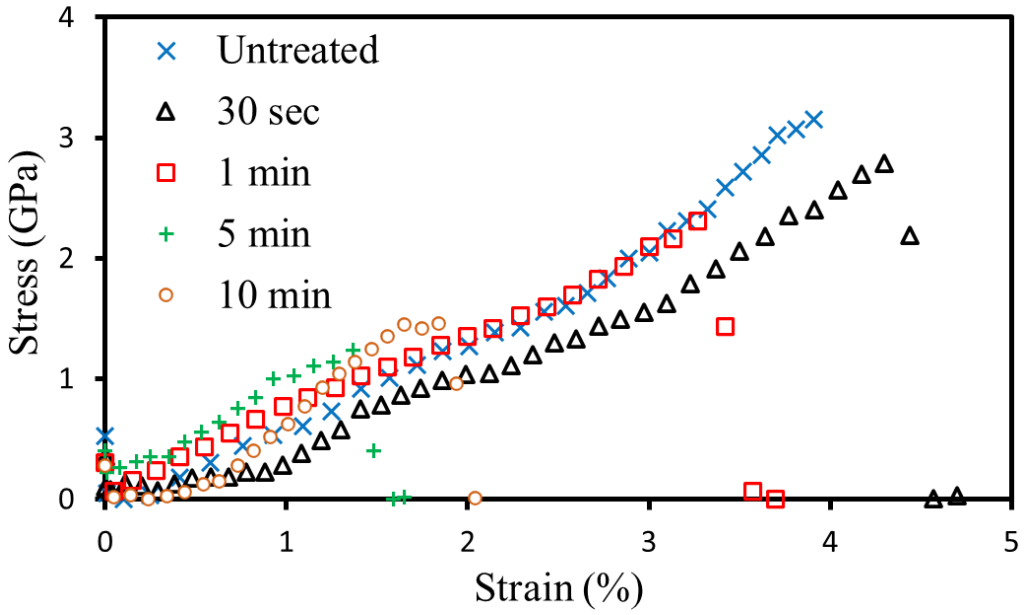

Figure 3.2 Stress versus strain curves of individual aramid fibers with different periods of plasma treatment.

Several testing methods have been used to measure the IFSS, including the micro-indentation test [63], the push-out test[38], the fragmentation test[1265], the pull-out test[394766], and the microbond test[43]. Among them, the pull-out test is simpler than other testing methods and has no limitation in sample size. Both microscale and nanoscale wires/rods can be pulled out from the matrix with the pull-out method. [61757677] To quantify IFSS, the pull-out testing was carried out to debond untreated, plasma treated, aged, and reactivated aramid fibers from matrix. Figure 3.3 shows the IFSS of all tested aramid fibers placed in the air for 0, 1, 3, 7, 14, and 28 days after plasma treatment. The untreated aramid fibers were first pulled out from matrix as a reference. The calculated IFSS was 22.93 ± 1.47 MPa. Five samples of the untreated individual aramid fibers were embedded in the polymers matrix and pulled-out to characteristic their average IFSS as shown in the Table 3.7.

Table 3.7 Interface mechanical properties of aramid microfibers without oxygen plasma treatment.

Sample	Test #	Embedded Length μm	IFSS MPa
Untreated	Test 1	191.67	21.90
	Test 2	170.00	24.23
	Test 3	146.33	21.53
	Test 4	204.67	22.20
	Test 5	222.67	24.77
Average± Standard deviation		187.07±29.79	22.93±1.47

The aramid fibers with 30 sec plasma treatment significantly promote the IFSS to 29.26 ± 1.32 MPa. After one day placement in the air, the plasma-treated aramid fibers well maintained their functional groups, which is evident from the measured IFSS of 30.13 ± 2.66 MPa. However, the IFSS quickly decreased to 24.98 ± 0.86 MPa after the plasma-treated aramid fiber was placed in the air for three days, suggesting that functional groups on the aramid fiber started to be passivated and the fibers were unable to bond to the matrix as tightly as the preceding trials.[34353637] The aramid fibers placed in the air for 7, 14, and 28 days

were embedded into the matrix and pulled out to study when the functional group would be fully passivated. The measured IFSS dropped down to 21.75 ± 1.53 for the fibers placed in the air for 7 days. There was no change in the IFSS for those fibers placed in the air longer. Therefore, the functional groups on the aramid fibers can be well preserved within a few days and survive in one week but are fully passivated after one week of placement in the air. Five test results of the IFSS and the embedded length for each of the 0, 1, 3, 7, 14, and 28 aging days after treating the individual aramid fibers by the oxygen plasma treatment are shown in the Table 3.8 - Table 3.13.

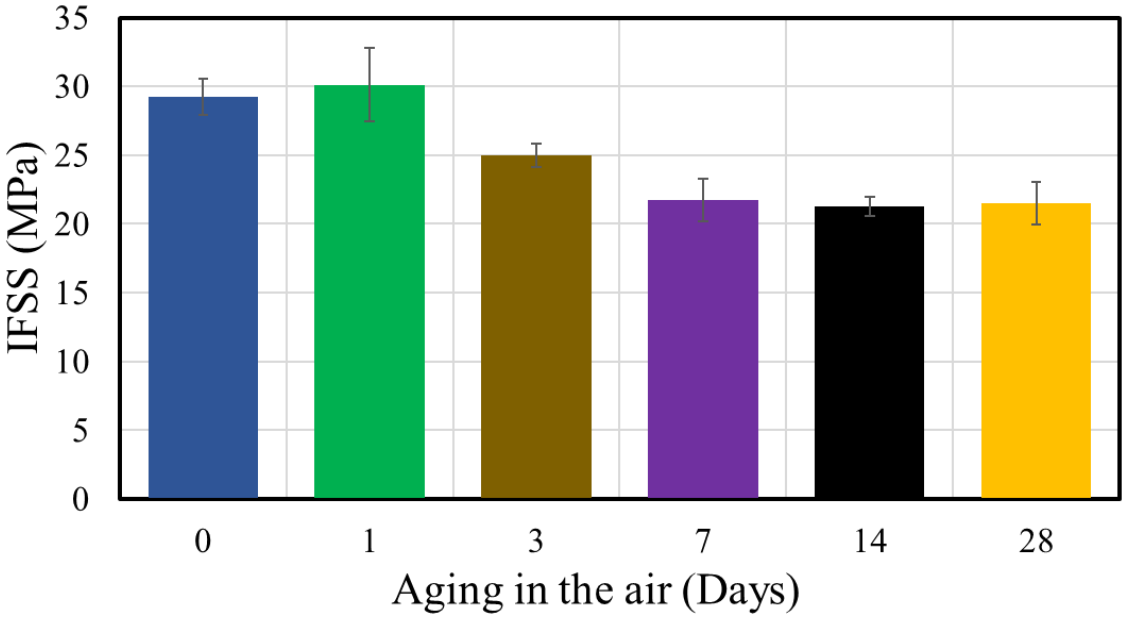

Figure 3.3 Decreasing of the IFSS resulting from placed the individual plasma-treated aramid fibers in the air from 0 to 28 days.

Table 3.8 Interface mechanical properties of aramid microfibers after 0 day of the oxygen plasma treatment.

Sample	Test #	Embedded Length µm	IFSS MPa
30 sec treatment	Test 1	176.67	28.24
	Test 2	269.33	28.17
	Test 3	97.33	30.81
	Test 4	191.00	30.59
	Test 5	276.00	28.51
Average± Standard deviation		202.07±73.70	29.26±1.32

Table 3.9 Interface mechanical properties of aramid microfibers after 1 day of the oxygen plasma treatment.

Sample	Test #	Embedded Length µm	IFSS MPa
30 sec treatment	Test 1	342.67	27.19
	Test 2	245.67	31.94
	Test 3	182.67	29.32
	Test 4	259.33	33.73
	Test 5	292.67	28.47
Average± Standard deviation		264.60±59.12	30.13±2.66

Table 3.10 Interface mechanical properties of aramid microfibers after 3 day of the oxygen plasma treatment.

Sample	Test #	Embedded Length µm	IFSS MPa
30 sec treatment	Test 1	131.67	23.96
	Test 2	239.67	25.52
	Test 3	133.67	24.13
	Test 4	211.67	25.59
	Test 5	138.67	25.73
Average± Standard deviation		171.07±50.88	24.98±0.86

Table 3.11 Interface mechanical properties of aramid microfibers after 7 day of the oxygen plasma treatment.

Sample	Test #	Embedded Length µm	IFSS MPa
30 sec treatment	Test 1	359.33	22.20
	Test 2	167.67	20.01
	Test 3	224.00	20.32
	Test 4	129.33	23.55
	Test 5	247.00	22.65
Average± Standard deviation		225.47±87.99	21.75±1.53

Table 3.12 Interface mechanical properties of aramid microfibers after 14 days of the oxygen plasma treatment.

Sample	Test #	Embedded Length µm	IFSS MPa
30 sec treatment	Test 1	136.33	21.82
	Test 2	461.33	20.50
	Test 3	168.33	20.77
	Test 4	209.33	21.23
	Test 5	244.33	22.16
Average± Standard deviation		243.93±128.21	21.30±0.70

Table 3.13 Interface mechanical properties of aramid microfibers after 28 days of the oxygen plasma treatment.

Sample	Test #	Embedded Length µm	IFSS MPa
30 s treatment	Test 1	158.00	21.37
	Test 2	192.33	20.34
	Test 3	213.67	22.52
	Test 4	226.33	19.79
	Test 5	283.00	23.58
Average± Standard deviation		214.67±46.14	21.52±1.55

Figure 3.4a-f show the morphology of the fibers embedded into matrix, residual grooves in the epoxy, and pulled-out fibers, where the fibers were placed in the air for 1 and 7 days. Figure 3.4c highlights several mounds of residual epoxy on the aramid fiber after the pull-out test, indicating a firm bonding between the fiber and matrix. Likewise, the matrix was heavily damaged due to the strong interface interaction. Once the fiber was placed in the air for 7 days, the residual epoxy was hardly seen on the pulled-out fiber (Figure 3.4f), corresponding to a weak bond between the fiber and matrix. The phenomena observed in Figsure 3.4a-f accurately reflected the measured IFSS of plasma treated and aged aramid fibers.

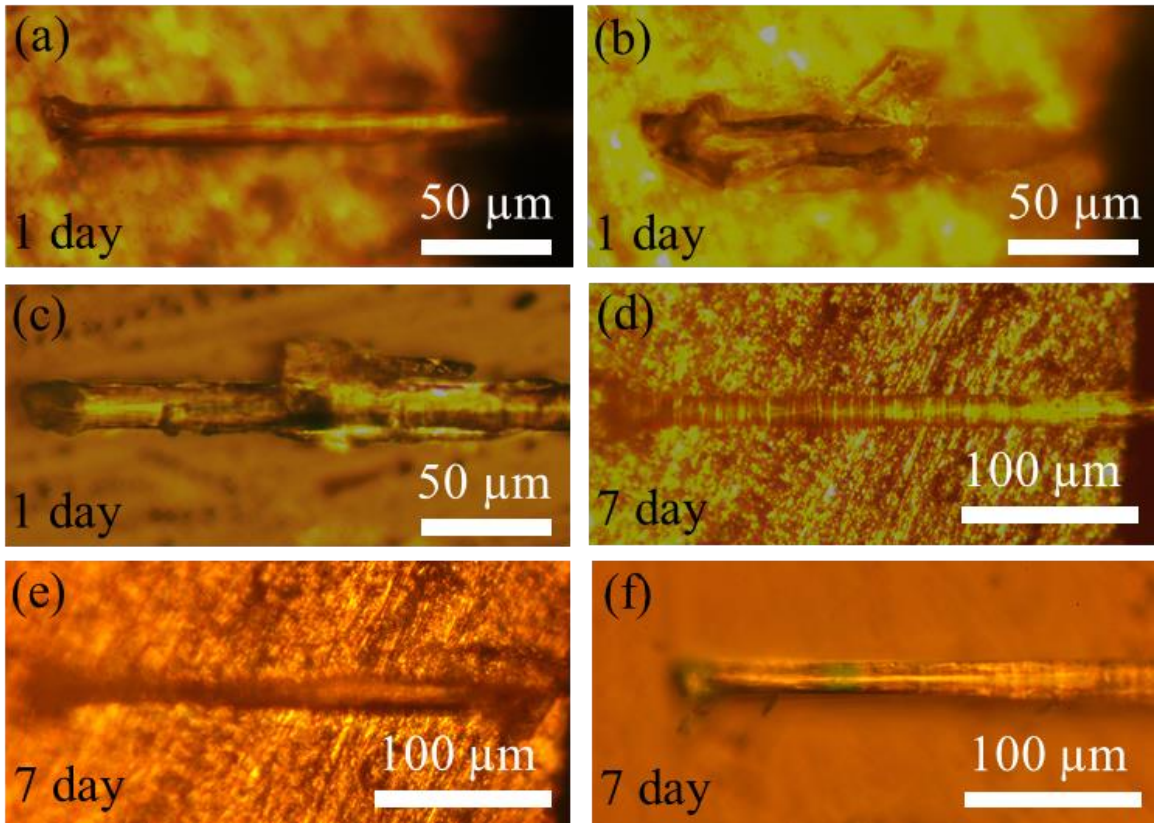

Figure 3.4 - (a)-(f) Optical images of a fiber embedded into epoxy, residual groove in the epoxy, and the pulled-out fiber. (a)-(c) The fiber was placed in the air for 1 day. (d)-(f) The fiber was placed in the air for 7 days.

As plasma-treated aramid fibers are passivated in the air and become fully inactive around 7 days, the raised question is how to reactivate the functional groups to form a strong interface with matrix. The functional groups are mostly dangling bonds, such as carboxyl groups (-COOH), hydroxyl groups (-OH), etc.[7879] These dangling bonds pair with polar molecules in the air. Due to water molecules being present everywhere, they could be ideal counterparts for the functional groups. Once this paring occurs, the functional groups will be unable to bond to the matrix to form strong covalent bonding. Instead, weak van der Waals bonding occurs, resulting in a weak interface interaction. To support this hypothesis, the plasma-treated fibers were treated by water vapor and then heated at 100 °C for two different durations of time, 1 hour and 10 hours. In addition, the aged aramid fibers were directly heated at 100 °C for 10 hours. Figure 3.5 shows the IFSS of the composites reinforced by passivated and reactivated aramid fibers. As the fiber was treated by water vapor and dried only 1 hour, the IFSS dramatically decreased to 13.95 ± 2.14 MPa, which retained only 39.16% of the IFSS of the plasma treated aramid fibers. The residual water molecules trapped by functional groups act as a lubricant, significantly weakening the interface interaction. Five test results of the IFSS and the embedded length of 1 hour water-heat treatment is presented in the Table 3.14.

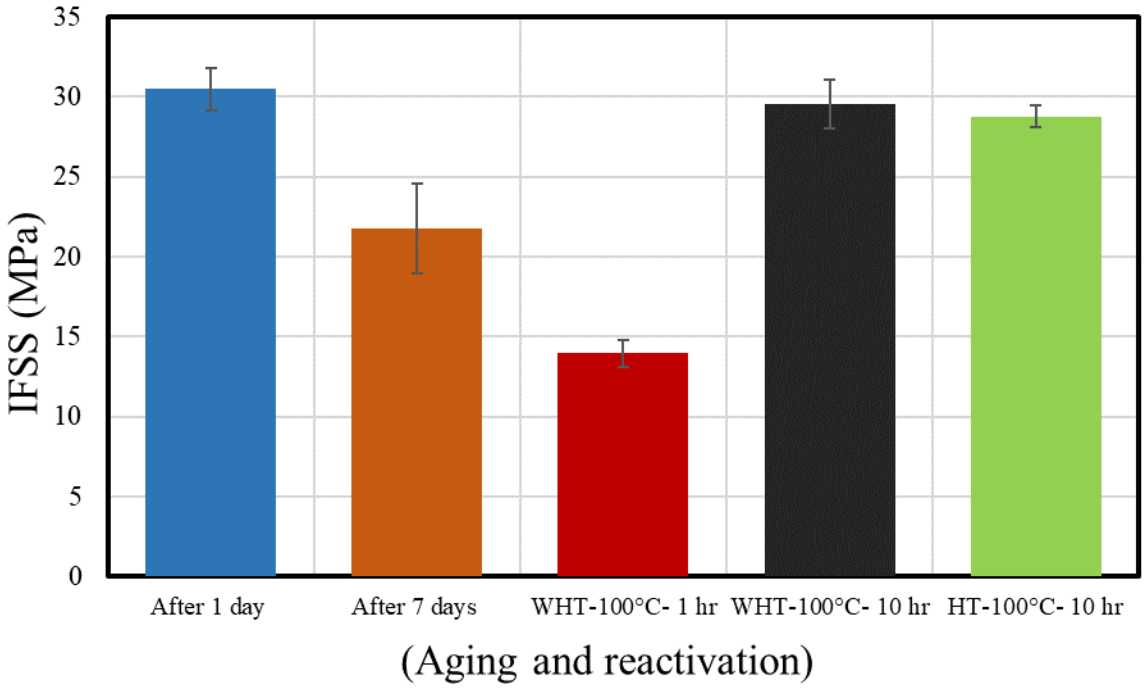

Figure 3.5 IFSS of the composites reinforced by passivated and reactivated aramid fibers (WHT is water treatment followed by heat treatment. HT is heat treatment).

Figure 3.6a-c demonstrate the morphology of a fiber embedded into epoxy, residual groove in the epoxy, and the pulled-out fiber, where the fiber was treated by water vapor and heated for 1 hour. The interaction zone during mechanical failure shown in Figure 3.6b is in ellipse shape, suggesting that the residual water molecules on the aramid fiber might diffuse into the matrix around. As a result, the affected matrix was weakened. Limited residual matrix was found on surface of the pulled-out fiber (Figure 3.6c), indicating a weak interface interaction.

To fully remove all the water molecules trapped by functional groups on surface of the plasma-treated aramid fibers, the heat treatment was extended from 1 hour to 10 hours. The IFSS was restored to 29.57±1.59 MPa during this procedure, which is very close to the result of plasma-treated aramid fiber with one day placement in the air. Figure 3.6d-f shows the morphology of the fiber embedded into epoxy, residual groove in the epoxy, and pulled-out fiber, in which the fiber was aged with water vapor and dried

for 10 hours. Figure 3.6f highlight the heavy damage on the aramid fiber after the pull-out test, implying a strong interface interaction between the fiber and matrix during mechanical failure. As the water molecules were brought to and released from the plasma-treated aramid fibers, the IFSS responded synchronously. Therefore, the functionalized surface of aramid fibers is passivated by water molecules in the air. Table 3.15 presents five test results of the IFSS and the embedded length of 10 hours water-heat treatment. To learn whether the passivated aramid fibers placed in the air for 7 days or even longer can be reactivated through drying in an oven, the passivated aramid fibers were dried for 10 hours directly. After drying, the fibers were carefully embedded into the matrix and pulled out. The IFSS reached 28.78 ± 1.99 MPa which is comparable to the results of the freshly plasma-treated aramid fibers. In addition, the load transfer between the fiber and the matrix is effective, which can be drawn from the residual epoxy that was found on the fiber surface after the pull-out test (Figure 3.6i). All data used to calculate the average of IFSS, including embedded length and IFSS of pulling out aramid fibers after they were exposed to 600 min heat treatment, are presented in the Table 3.16.

Table 3.14 Interface mechanical properties of aramid microfibers after the oxygen plasma treatment and water plus heat treatment for 60 min at temperature 100°C.

Sample	Test #	Embedded Length µm	IFSS MPa
30 sec treatment	Test 1	180.67	12.46
	Test 2	131.33	15.07
	Test 3	265.67	13.34
	Test 4	207.33	17.09
	Test 5	259.33	11.79
Average± Standard deviation		208.87±56.09	13.95±2.14

Table 3.15 Interface mechanical properties of aramid microfibers after the oxygen plasma treatment and water plus heat treatment for 600 min at temperature 100°C.

Sample	Test #	Embedded Length µm	IFSS MPa
30 sec treatment	Test 1	85.33	29.73
	Test 2	136.67	28.71
	Test 3	69.67	30.46
	Test 4	201.00	31.55
	Test 5	237.33	27.42
Average± Standard deviation		146.00±72.39	29.57±1.59

Table 3.16 Interface mechanical properties of aramid microfibers after the oxygen plasma treatment and heat treatment for 600 min at temperature 100°C without water treatment.

Sample	Test #	Embedded Length µm	IFSS MPa
30 sec treatment	Test 1	524.67	27.88
	Test 2	229.67	30.60
	Test 3	395.33	26.02
	Test 4	281.00	28.60
	Test 5	221.67	30.80
Average± Standard deviation		330.47±128.81	28.78±1.99

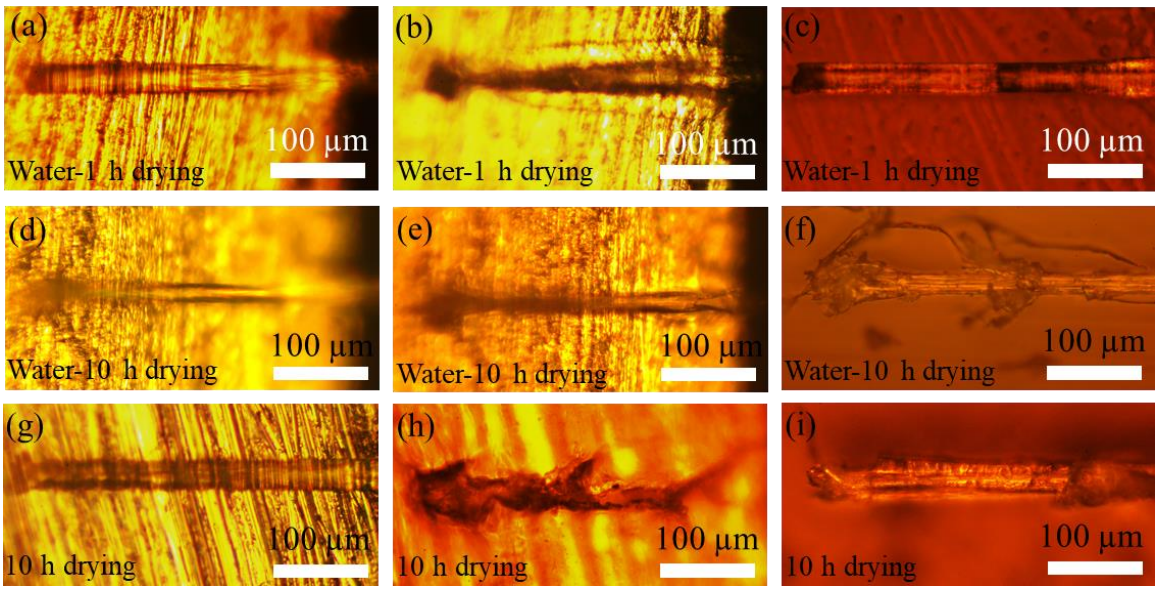

Figure 3.6 Optical images a fiber embedded into epoxy, residual groove in the epoxy, and pulled-out fiber. (a)-(c) The aged fiber was treated with water and heated for 1 hour. (d)-(f) The aged fiber was treated with water and heated for 10 hours. (g)-(i) The aged fiber was heated for 10 hours.

Figure 3.7 shows high-magnification SEM images of the pulled-out aramid fibers. Figure 3.7a demonstrates the plasma-treated fiber surface which was passivated by water vapor and subsequently heated for 1 hour. Little residual epoxy can be found, and the fiber is also not heavily damaged. In contrast, when the aramid fiber was heated for 10 hours (Figure 3.7 b, and 3.7 c), large mounds of epoxy are remained on the pulled-out fibers and the fibers were also severely damage. These observations are similar to those observed in the optical images. The damage to the fibers and the amount of residual epoxy found in Figure**3.7** can be directly linked to the measured IFSS as well as the interface interaction.

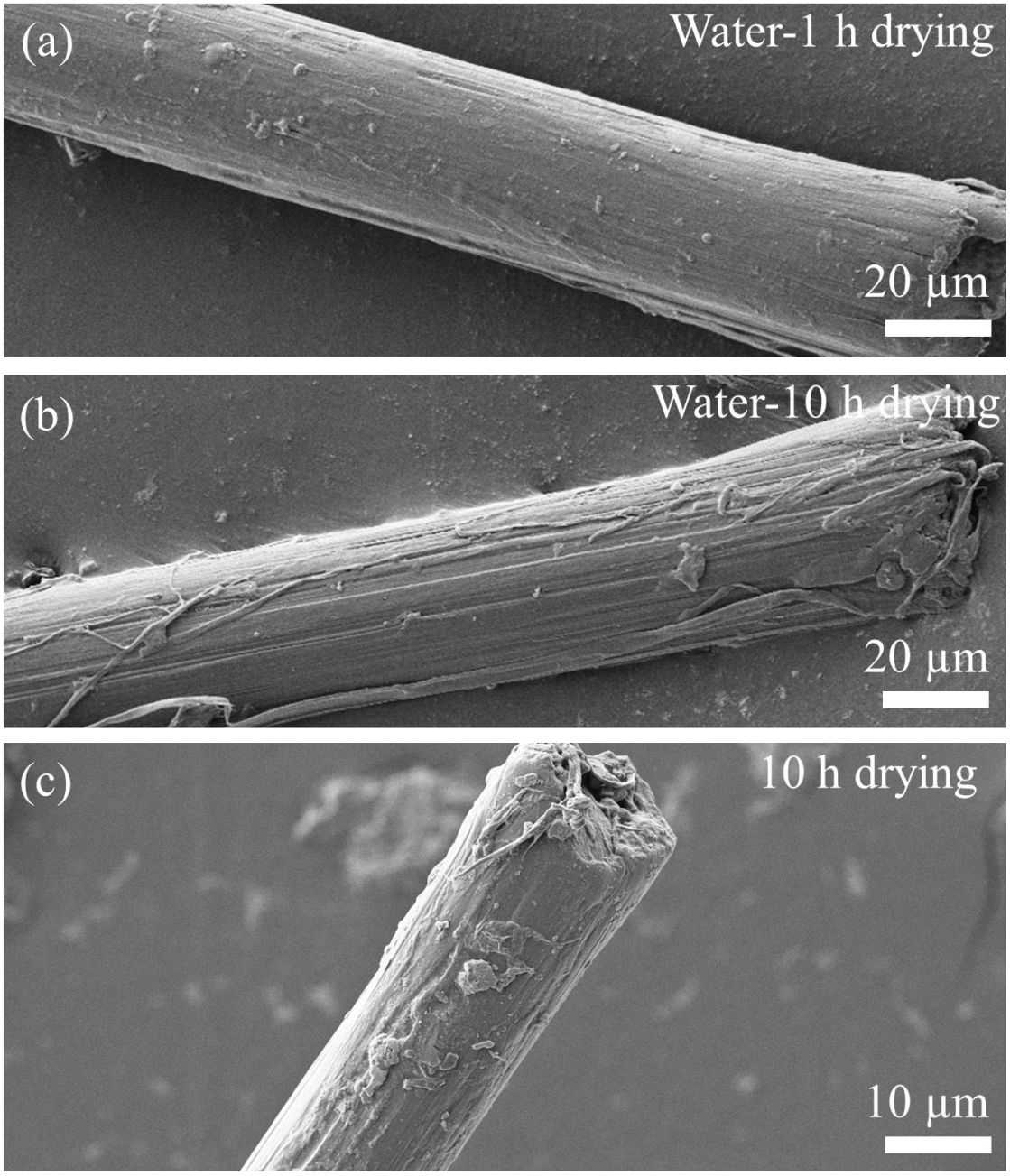

Figure 3.7 SEM images of the pulled-out aramid fibers. (a) The plasma-treated fiber was passivated by water vapor and heated for 1 hour. (b) The plasma-treated fiber was passivated by water vapor and heated for 10 hours. (c) The aged fiber was heated for 10 hours

FTIR has been widely used to demonstrate the absorbance of peaks assigned to various bond stretching bands and to identify the existent bonds and associated changes due to chemical or physical

reaction, curing, aging, etc.[808182] For example, González-Benito investigated the curing process of an epoxy system at the interface formed by a silane coated glass fiber using FTIR imaging and obtained images for -OH and amino groups (H-N-H).[83] Based on the obtained results, the IFSS of the aramid fibers reinforced epoxy responded to the water vapor treatment. To visualize the existence and change of water on the aged and activated aramid fibers, FTIR analysis was performed in this work. To get a high signal intensity, aramid fibers were chopped into small pieces (~1 mm) and mixed with potassium bromide for FTIR analysis. Figure 3.8 shows the FTIR spectra of the plasma-treated aramid fibers aged in the air for 7 days, passivated by water vapor followed by 1 hour and 10 hours drying. The presence of the peak at ~3,000 cm^{-1} corresponds to the aromatic rings of C-H bond stretching vibrations, while the peak at ~1,600 cm^{-1} confirms amide C=O bonds in the structure. The broad band at ~3,000 cm^{-1} is a hydrogen-bonded O-H stretch, which can be used to indicate water adsorption.[808485] To have a direct comparison of water adsorption, all three FTIR spectra are normalized with respect to the intensity of aromatic rings of the C-H bond which is not affected by the adsorption of water. The hydrogen-bonded O-H stretch of the fibers that was naturally passivated in the air for 7 days is the baseline for the comparison of water adsorption. As the fibers were dried at 100 °C for 1 hour right after water passivation, the intensity of the hydrogen-bonded O-H stretch increased by 14.0 %. Interestingly, if the water vapor passivated aramid fibers are dried at 100 °C for 10 hours, the intensity of hydrogen-bonded O-H stretch decreases 3.8% compared to that of the fibers without water vapor passivation, but instead placed only in the air.

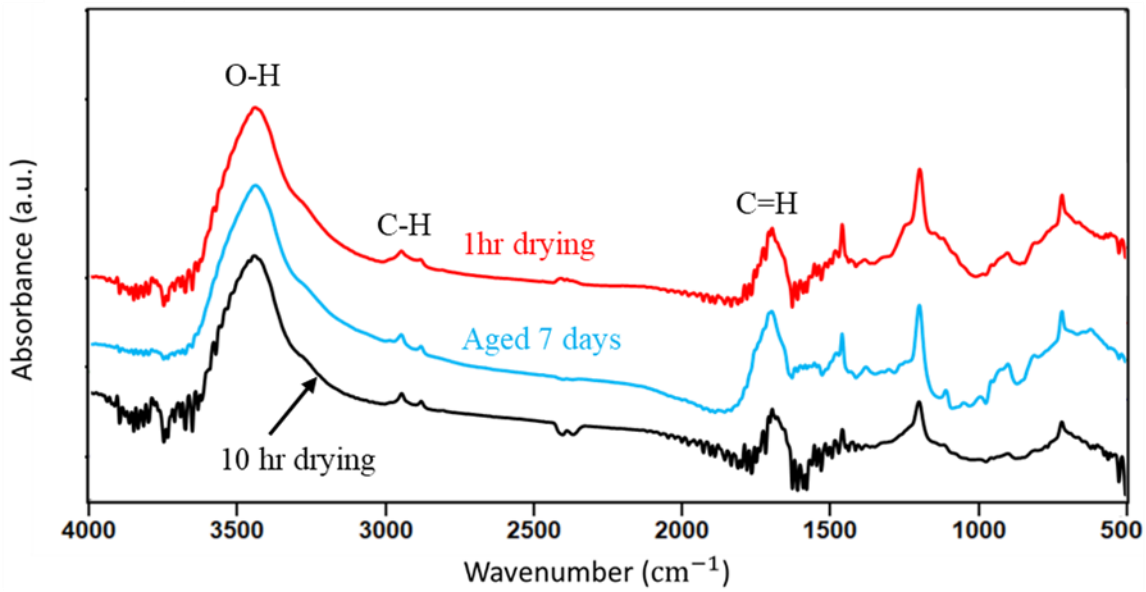

Figure 3.8 FTIR spectra of the plasma-treated aramid fibers aged in the air for 7 days, passivated by water vapor followed by 1 hour and 10 hours drying.

The comparison reveals that water adsorption can be released through drying. Shorter time treatments, such as 1 hour, is not enough to get rid of all trapped water molecules in the fibers. Regarding the strength of interface interaction, the IFSS dramatically decreased to 13.95 ± 2.14 MPa for the fibers treated by water vapor that only experienced 1 hour of drying. Unveiled by FTIR analysis, the residual water on the fibers dominates and then weakens the interface interaction. As the heat treatment was extended from 1 hour to 10 hours, the IFSS was restored to 29.57±1.59 MPa which is very close to the result of the freshly plasma-treated aramid fibers. Therefore, the water molecules trapped in the plasma treated fibers are responsible for the aging of functional group and weakening the interface interaction if the treated fibers are placed in the air for multiple days.

CHAPTER 4

4 COATING THE ARAMID FIBERS WITH CERAMIC NANO-PARTICLES TO IMPROVE THE IFSS

4.1 Introduction

The superior performance of any composite structure depends on the intrinsic properties of the fibers, reinforcement/matrix and the bonding between them. [1,12,13,55,56,57,58] A firm bonding between the fiber and its matrix means the load will be efficiently transfer from the matrix to the fiber if the fracture strengths for both are high. In opposite, a weak bonding leads to deteriorate the composite because the fiber is unable to carry the applied load.

One of the most common reinforcements is the aramid fiber, where it has high fracture strength, low mass at constant size, high toughness, remarkable corrosion resistance and accepted thermal stability due to their dense hydrogen bonds and high crystallinity. These properties make it the best candidate for structure of body armor, marine hulls, aerospace components, and automotive components as shown in the chapter one.[3,4,5,6] In opposite, the aramid fibers are suffering from a smooth and chemically inert surface, which is responsible for thw low mechanical performance and undesirable properties such as poor interfacial interaction between the aramid fiber and its matrix.[14,15,29]

The IFSS could be improved by using surface roughness and enrich the fiber surface with functional groups. The plasma treatment is usually used for increasing the surface roughness by inducing a high temperature and melt the outer layer of the aramid fiber to increase the sliding resistance and allow an efficient load transfer between fibers and its matrix. [19,20,21,59] The stated method leads to increase the number and size of defects, where the stresses will concentrate around these defects and deteriorate the fracture strength of the fibers at specific period of plasma treatment.[75] Therefore, the period of plasma treatment is important to balance the fracture strength and the surface defects which is usually complex. Using chemical treatment to enrich the fiber surface with functional groups such as carboxyl and hydroxyl is the second method to increase the IFSS.[3349] One of the most important advantages of

using this method, it will not generate new defects which keep the mechanical properties same such as the tensile strength and improve the IFSS.[50] Unfortunately, the fiber surface becomes inactive after several days - few weeks due to the surface passivation that makes the aramid fibers unable to bond with the matrix.[35]

In this work, the CVD will be used as an alternative method to increase the surface roughness by synthesis the ceramic nano-particles on the aramid fibers surface to improve the IFSS. This method will solve the issue of using plasma treatment because the CVD method will not generate a new defect. Also, the CVD method will keep the aramid fiber with the same performance because there is no concern regarding the passivation of the functional groups on the fiber surface. The CVD is usually used to improve the mechanical properties of the carbon due to the high decomposition temperatures (T_d) of the carbon (700 °C - 1200°C).[52] The high T_d of carbon fibers made the CVD an optimal method for improving the IFSS. Also, it was used for getting three dimensions hybridized structure that consists of the carbon sheets and carbon nanotubes (CNTs). [53,54] Moreover, the CVD could be used for grafting the CNTs on the surface carbon fibers to enhance the IFSS between the fiber and its matrix.[11] To use the CVD method for synthesis the ceramic nanoparticles on the aramid fiber and improve its IFSS, it is important to sythesis these particles without damaging the aramid fibers, where the aramid fiber has very low T_d (510 °C – 560 °C).[27] To solve this obstacle, the ceramic nanoparticles were placed in the center of the furnace while the aramid fibers were kept closing to the end of the tube with increasing the flow rate of the nitrogen gas from the other side of the tube.

4.2 Experimental Section

4.2.1 Coating aramid fibers by the CVD method

Aramid fibers under name DAF III, polyheteroarylene-co-p-phenyleneterephthalamide with radius ~8.5 were used to apply the CVD method. These fibers were purchased from Bluestar Chengrand Chemical Co. Ltd. Before the using, aramid fibers should be cleaned very well by a suitable chemical such as the acetone and dry them at the elevated temperature.[75] MoO_3 works as a precursor of the ceramic nanoparticles that will be synthesized on the surface of the aramid fibers. The MoO_3 was placed in the center of the furnace to exposure it to the highest temperature (~800 °C) while the aramid fibers were placed at the left side of the tube to keep it away from the high temperature. On the meantime, the right side of the tube was connected to the Aragon gas with 200 Standard cubic centimeters per minute (SCCM) to force the ceramic particles moving quickly to the other side and deposing on the fibers' surfaces

4.2.2 Matrix preparation

Four solutions with a different percentage represent the resin for forming the epoxy, including Embed 812, Dodecenylsuccinic anhydride (DDSA), N-Methylaniline (NMA), and 2,4,6-Tris (dimethylaminomethyl) phenol (DMP-30). All of them were purchased from Electron Microscopy Sciences, Hatfield, PA. Embed 812 represent the matrix resin with 44.7 %, while DDSA, and NMA are the hardeners with percentages 35.8 % and 17.9 %, respectively. These three solutions were mixed carefully with aid of a magnetic stirrer for 10-15 minutes. 1.6 % of DMP-30 was added to the mixture as an accelerator and then they were stirred for 10 minutes. The last step is placing the mixture in the ultrasonic vibration to get the bubbles out of the resin.

4.2.3 Preparation for debonding tests and the pull-out tests

A carefully polished aluminum plate with a dimension of 10 mm x 10 mm x 2 mm (length x width x height) was placed under the microscope and then a small droplet of the prepared epoxy was dropped closing to the sharp edge of the substrate. The untreated and coated fibers were carefully embedded in the matrix with embedded length less than 1 mm. The whole assembly then placed in the drying oven for curing at 60 °C for 24 hours. The sample after became ready for the pull-out test is demonstrated in the schematic of the Figure 4.1a. The left end of the sample is firmly clamped to the micro tester while the other end represents the free fiber, that is should be clamped to the moveable chew of the tester. Figure 4.1b shows schematic demonstration for the sample after conducting the test, where the fiber leaves a groove with length equal to the embedded length of the fiber. Uniform groove and no residual epoxy mean the interaction between the fiber and the matrix is week.

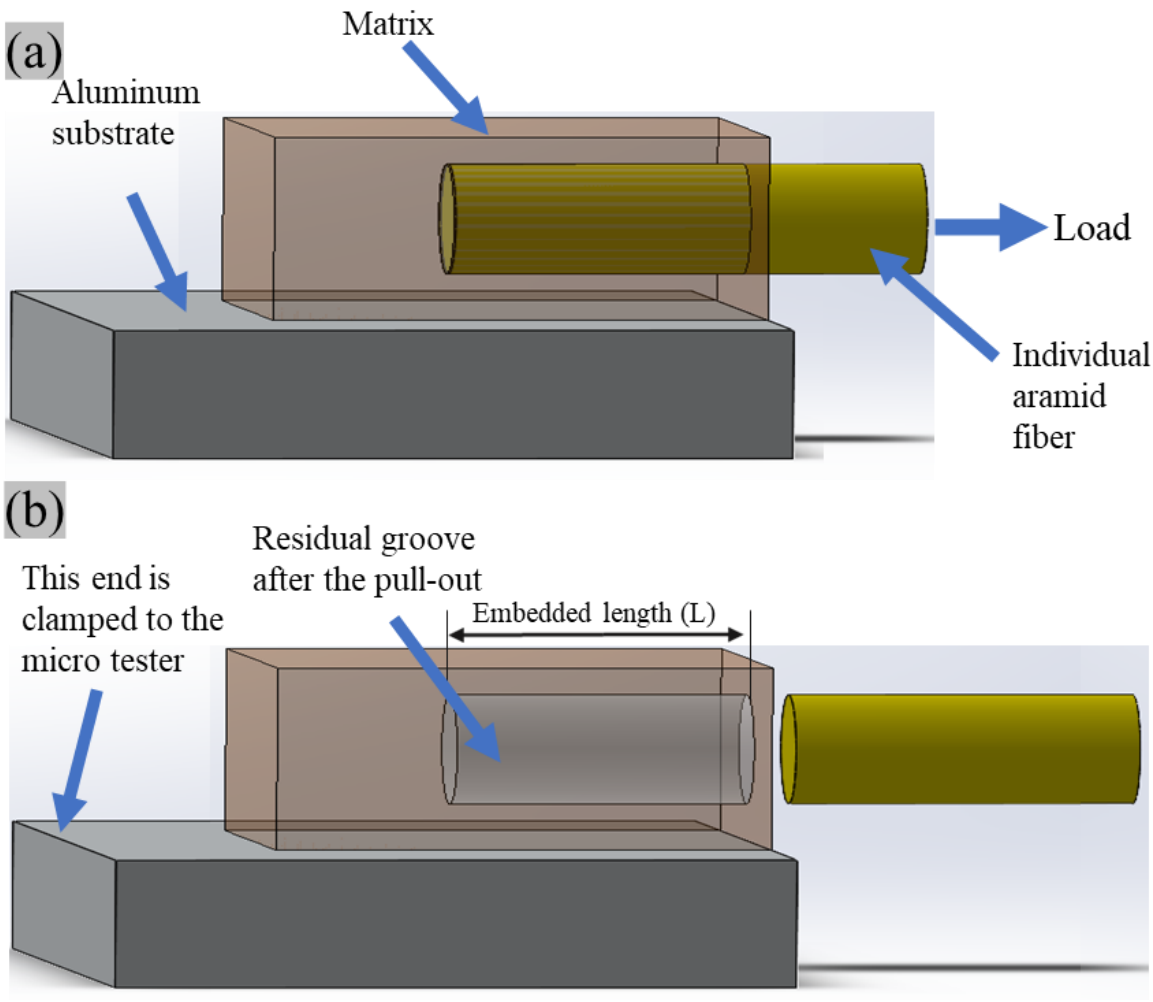

Figure 4.1 Schematic demonstration of the prepared sample (a) before the pull-out test (b) after the pull-out test.

4.2.4 Other characterizations

For conducting the pull-out tests, A Deben Micro Tensile Tester (Gatan Inc.) was used. The tester was installed with a 200 N load cell with a force resolution of 0.001 N. The loading speed was maintained to be 0.5 mm/min.

4.3 Results and Discussion

To precisely characteristic the IFSS by using the CVD method of the aramid fibers, the surface of the fiber should be dominated by the grafted particles rather than the generated functional groups. As the we proved in the chapter three, the aramid fiber surface is fully passivated after passing seven days. The interfacial load transfer will be dominated by the interface interlocking rather than functional groups. The uncoated fiber was used as a reference to show the change on the fibers' surface. Figure 3.1a-c show SEM images of the pristine aramid fibers, coated with ceramic nanoparticles, and high magnification of the coated fiber. The untreated fibers have a very smooth surface as shown in the Figure 4.1a. In contrast, according to our visual test of the fibers' surface, it has roughness after using the CVD method to synthesis the ceramic particles as demonstrated in the in Figure 4.1b, which is a good sign for improving the IFSS. Also, Figure 4.1c shows a high magnification SEM image of the coated fiber, the entire surface is coated with new particles that promises to give stable mechanical properties of the structure.

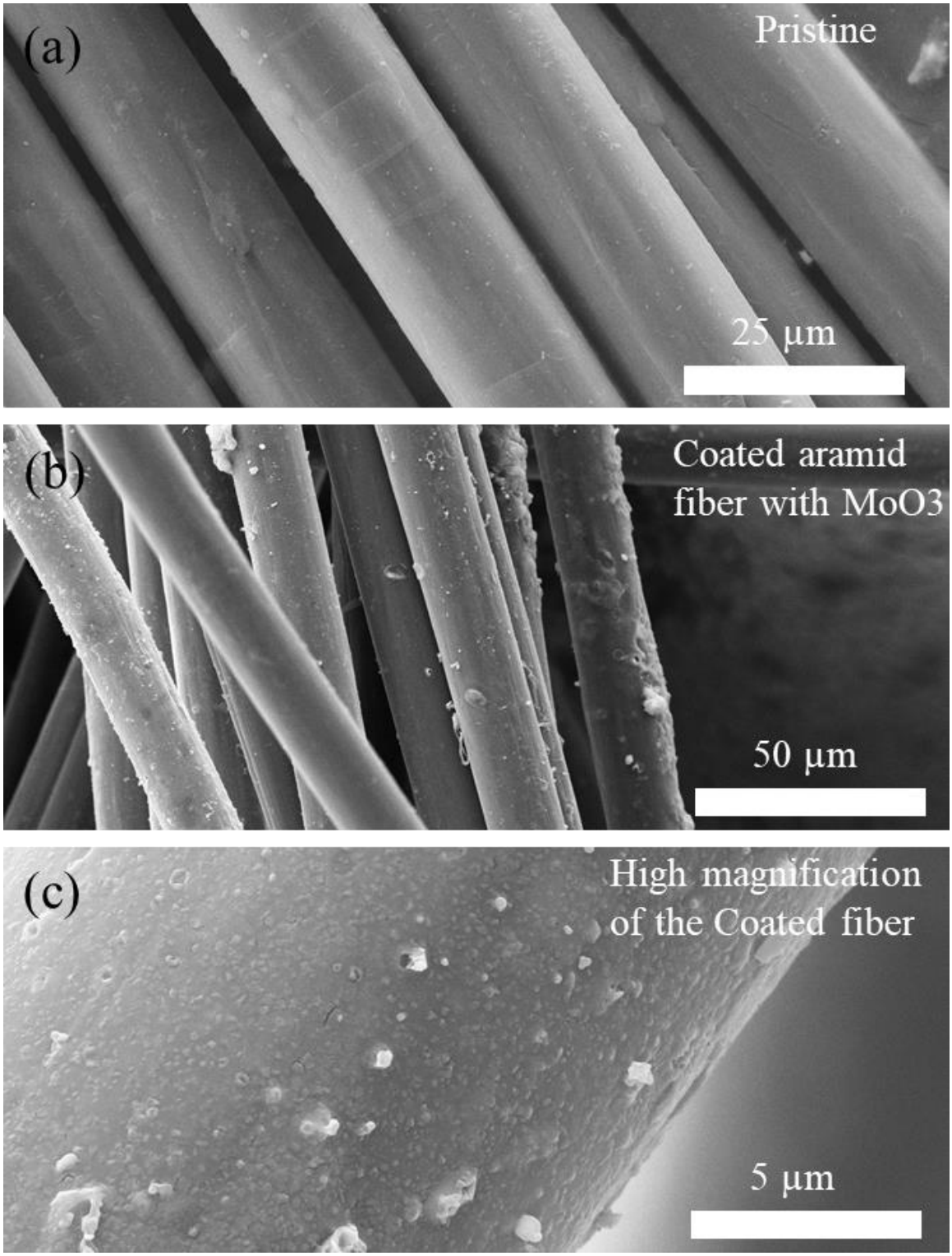

Figure 4.2 SEM of (a) pristine the aramid fiber (b) the coated aramid fiber with ceramic partials (c) a high magnification of the coated aramid fiber with ceramic partials.

For better evaluation the impact of CVD method on the mechanical property of aramid fibers, the tensile tests were conducted for both uncoated and coated fibers. Figure 4.3 show the most representative of stress-strain curves of pristine and coated fibers. The untreated fibers have a tensile strength of 3.56± 0.40 GPa. Table 4.1 shows all the conducted tests for characteristic the elastic modulus and the fracture strength of aramid fibers before coating the fibers by the MoO3 particles. Also, the coated fibers with MoO_3 particles have a tensile strength of 3.29 ± 0.29 GPa. Table 4.2 shows all the conducted test for characteristic the elastic modulus and the fracture strength of aramid fibers after coating the surface by the MoO3 particles. By comparing the results of the coated and uncoated fibers, the tensile strength reduced by ~7% which can be consider as a good result comparing to the increasing surface roughness by using the oxygen plasma treatment. Maintaining the tensile strength in high performance means the CVD method did not generate new defects on the fibers' surface.

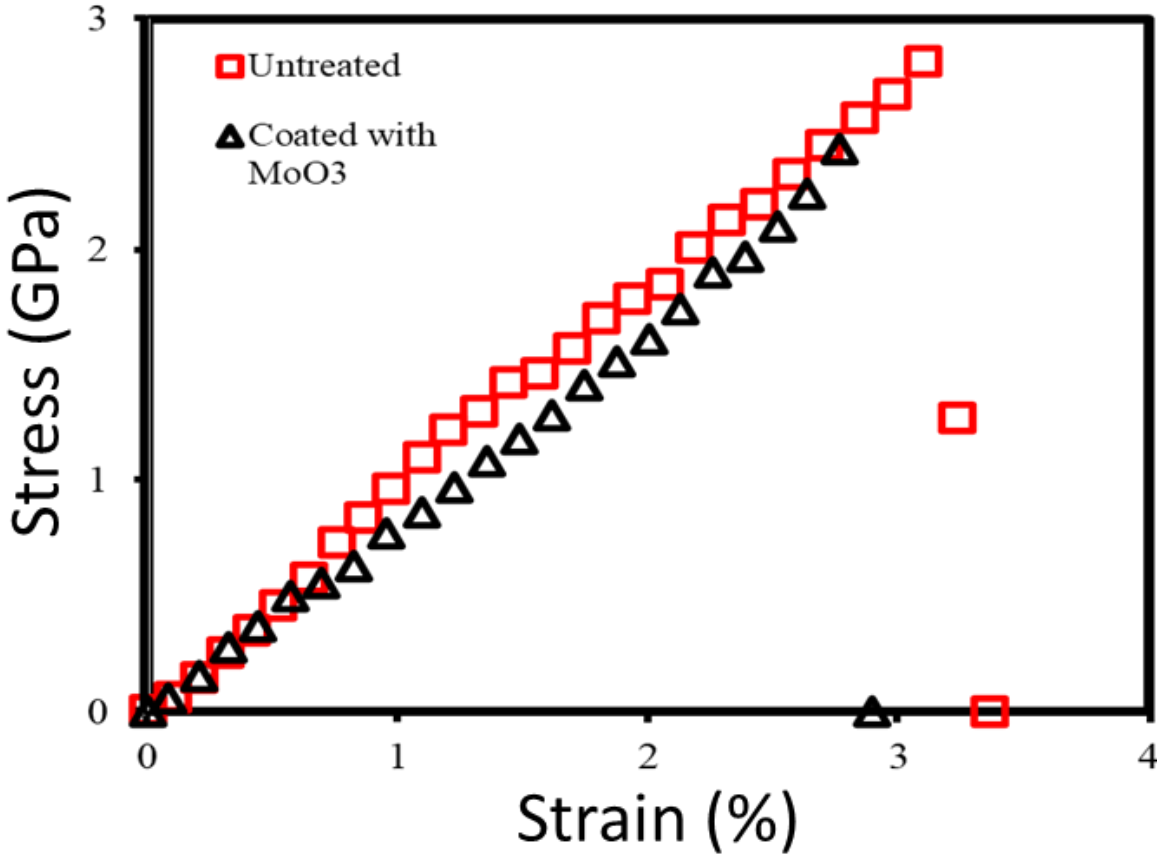

Figure 4.3 Stress-strain curves before and after using the CVD method for coating the aramid fiber.

Table 4.1 Mechanical properties of aramid fibers before coating the surface by the MoO3 particles.

Sample #	**Tensile Strength GPa**	**Elastic Modulus GPa**
1	2.93	90.48
2	3.44	86.00
3	3.89	130.00
4	3.93	100.00
5	3.64	125.00
Average	3.57±0.41	106.30±20.08

Table 4.2 Mechanical properties of aramid fibers after coating the surface by the MoO3 particles.

Sample	Tensile Strength GPa	Elastic Modulus GPa
1	3.21	71.43
2	3.10	80.00
3	3.81	100.00
4	3.20	125.00
5	3.15	86.67
Average	3.29±29	92.62±20.90

The high performance of the tensile strength should accompany by improving the IFSS, otherwise the goal was not achieved. For quantifying the IFSS, individual uncoated and coated (either PVD method or CVD method) fibers carefully embedded in the matrix and then they were pulled out after the curing. The uncoated fiber has IFSS value equals to 22.90 ± 1.50 MPa. Also, using the PVD method did not significantly increase the IFSS, where the IFSS value is 25.17 ± 3.38 MPa. Five results of the IFSS beside the average and the standard deviation of the coated individual aramid fibers with MoO3 by using the PVD method are shown in the Table 4.3. On the other hand, by using the CVD method, the IFSS significantly increased and reached 31.16±3.11 MPa Figure 4.4 shows the IFSS values before and after the coating process. Such a great result can enhance the composite without affecting the tensile

strength of the fibers. Table 4.4 shows five results of IFSS of the coated individual aramid fibers with MoO3 by using the CVD method.

Table 4.3 Interface mechanical properties after coating the aramid fibers with MoO3 by using the PVD method.

Sample	Test #	Embedded Length µm	IFSS MPa
30 sec treatment	Test 1	559.21	23.65
	Test 2	148.03	29.84
	Test 3	477.63	21.06
	Test 4	364.47	24.197
	Test 5	213.16	27.09
Average± Standard deviation			25.17±3.38

Table 4.4 Interface mechanical properties after coating the aramid fibers with MoO3 by using the CVD method.

Sample	Test #	Embedded Length µm	IFSS MPa
1	Test 1	225.00	32.67
2	Test 2	287.0	28.78
3	Test 3	361.84	34.03
4	Test 4	268.42	34.98
5	Test 5	281.58	27.703
Average± Standard deviation			31.16±3.11

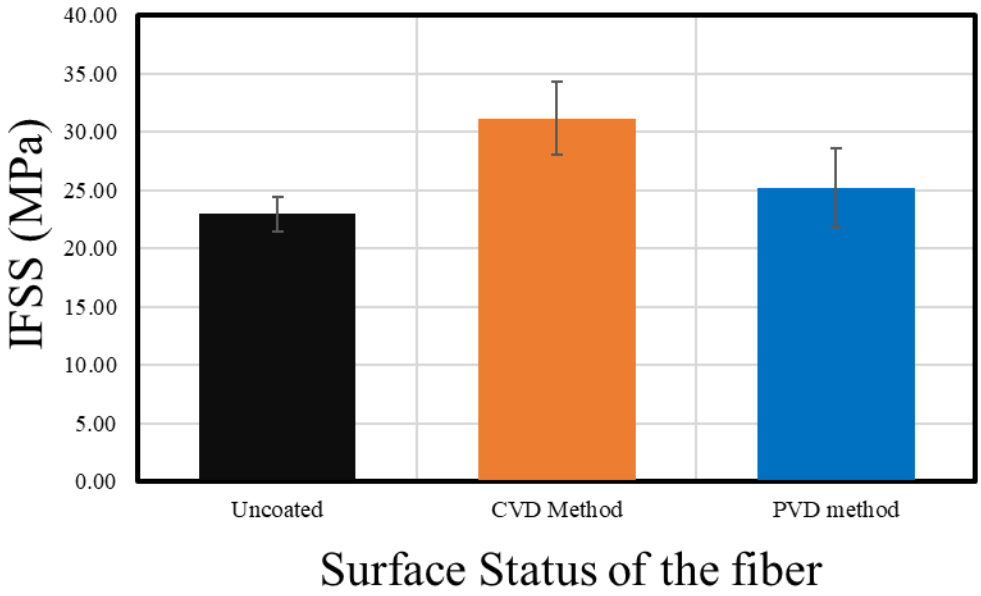

Figure 4.4 IFSS results of the individual aramid fibers before and after using CVD and PVD methods.

Figure 4.5a-c show the optical images of the uncoated individual fiber embedded into the polymer matrix, residual grooves in the epoxy after the fiber was pulled out, and the pulled-out individual fiber. The uncoated fibers have been used as a reference for improving the IFSS. The embedded length was kept less than 0.6 mm to force the fiber to be pulled out rather than fracture as shown in the Figure 4.5a. Figure 4.5b shows no damage or dislocation in the matrix, indicating a low interaction between the matrix and the fibers. Also, the residual epoxy on the fiber barely seen on the fiber surface as shown in the optical image of the Figure 4.5c. These results are expected because the aramid fibers are suffering from a smooth and chemically inert surface, which gives a low mechanical performance and undesirable properties such as poor interfacial interaction between the aramid fiber and its matrix.

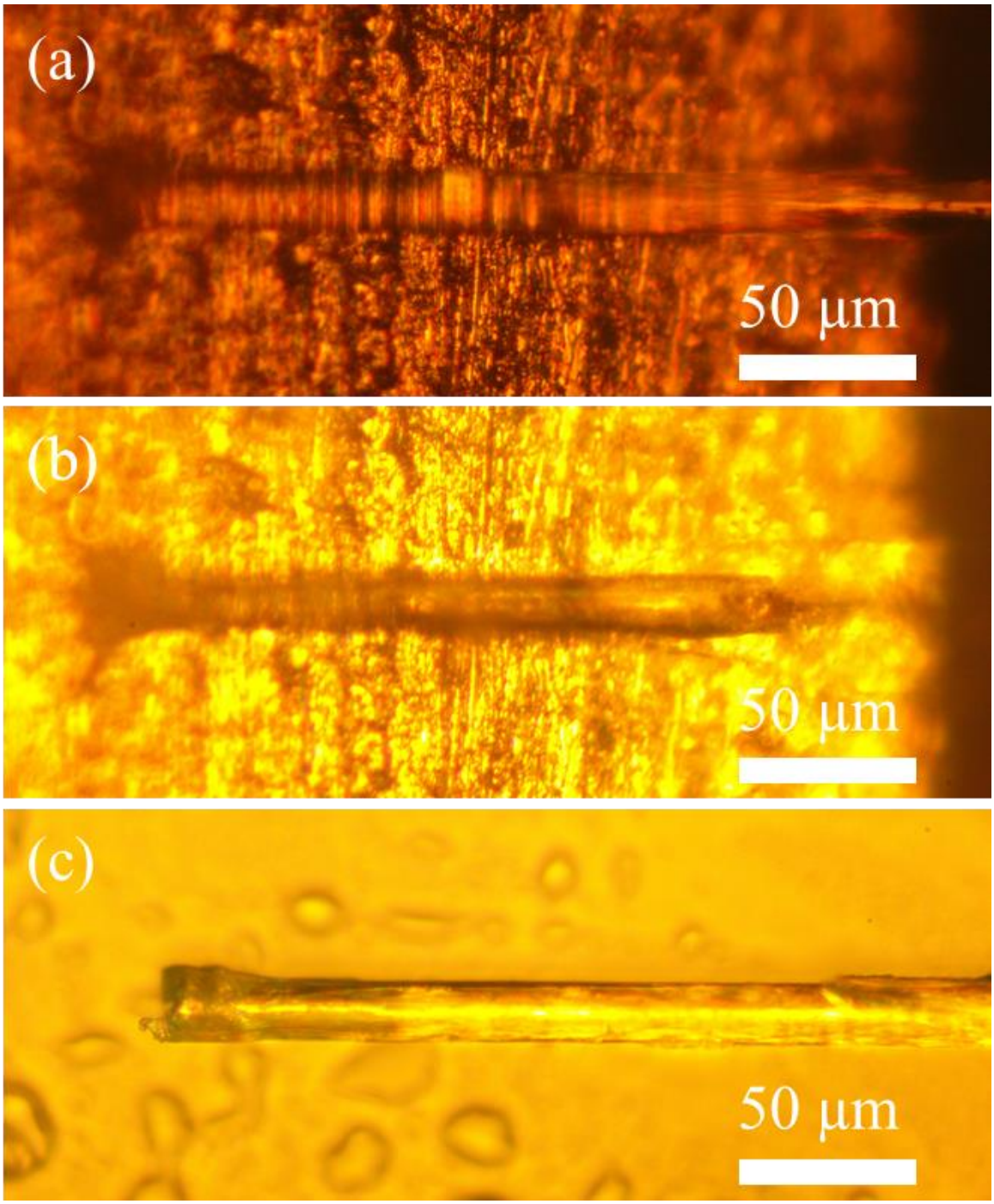

Figure 4.5 (a)-(c) Optical images of (a) uncoated individual fiber after embedded into epoxy (b) residual groove in the epoxy after the pull-out tests, and (c) the pulled-out fiber.

As forementioned, for improving the IFSS, increasing the surface roughness by using the CVD method is an optimal method that can maintain the fracture strength in a high performance. The ceramic particles were grafted on fibers' surface by applying the CVD method. Figure 4.6a-c show the optical images of the coated individual fiber before the pull-out test, residual groove in the epoxy after the fiber have been pulled out, and the pulled-out individual fiber, respectively, of the CVD method. The measured embedded length is better to be less than ~0.35 mm due to the high interaction between the polymer matrix and the aramid fibers as shown in the Figure 4.6a. Also, the dislocation in the matrix after the pull-out test is another evidence of the strong bonding between the matrix and the fiber. Regarding the PVD method, Figure 4.7a-c show the optical images of the coated individual fiber before the pull-out test, residual groove in the epoxy after conducting the pull-out test, and pulled-out individual fiber, respectively. In opposite to the CVD method, the embedded fiber can be more than ~0.35 mm due to the low interaction between the fiber and the matrix as shown in the Figure 4.7a. Also, there is no damaging in the matrix and no residual epoxy on the fiber's surface as shown in the Figure 4.7b-c, respectively.

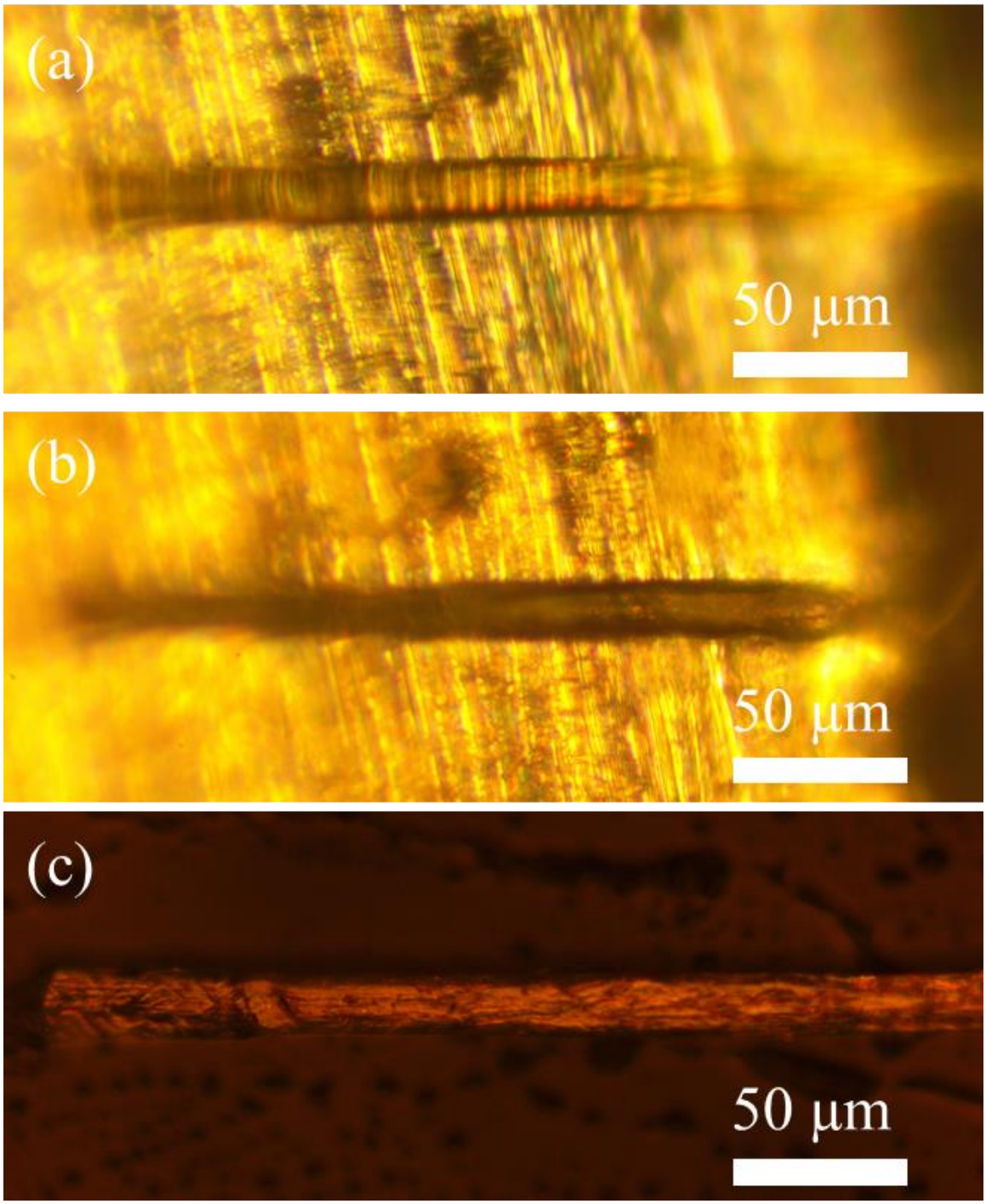

Figure 4.6 (a)-(c) Optical images of CVD method (a) coated individual fiber with MoO_3 and embedded into epoxy (b) residual groove in the epoxy, and (c) the pulled-out fiber.

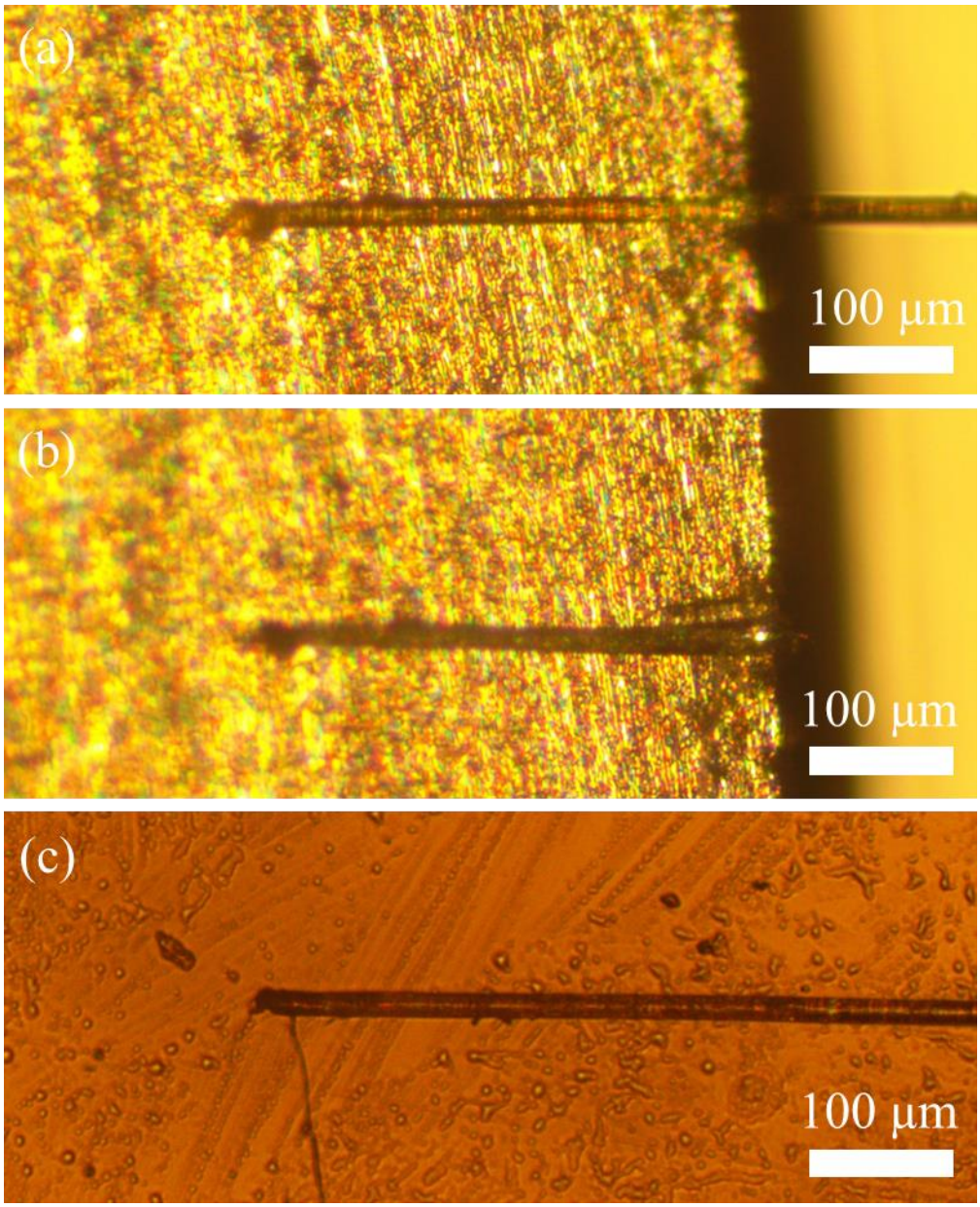

Figure 4.7 (a)-(c) Optical images of the PVD method (a) coated individual fiber with MoO_3 before embedding it into epoxy (b) residual groove in the epoxy, and (c) the pulled-out fiber.

4.4 Fourier-transform infrared spectroscopy (FTIR)

FTIR has been used to study various stretching bonds and bending bond to identify the existent elements and surface changes due to chemical or physical reaction, curing, aging, etc.[8081] In this work, the FTIR spectroscopy was performed to prove that the MoO_3 particles have been synthesized on the fiber surface and new bonds were generated. The FTIR spectroscopy confirmed that the MoO3 have been successfully synthesized on the surface of aramid fibers as explained in the Figure 4.8. At the temperature 600°C or higher, several function group can be seen such as Mo=O and Mo-O-Mo at ~810 cm^{-1} and ~1100,respectively due to the synthesized MoO_3 particles on the fiber's surface.[86] Both of the mentioned functional groups appeared on the surface of aramid fiber as presented in the FTIR of the Figure 4.8. Also, the terminal Mo=O bond can be seen at the peak of 995 cm^{-1}.[87] the peak intensity in some places decrease when the temperature reaches 700 °C because the structure have been changed due to the resolved stretch peak of the double oxygen.[88] The peak at ~3400cm^{-1} is the OH stretching bond, which can be attributed to the hydrogen-bonded water molecules.[8889]

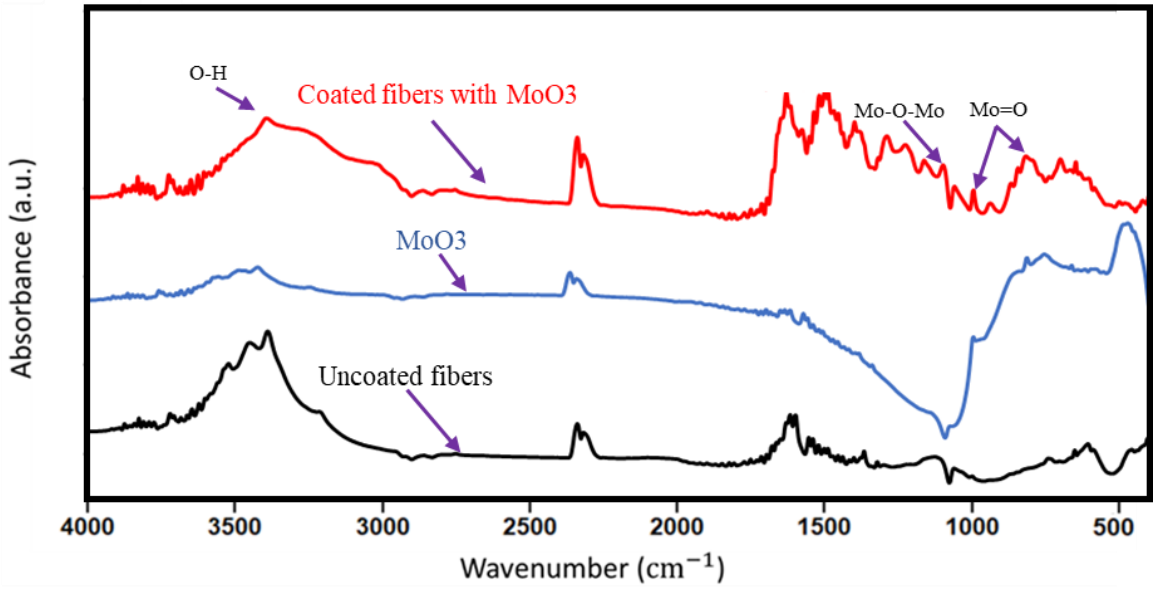

Figure 4.8 FTIR spectra of the coated aramid fibers with synthesized MoO3, MoO3 powder, and the pristine aramid fibers.

CHAPTER 5

5 IDENTIFYING VAN DER WAALS FORCE AND THE HYDROGYN BONDING BETWEEN ARAMID FIBERS AND SILICON WAFER

5.1 Introduction

With an upsurge of interest in fabrication and manufacture of soft and smart materials, van der Waals (vdW) force and hydrogen bonding have been believed playing a key role in a variety of systems.[909192] The interface exists between different matters. Its importance highly depends on the surface-to-volume ratio of the systems, where incredible physical behaviors may occur because of the augmented interfacial interaction (mainly vdW force and hydrogen bonding). For example, square ice and superdense lithium have been observed under bilayer graphene confinement due to the ultra-strong vdW pressure.[9394] Self-healing in hydrogel can be also generated because of the reversibility and tunable strength of hydrogen bonding.[95]

Both vdW force and hydrogen bonding are too subtle to capture and quite easy to be disturbed due to their reversible nature.[96] The vdW force is a distance-dependent interaction, which has diverse measurements from varied experimental platforms.[979899] The hydrogen bond, a primarily electrostatic force of non-covalent attraction between an electropositive hydrogen donor and a strongly electronegative acceptor (F, O, N or Cl), is ubiquitous in nature and central to biological functions, which only forms between specific functional groups or small molecules, such as water molecule (H_2O). In fact, small molecules could be trapped in the interfacial region due to the hydrogen bonding and vdW interaction, filling the gap and bridging the interface.[100101102103] Within the interfacial region, hydrogen bond network tends to dynamically form and further glue the surroundings together, which will renormalize the local interfacial interaction and further mediate the entire mechanical performance.[104105106107]

As one of carbon-based engineering structures, carbon fibers with ultrahigh surface-to-volume ratio are usually bundled together to reinforce other materials.[108109] The entire mechanical performance is mainly restricted by the interfacial bonding scenario.[11011161] Given the fact that carbon fibers are technically synthesized by small organic molecules such as polyacrylonitrile (PAN), stabilized, carbonized at >1,000 ^{o}C and treated to obtain active surface, a number of residual -OH groups can be found.[112113114] As a result, hydrogen bonds are richly supportive to form around the surface of carbon fibers.

In this study, we have developed a straightforward and sensitive method to quantify the interfacial interaction between an isolated carbon fiber and various substrates. Through the introduction of polar (water) and nonpolar (hexane) medium into the interfacial region, hydrogen bonding and vdW force between the fiber and the substrate will be generated separately to mediate the interfacial interaction. By the joint efforts of experimental observation and atomistic simulation, it clearly shows that water pretreatment can significantly enhance the ISR and tighten the contact facilitated by hydrogen bonding. Our study would benefit the rational design and assembly of new materials together by the tunable interfacial interaction.

5.2 Experimental Section

5.2.1 Materials and characterizations

Aramid fibers (DAF III, Bluestar Chengrand Chemical Co. Ltd. China) and carbon fibers (T700-SC, Toray) were characterized by optical workstation (Micromanipulator 6200), SEM (AMR 1820) at voltage of 10 kV, and FTIR (ABB-Bomem FTLA 2000). The epoxy to bridge the carbon fiber and aramid fiber is Hardman double bubble blue general purpose slow-setting epoxy. The water used in this study is deionized water. Anhydrous hexane was ordered from Sigma-Aldrich, Inc. The Au was coated on silicon

wafer by a Denton desk sputter. The contact angle between H_2O and Au coated glass was measured by optical contact angle measurement tester (OCA200, Dataphysics).

5.2.2 Mechanical characterization of aramid fibers for force sensing

To measure elastic modulus of aramid fibers, tensile test was performed using a Gatan™ Deben micro-tester (Gatan, Inc., U.K.). A load cell of 200 N was used to monitor and collect the load continuously. During tensile test, the loading rate was set as 1.2 mm/s. The force-displacement was directly obtained after tensile testing.

5.2.3 In-house nanomechanical tester

The in-house nanomechanical tester is composed of a XYZ motorized five-axis aligner (8081.UHV, Newport, CA) and a sensing fiber made of an aramid fiber. The linear stages are driven by picomotors. The displacement resolution is 30 nm/step. The force resolution depends on the spring constant of the sensing fiber. The nanomechanical tester can be placed on the stage of the optical workstation which will facilitate the observation of mechanical behaviors of tested samples. A digital camera mounted on the workstation can capture video as well.

5.2.4 Debonding carbon fiber out of substrate

A carbon fiber was bridged to the sensing fiber by a tiny epoxy. The carbon fiber was loaded at edge of an FTO glass with contact length of ~0.30 mm. To quantify the interfacial interaction, the carbon fiber was pulled out by the sensing fiber. The force was specific by the force divided by the contact length between the carbon fiber and the substrate, regarding the contact could be different. To quantify the interfacial interaction dominated by hydrogen bonding, a drop of water (~50 μL) was loaded onto

the contact area between the carbon fiber and the FTO glass. The whole setup was exposed in air for 24 hours to evaporate the water. Subsequently, the carbon fiber was pulled out of the FTO glass. To quantify the interfacial interaction dominated by vdW force, a drop of hexane (~50 μL) was loaded between a carbon fiber and an FTO glass as well as between a carbon fiber and an Au coated substrate. The other procedures are exactly same as those in the test with water pretreatment. The direct competition between hydrogen bonding and vdW force was created between the carbon fiber and the Au coated substrate with water bridging. The debonding testing was carried out after the water evaporates.

5.3 Results and discussion

Among 1D fibers as well as between individual 1D fiber and a substrate, both vdW force and hydrogen bonding are very challenging to be quantified due to their reversibility. To this end, a facile in-house nanomechanical tester with tunable force resolution has been built and schematically demonstrated in Figure 5.1a. The aligner, which is driven by picomotors along X, Y, and Z axes, can bring two objects to engage together. The applied load is sensed by an aramid fiber, which is fixed at the edge of a silicon wafer. Depending on the requirement of force resolution, fibers with selected sizes can be used to measure the critical force. Under small deformation assumption ($\delta << L$),[115116] the load P and the deflection δ (Shown in the Figure 5.1b) will maintain a linear relationship which can be written as $P=k\delta$, where the spring constant k depends on the diameter d, elastic modulus E, and suspended length L of the sensing fiber:

$$k = \frac{3\pi d^4 E}{64 L^3} \qquad \text{Equation 5.1}$$

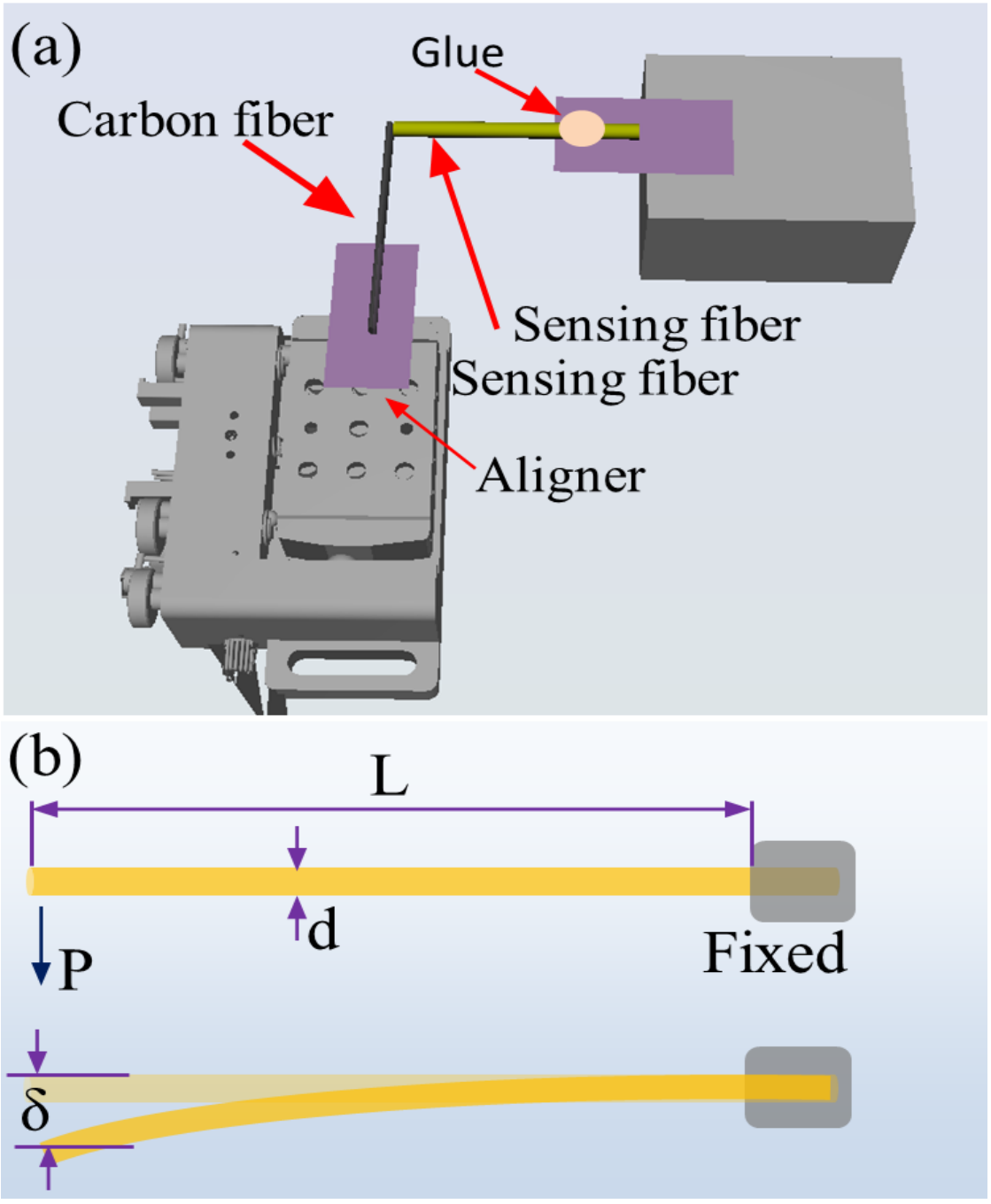

Figure 5.1 Setup for sensing interfacial interaction. (a) An in-house setup with aligner driven by picomotors for measuring the ISR. (b) Anchored aramid sensing fiber before and after loading with load calculated by the product of deflection and spring constant.

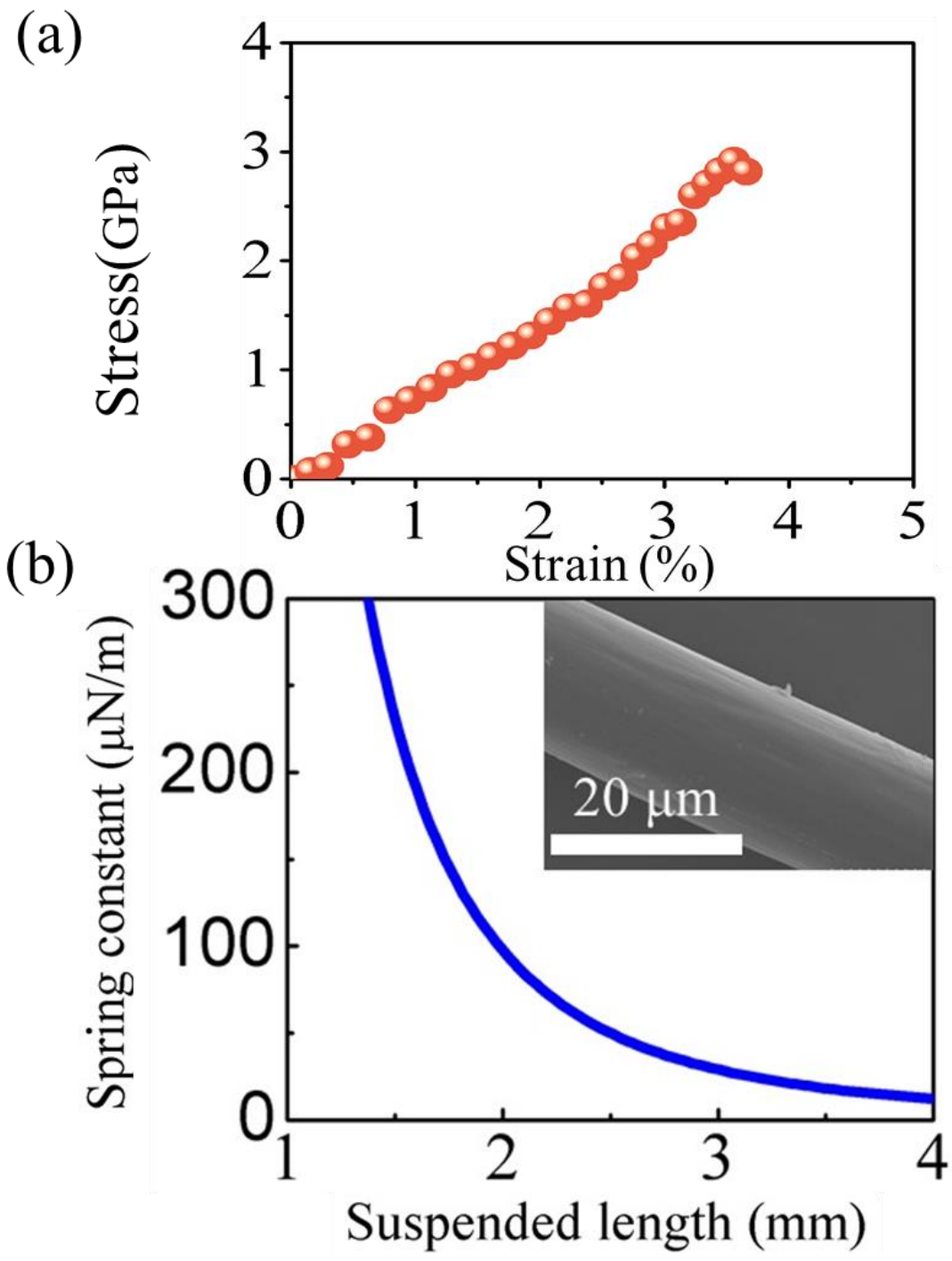

Figure 5.2 Shows (a) A representative stress-strain curve of the aramid fiber for elastic modulus measurement. (b) The relationship between the spring constant *k* and suspended length *L* with given diameter of 17.4 μm and elastic modulus of 78.7 GPa. The inset in (b) is a scanning electron microscope (SEM) image of the aramid fiber

Seven aramid fibers were tested through the uniaxial tensile testing to get their elastic modulus. A representative stress-strain curve is included in Figure 5.2a. The measured elastic modulus of the aramid fibers is 78.73±14.73 GPa. Also, the mechanical properties of all tested fibers can be seen in the Table 5.1. The inset in Figure 5.2b shows a SEM image of an aramid fiber. The advantage of the in-house nanomechanical tester is to maintain a high-degree and compatible force resolution as the above formula suggests. Generally, the spring constant of a commercial atomic force microscopy (AFM) probes ranges from 0.01 N/m to 450 N/m. The spring constant of the sensing fibers used in this study is 0.0043.0.157 N/m as shown in the Table 5.2.

Table 5.1 Mechanical Properties of Aramid Sensing Fibers

Test #	Fiber Diameter μm	Tensile Strength GPa	Elastic Modulus GPa
Test 1	17.4	2.08	50.76
Test 2	17.4	3.94	93.18
Test 3	17.4	2.71	81.04
Test 4	17.4	2.85	93.41
Test 5	17.4	3.64	70.14
Test 6	17.4	3.60	82.46
Test 7	17.4	2.63	80.14
Average ± standard deviation		3.06 ±0.67	78.73±14.73

Table 5.2 Spring constant measurement of individual aramid sensing cantilevers.

Sensor #	Fiber Diameter μm	Elastic Modulus GPa	Length mm	Spring constant N/m
Sensor 1	17.4	78.73	5.60	0.0043
Sensor 2	17.4	78.73	2.55	0.046
Sensor 3	17.4	78.73	1.69	0.157
Sensor 4	17.4	78.73	3.56	0.017
Sensor 5	17.4	78.73	2.67	0.040
Sensor 6	17.4	78.73	2.56	0.045
Sensor 7	17.4	78.73	2.97	0.029
Sensor 8	17.4	78.73	2.56	0.045

The smallest spring constant is below the minimal resolution of the commercial AFM probes. The fiber with longer suspended length and smaller diameter can be applied to sense imperceptible force. For example, if a carbon fiber has a diameter of 7.5 μm and a suspended length of 10 mm, the calculated spring constant will be ~0.0001 N/m, which is two-order lower than the minimal resolution of the commercial AFM probes. The spring constants in our study are high enough to quantitatively measure the vdW force and hydrogen bonding precisely. Figure 5.1b interprets the relation between the spring constant k and the suspended length L with a fixed diameter d = 17.4 μm.

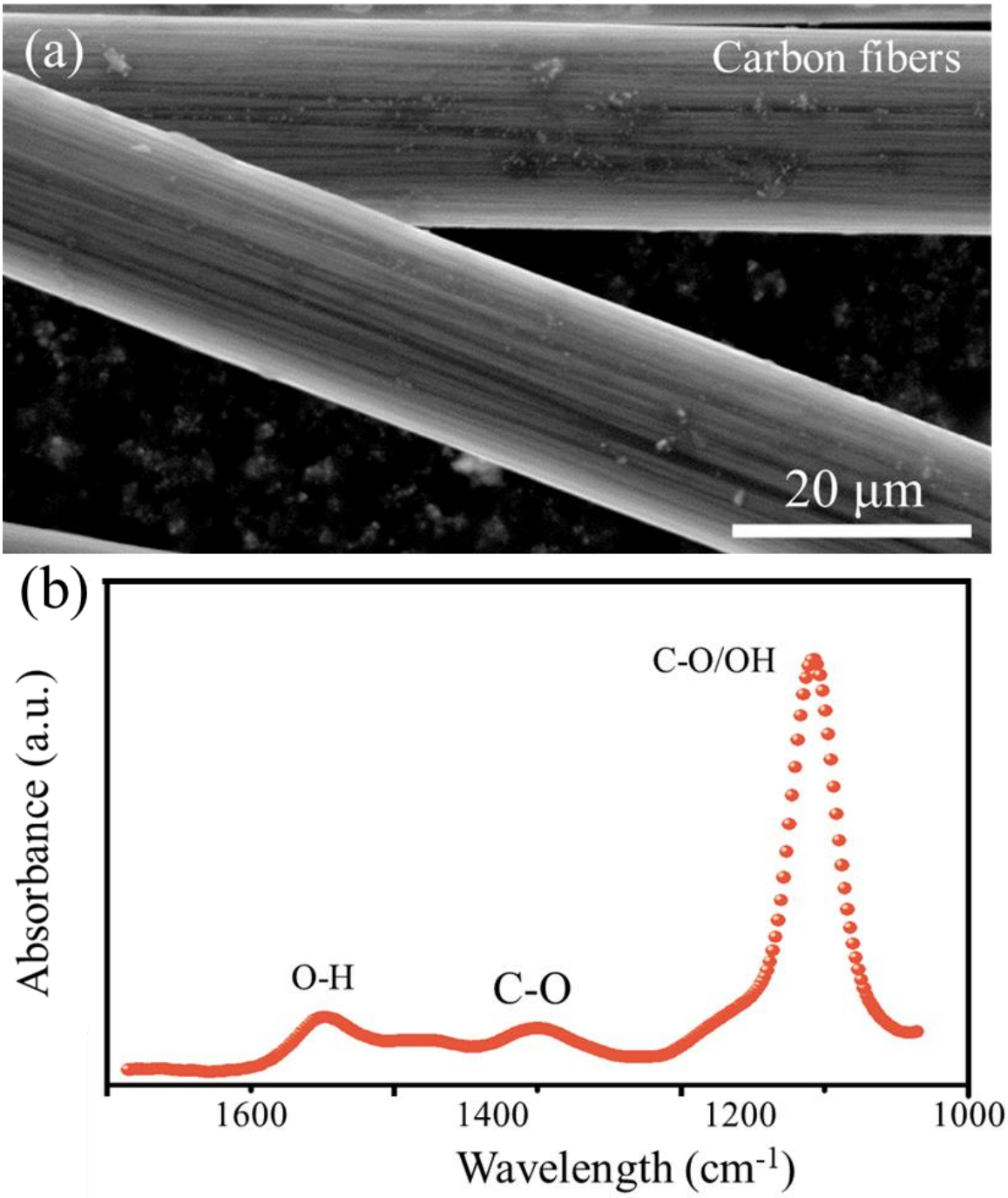

Figure 5.3 Show (a) SEM image of carbon fibers. (b) Fourier-transform infrared spectroscopy (FTIR) spectrum of the carbon fibers.

Carbon fibers (Figure 5.3a) with a diameter of 7.5 μm, on which hydrophilic phenol and carboxyl groups are identified by the FTIR spectrum (Figure 5.3b), are chosen to create hydrogen bonding and vdW

force with substrates. The measurement of ISR was realized by debonding a carbon fiber out of the substrate. The interfacial region between two surfaces was pretreated by polar (H_2O) or nonpolar (Hexane) medium. Table 5.3 summerizes the designed experiment for debonding tests under interfacial interaction dominated by either hydrogen bonding or vdW force.

Table 5.3 Experimental design for debonding tests under interfacial interaction dominated by either hydrogen bonding or vdW force.

Tested fiber	**Substrate**	**Medium**	**Bonding between carbon fiber and medium**	**Bonding between medium and substrate**
Carbon fiber	FTO glass	-	-	-
Carbon fiber	FTO glass	H_2O	Hydrogen bonding	Hydrogen bonding
Carbon fiber	FTO glass	Hexane	vdW force	vdW force
Carbon fiber	Au coated glass	-	-	-
Carbon fiber	Au coated glass	H_2O	Hydrogen bonding	vdW force
Carbon fiber	Au coated glass	Hexane	vdW force	vdW force

The FTO substrate can form hydrogen bonds with water molecules via the fluorine and oxygen atoms, while the Au substrate is incapable of forming any hydrogen bonding but only vdW force because of inert Au atoms. In contrast to polar water forming hydrogen bond, nonpolar hexane can only bridge the interfacial region with vdW force.

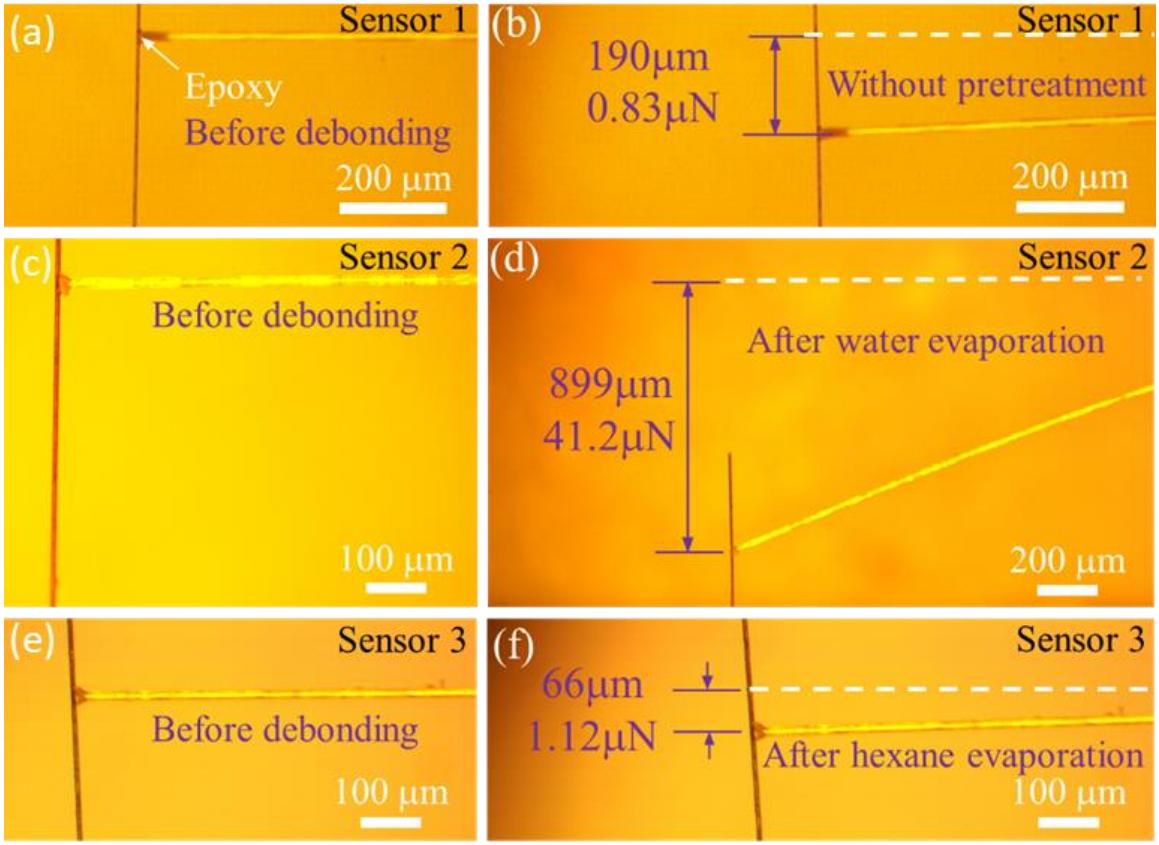

Figure 5.4 Debonding tests between individual carbon fiber and FTO glass. (a) Optical image of a bridged carbon fiber and an aramid sensing fiber. (b) The last moment before debonding of the fiber in (a) without any pretreatment. (c) Original bridged carbon fiber and sensing fiber before debonding test. (d) The last moment before debonding of the fiber in (c) with water pretreatment. (e) Original bridged carbon fiber and sensing fiber before debonding test. (f) The last moment before debonding of the fiber in (e) with hexane pretreatment. The insets are the segment of the carbon fiber sitting on the FTO glass.

Firstly, we conducted three comparative debonding tests through the mentioned device to unveil the role of polar and nonpolar medium in the interfacial region. Figure 5.4 compares the debonding of the carbon fiber out of the FTO glass without and with either H_2O or hexane pretreatment. A carbon fiber was first fixed to a sensing fiber perpendicularly with a tiny epoxy. The carbon fiber together with the sensing fiber was then loaded on the XYZ motorized aligner with a step resolution of 30 nm toward the FTO glass.

The dry carbon fiber is first placed onto the FTO glass. The contact length between the carbon fiber and the FTO glass is 0.29 mm. The spring constant of the used sensing fiber is 0.0043 N/m (Sensor 1). The carbon fiber was pulled along axial direction at a constant speed of 180 nm/s. The entire debonding test was monitored by a digital camera mounted to the probe station. During the debonding test, the maximum deflection of the sensing fiber is 190 μm as shown in Figure 5.4 b and the specific ISR (load per contact length between the carbon fiber and the substrate) is 2.86 μN/mm. Three more tests were conducted. Details of spring constants, deflections, and ISR are shown in the Table 5.4. The average specific ISR is as low as 2.65±0.51 μN/mm. Also, all the debonding tests of the individual carbon fiber out of FTO glass without water pretreatment are shown in the Figure 5.5.

Table 5.4 Specific ISR between individual carbon fiber and FTO glass without water pretreatment.

Test #	Sensor #	Spring constant (N/m)	Contact length (mm)	Deflection (μm)	Debonding force (μN)	Specific ISR (μN/mm)
1	1	0.0043	0.29	220	0.95	3.27
2	1	0.0043	0.29	143	0.62	2.14
3	1	0.0043	0.29	190	0.83	2.86
4	1	0.0043	0.29	154	0.68	2.34
Average ± standard deviation						2.65±0.51

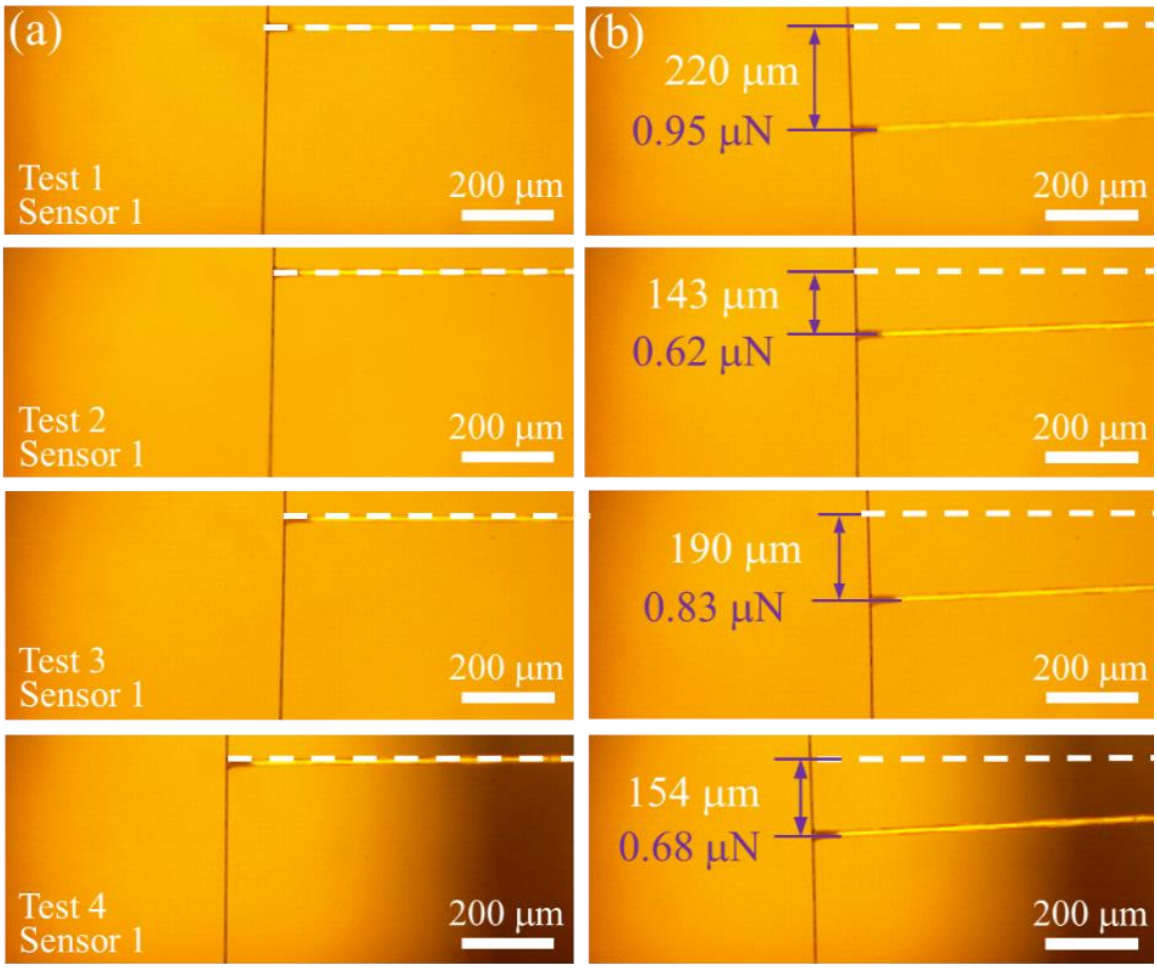

Figure 5.5 Debonding of individual carbon fiber out of FTO glass without water pretreatment. Column (a) Optical image of bridged carbon fiber and aramid sensing fiber before debonding test. Column (b) Last moment before debonding the carbon fiber out of the FTO glass.

To mediate the interfacial bonding through the water pretreatment, a drop of deionized (DI) water (~50 µL) was dropped onto the contact area between the carbon fiber and the FTO glass. The setup was exposed at ambient condition for 24 hours to get rid of the water. The spring constant of the used sensing fiber is 0.046 N/m (Sensor 2). During the debonding test, the maximum deflection of the sensing fiber surprisingly reached as high as 899 µm as shown in Figure 5.4 d and the specific ISR is 147.14 µN/mm, which indicates that the interfacial interaction is dramatically enhanced after water bridges the interfacial gap and then fully evaporates. Three more tests were conducted. Details of spring constants, deflections,

etc, are shown in the Table 5.5. Also, all the debonding tests of the individual carbon fiber out of FTO glass with water pretreatment are shown in the Figure 5.6. The average specific ISR is 157.86±44.18 μN/mm, which is ~60 times higher than the ISR from debonding the carbon fiber out the FTO without any pretreatment. It has been confirmed by the FTIR spectrum (Figure 5.3b) that there are several types of hydrophilic functional groups on the surface of carbon fibers, such as hydroxyl group (O−H), carboxyl group (O=C−O−H). These residual −OH groups, which can be sourced from the typical manufacture process of carbon fiber, [112113114] serve as the latent binding sites of hydrogen bond network. With the introduction of water into the interfacial region, hydrogen bond network is immediately formed between the carbon fiber and the FTO substrate due to their hydrophilic surface. The water evaporation will bring the two surfaces to the distance forming hydrogen bonding. In contrast, if there is no water involved, the large surface distance will prevent the formation of hydrogen bonding between the carbon fiber and the FTO glass, accounting for the lower specific ISR.

Table 5.5 Specific ISR between individual carbon fiber and FTO glass with water pretreatment.

Test #	Sensor #	Spring constant (N/m)	Contact length (mm)	Deflection (μm)	Debonding force (μN)	Specific ISR (μN/mm)
1	2	0.046	0.28	899	41.35	147.14
2	2	0.046	0.28	869	39.97	142.14
3	2	0.046	0.28	736	33.86	120.36
4	3	0.157	0.28	395	62.02	221.79
Average ± standard deviation						157.86±44.18

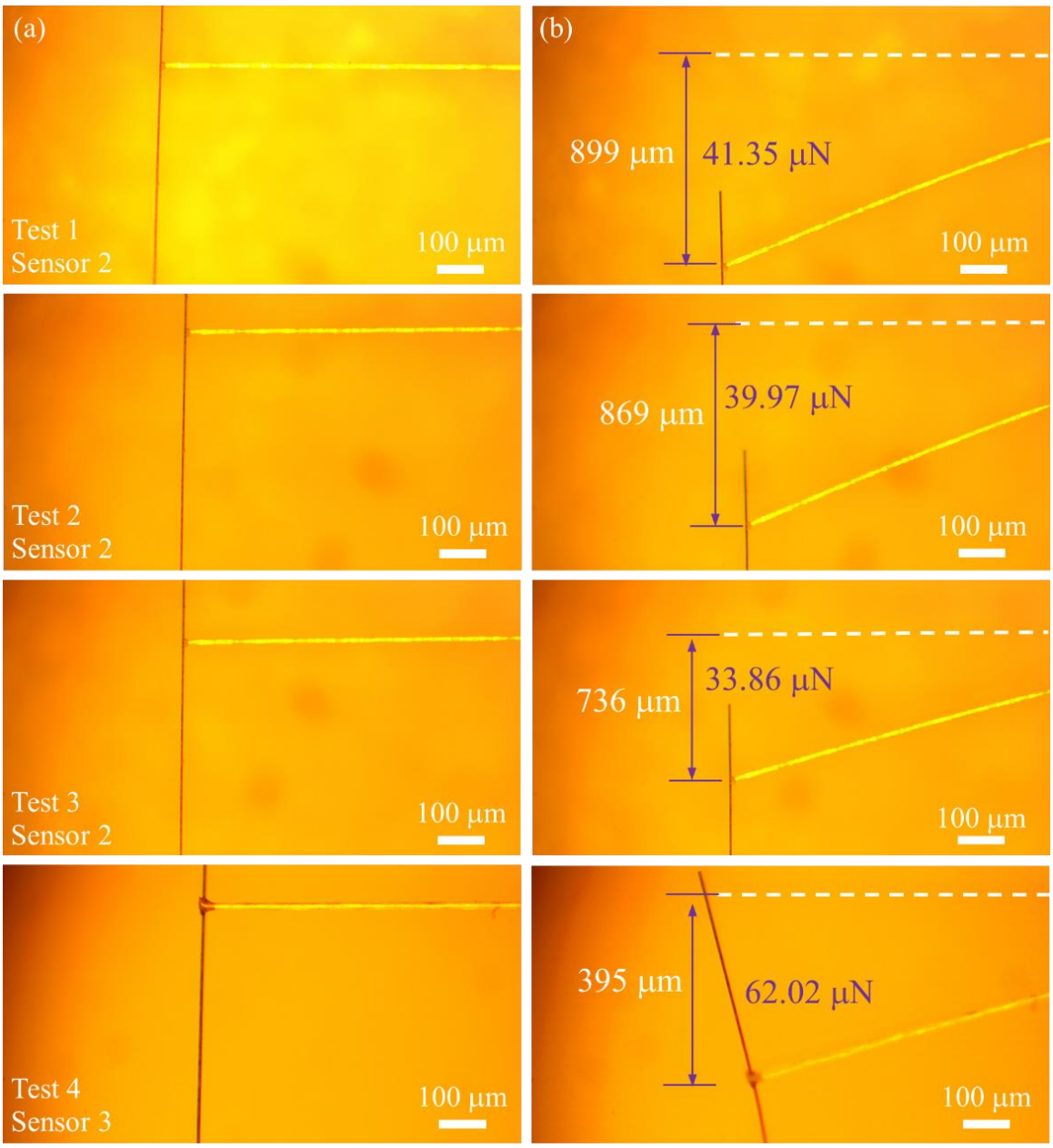

Figure 5.6 Debonding of individual carbon fiber out of FTO glass with water pretreatment. Column (a) Optical image of bridged carbon fiber and aramid sensing fiber before debonding test. Column (b) Last moment before debonding the carbon fiber out of the FTO glass with water pretreatment.

To further confirm that the enhanced ISR is mainly from the hydrogen bonding rather than vdW force, liquid hexane as a nonpolar medium, which is apparently absent from forming hydrogen bond, is introduced into the interfacial region as a comparative study. Nonpolar hexane is volatile at room temperature with a boiling temperature at 68 °C. Following the same debonding test route, a carbon fiber was pulled out of the FTO glass after the hexane fully evaporated. The optical images of the carbon fiber bridged to the sensing fiber and the moment right before debonding are shown in Figure 5.4e and 5.4f, respectively. The contact length of the carbon fiber sitting on the FTO glass. The maximum deflection is 66 μm and the specific ISR is 4.0 μN/mm. With three more tests, Table 5.6 shows the details of spring constants, deflections, etc. The average specific ISR is 3.55±0.50 μN/mm, which is slightly higher than the average specific ISR with no pretreatment, 2.65±0.51 μN/mm. Also, all the debonding tests of the individual carbon fiber out of FTO glass with hexane pretreatment are shown in the Figure 5.7.

Table 5.6 Specific ISR between individual carbon fiber and FTO glass with hexane pretreatment.

Test #	Sensor #	Spring constant (N/m)	Contact length (mm)	Deflection (μm)	Debonding force (μN)	Specific ISR (μN/mm)
1	4	0.017	0.28	66	1.12	4.00
2	4	0.017	0.28	65	1.10	3.93
3	5	0.040	0.28	21	0.83	2.96
4	5	0.040	0.28	23	0.93	3.32
Average ± standard deviation						3.55±0.50

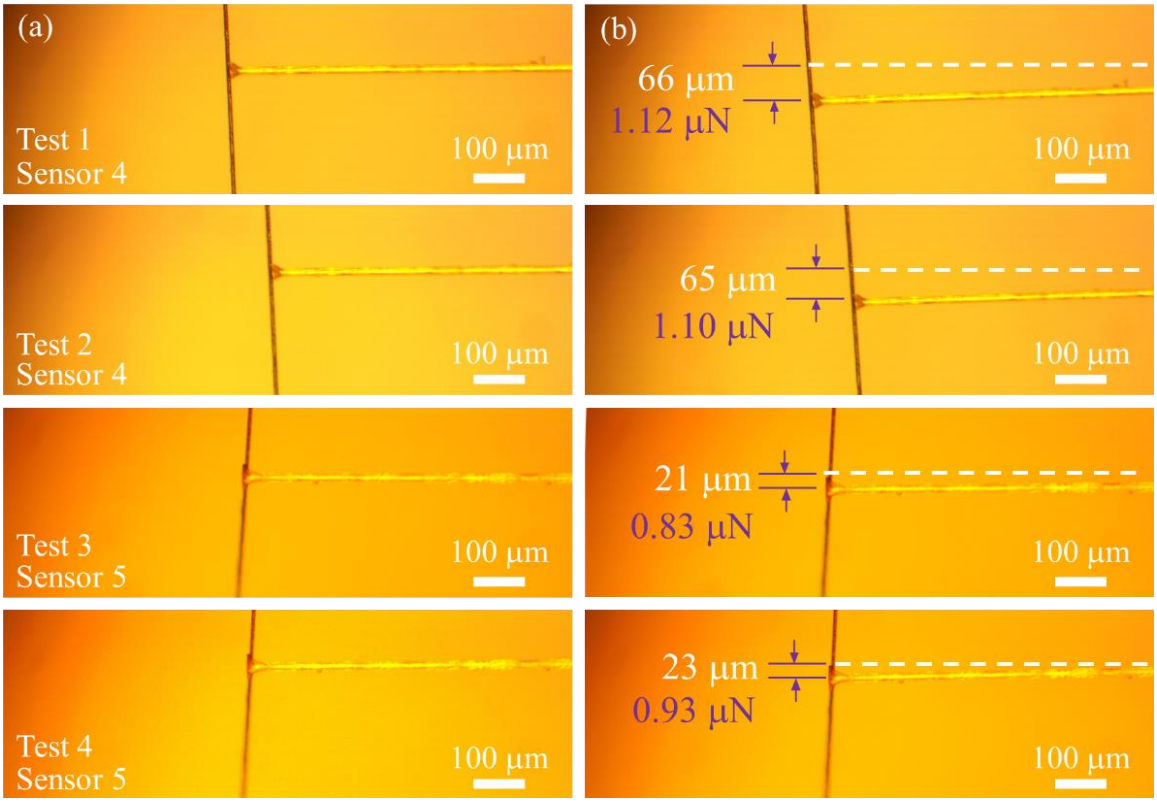

Figure 5.7 Debonding of an individual carbon fiber out of FTO glass with hexane pretreatment. Column (a) Optical image of bridged carbon fiber and aramid sensing fiber before debonding test. Column (b) Last moment before debonding the carbon fiber out of the FTO glass with hexane pretreatment.

For macroscopic bodies with known volumes and numbers of atoms per unit volume, theoretically, the total vdW force can be calculated by integration of all interacting pairs. For example, the vdW interaction energy between two spherical bodies with radius of R_1 and R_2 and with the closest surface distance $d_{1.2}$ was predicted by H.C. Hamaker.[117] If $d_{1.2}$ is much less than R_1 and R_2, the potential energy U can be written as

$$U(r; R_1; R_2) = -\frac{AR_1R_2}{6(R_1+R_1)d_{1-2}} \qquad \text{Equation 5.2}$$

Where *A* is the Hamaker coefficient (~10^{-19}-10^{-20} J) which depends on the material properties. Since the force on an object is negative to the derivative of the potential energy function and the radius of flat FTO glass can be regarded as infinite. The vdW force can be rewritten as:

$$F_{vdW}(r) = -\frac{AR_c}{6d_{c-f}^2} \qquad \text{Equation 5. 3}$$

Where the radius of carbon fiber R_c is 3.75 μm and $d_{c\text{-}f}$ is surface distance between the carbon fiber and the FTO glass. Since hydrogen bonding is not supportive to form on the surface of carbon fiber and FTO substrate after the hexane pretreatment, weak vdW force offered by nonpolar hexane has limited capability to bring the two surfaces closer. Therefore, the specific ISR dominated by weak vdW force is still low after the hexane pretreatment. In contrast, the ISR after water evaporation is ~60 times higher than that without water pretreatment, which suggests that hydrogen bonding would dominate the interfacial region and sew the interface between carbon fiber and FTO glass.

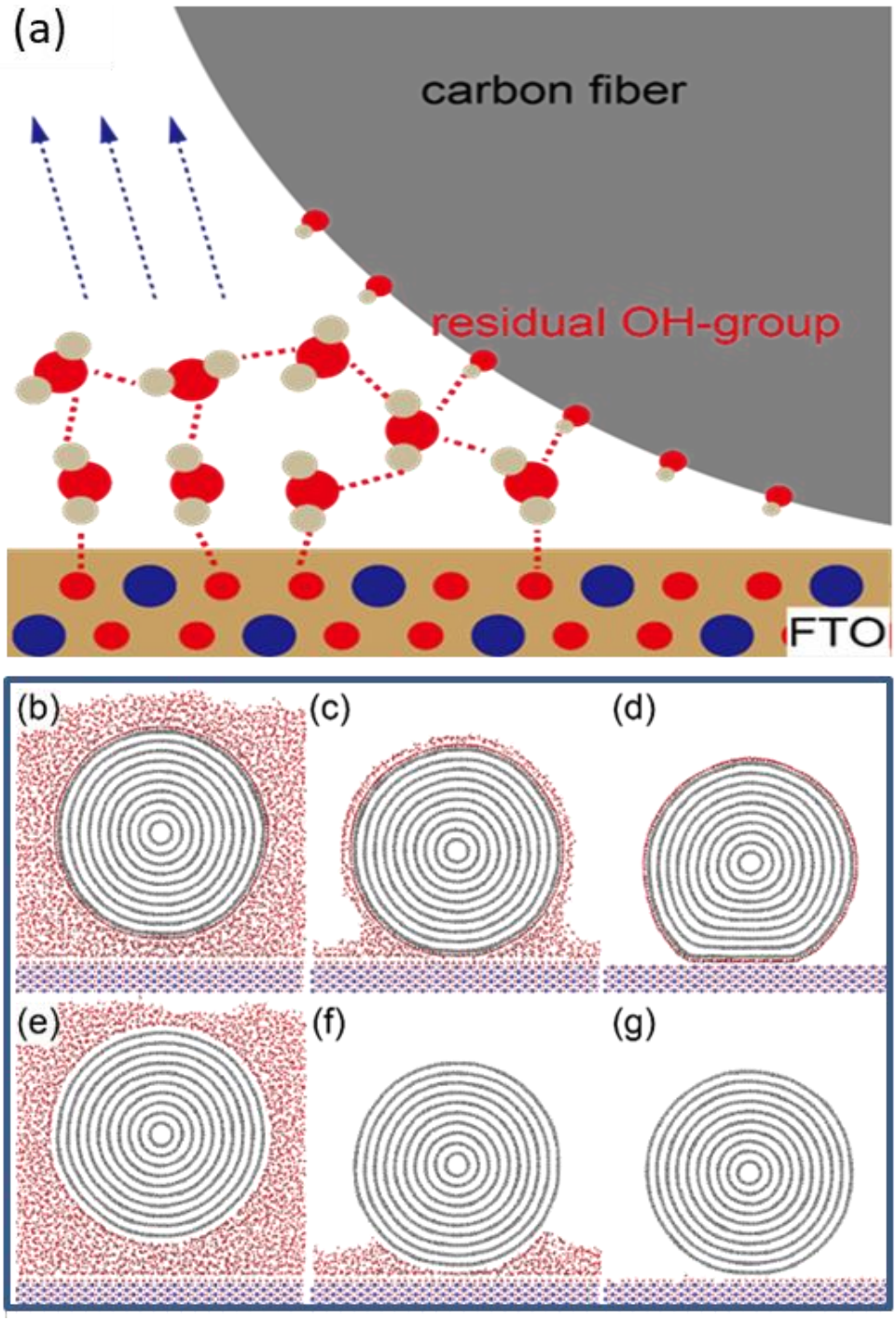

Figure 5.8 A minimal simulated model of water evaporation process in the interface between the carbon fiber and FTO glass. (a) Schematic of water evaporating from the interface; (b-d) water evaporating from the interface between FTO glass and carbon fiber with residual OH-group; (e-g) water evaporating from the interface between FTO glass and carbon fiber without residual OH-group.

These comparative results indicate that, regardless of polar or nonpolar medium, the liquid pretreatment can intrinsically strengthen the interfacial interaction by tightening the contact of two surfaces. The improvement is directly reflected by the increased ISR. However, the underlying physical origin of the increased ISR is quite different. After the water pretreatment, a huge increase in ISR is beneficial from the formation of hydrogen bond network between FTO substrate and carbon fiber, which is absent from a negligible increase in the hexane pretreatment.

To visualize the role of water pretreatment in the debonding test, a set of atomistic simulations is presented to provide the atomic insights of the enhanced interfacial bonding induced by water pretreatment. A minimal simulated model of water evaporation process is set up in Figure 5.8a. The carbon fiber is modelled as a 2 nm-long multiwalled carbon nanotube (MWCNT, 10 walls) with radius of 5 nm and the FTO is simplified as a crystalline SnO_2 substrate. The interface between MWCNT and SnO_2 substrate are fully drown in water solution with 3973 water molecules. As a comparative study, both MWCNT with and without residual OH-group are investigated, where the residual OH-group is randomly distributed on the outside of the MWCNT with 50% oxidation ratio (carbon number occupied by OH-group/total carbon number). The whole system is equilibrated under temperature 300 K for more than 5 newton-second (ns) and the gap between MWCNT and substrate is kept at about 2 nm. The force field is OPLS-AA (OPLS-AA id Optimized Potentials for Liquid Simulations all atom), which can capture the interfacial properties between water and carbon nanostructures accurately. The water evaporation process is simulated by random delete algorithm implemented in Large-scale Atomic/Molecular Massively Parallel Simulator (LAMMPS) package and the temperature of remaining water solution is dynamically controlled at 300 K during the evaporation process with low evaporation rate at 6 molecules/ps.

It clearly shows that the residual OH-groups make the MWCNT more hydrophilic and water molecules intend to encapsulate the MWCNT and stick around the interface as shown in Figure 5.8c, which facilitates the forming of compact hydrogen bond network. As the evaporation process goes on, the water layer drags the MWCNT closer to the substrate and the hydrogen bond network sews the interface gradually and renormalizes the interfacial interaction. Finally, a more compact interface is formed with strengthened ISR and larger contact area in Figure 5.8d. If the surface is without residual OH-group, in a sharp contrast, water molecules will fully evaporate and leave the substrate dry as same as before wetting as shown in Figure 5.8e-g.

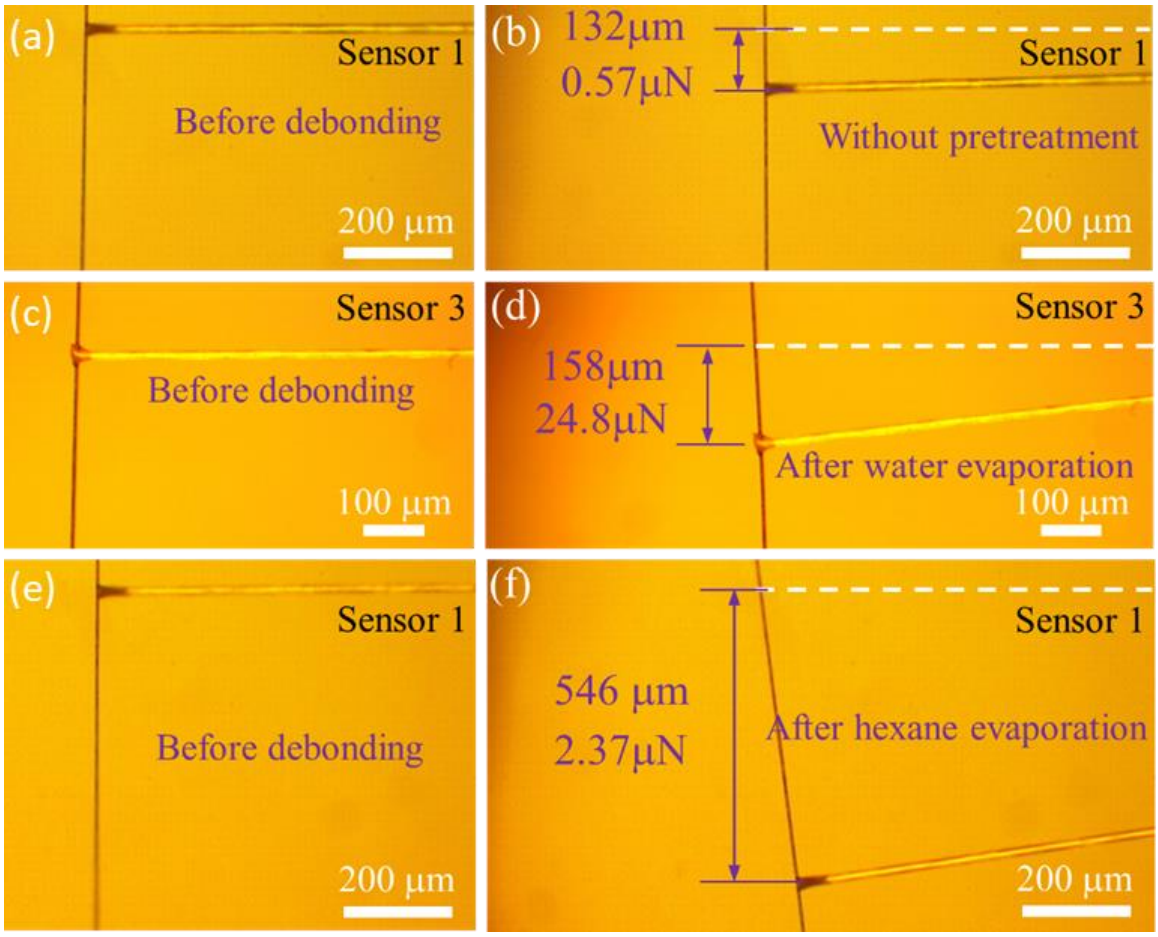

Figure 5.9 Debonding tests between individual carbon fiber and Au coated glass. (a) Optical image of a bridged carbon fiber and an aramid sensing fiber. (b) The last moment before debonding in (a) without any pretreatment. (c) Original bridged carbon fiber and sensing fiber for debonding test. (d) The last moment before debonding in (c) with water pretreatment. (e) Original bridged carbon fiber and sensing fiber before debonding test. (f) The last moment before debonding in (e) with hexane pretreatment. The insets are the segment of the carbon fiber sitting on the Au coated glass.

Regardless of the pretreatment by H_2O or hexane, the FTO glass always has the possibility to form hydrogen bonds with the residual OH-group on the surface of carbon fiber. To completely rule out the contribution of hydrogen bonds during the pretreatment process, Au coated glass, which cannot form

hydrogen bonds with carbon fiber and polar H_2O, is chosen as the substrate for the comparative study. The interaction between the Au substrate and liquid medium will be mainly in the form of vdW force. Figure 5.9 demonstrates three comparative debonding tests between individual carbon fiber and Au substrate without and with either water or hexane pretreatment. When there is no pretreatment between individual carbon fiber and substrate, the specific ISR on the Au substrate (Figure 5.9a and 5.9b) is 1.97 μN/mm. Three more tests were conducted. The average specific ISR is 1.42±0.49 μN/mm, which is close to that on the FTO glass (Figure 5.4a and 5.4b). Details of spring constants, deflections, and specific ISR without pretreatment are shown in the Table 5.7. The results suggest that the interfacial interaction between carbon fiber and Au or FTO substrate is mainly dominated by vdW force, if there is no pretreatment. Figure 5.10 show all the debonding tests (before and after the debonding) of the individual carbon fiber after using Au coated glass substrate without pretreatment.

Table 5.7 Specific interfacial sliding resistance between individual carbon fiber and Au coated glass without pretreatment.

Test #	Sensor #	Spring constant (N/m)	Contact length (mm)	Deflection (μm)	Debonding force (μN)	Specific ISR (μN/mm)
1	1	0.0043	0.29	62	0.27	0.93
2	1	0.0043	0.29	132	0.57	1.97
3	1	0.0043	0.29	113	0.49	1.69
4	1	0.0043	0.29	73	0.32	1.10
Average ± standard deviation						1.42±0.49

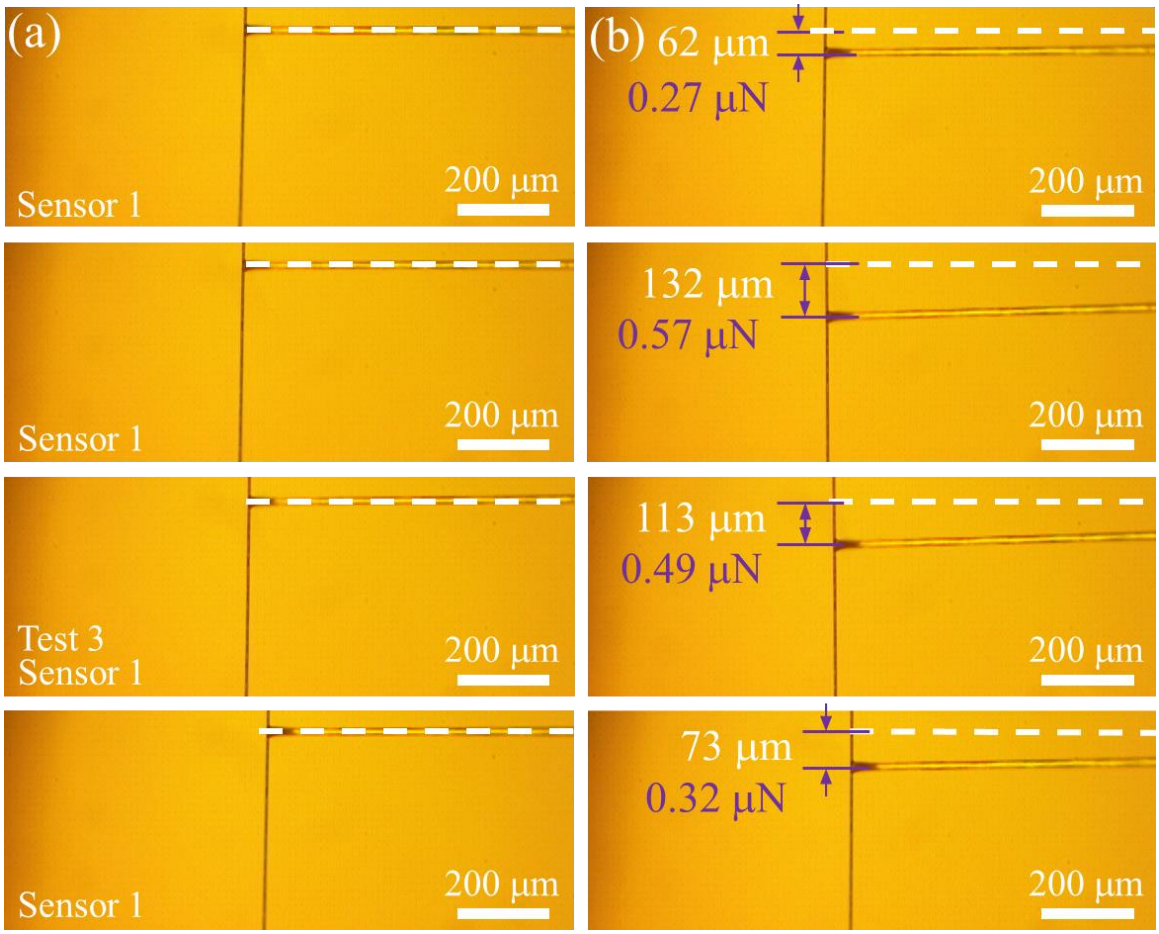

Figure 5.10 Debonding of individual carbon fiber out of Au coated glass without pretreatment. Column (a) Optical image of bridged carbon fiber and aramid sensing fiber before debonding test. Column (b) Last moment before debonding the carbon fiber out of the Au with water pretreatment.

Subsequently, a drop of water was used to fill the gap between carbon fiber and Au substrate, hydrogen bond network glues the water droplet and the carbon fiber, while vdW force bridge the Au substrate and the water droplet. After water evaporation, the debonding tests were conducted on the Au substrate as shown in Figure 5.9c and 5.9d. The calculated debonding force is 24.8 μN and the corresponding specific ISR is 88.57 μN/mm. Three more debonding tests were conducted to confirm this result and the average specific ISR is 98.21±7.03 μN/mm. Details of spring constants, deflections, and

specific ISR with water pretreatment are shown in the Table 5. 8. Figure 5.11 show optical images before and after the debonding of individual carbon fiber out of Au coated glass with water pretreatment.

Table 5. 8 Specific interfacial sliding resistance between individual carbon fiber and Au coated glass with water pretreatment.

Test #	Sensor #	Spring constant (N/m)	Contact length (mm)	Deflection (μm)	Debonding force (μN)	Specific ISR (μN/mm)
1	3	0.157	0.28	158	24.80	88.57
2	3	0.157	0.28	174	27.40	97.86
3	6	0.045	0.26	605	27.25	104.81
4	6	0.045	0.26	587	26.42	101.62
Average ± standard deviation						98.21±7.03

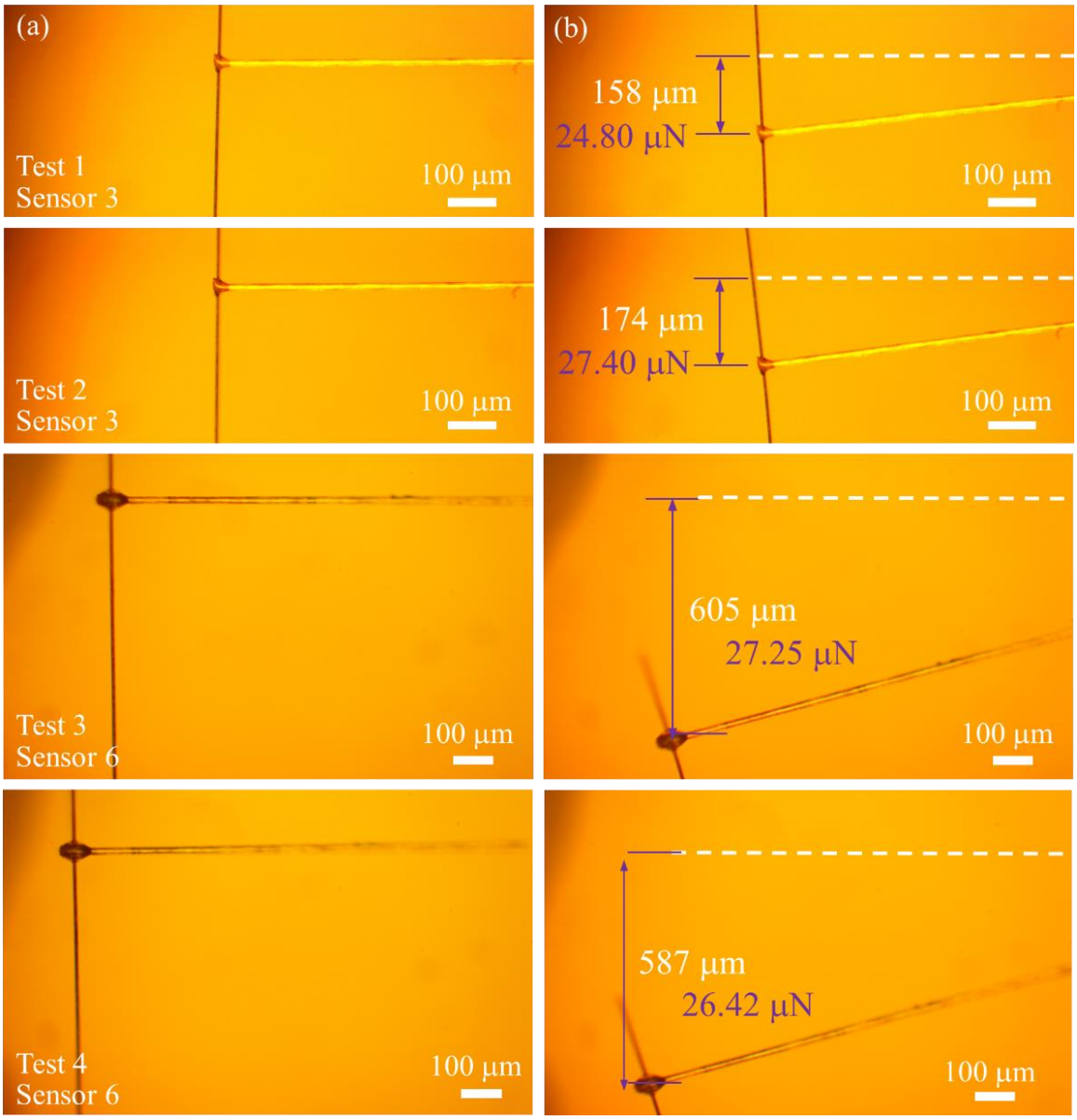

Figure 5.11 Debonding of individual carbon fiber out of Au coated glass with water pretreatment. Column (a) Optical image of bridged carbon fiber and aramid sensing fiber before debonding test. Column (b) Last moment before debonding the carbon fiber out of the Au with water pretreatment.

From the previous analysis, the contact between Au substrate and carbon fiber is dominated by vdW force, which is supposed to be very weak. Interestingly, this specific ISR after water pretreatment is

much higher than that after hexane pretreatment, which suggests that a much better contact is achieved through water renormalizing the interface. In order to reveal the role of water in the interfacial region, the contact angle between H_2O and Au was measured as 69.9° as shown in the Figure 5.12, which is close to the previous measurement.[118] Regarding the hydrophilic nature of Au surface, water fills in the interfacial gap between carbon fiber and Au substrate more smoothly than hexane, realizing a much closer contact with both sides. Thus, the vdW attraction is significantly enhanced due to the closer contact, which increases the contact area further and leads to a much stronger vdW attraction. Therefore, a much higher specific ISR is obtained due to the water pretreatment rather than hexane pretreatment because of the augmented vdW attraction.

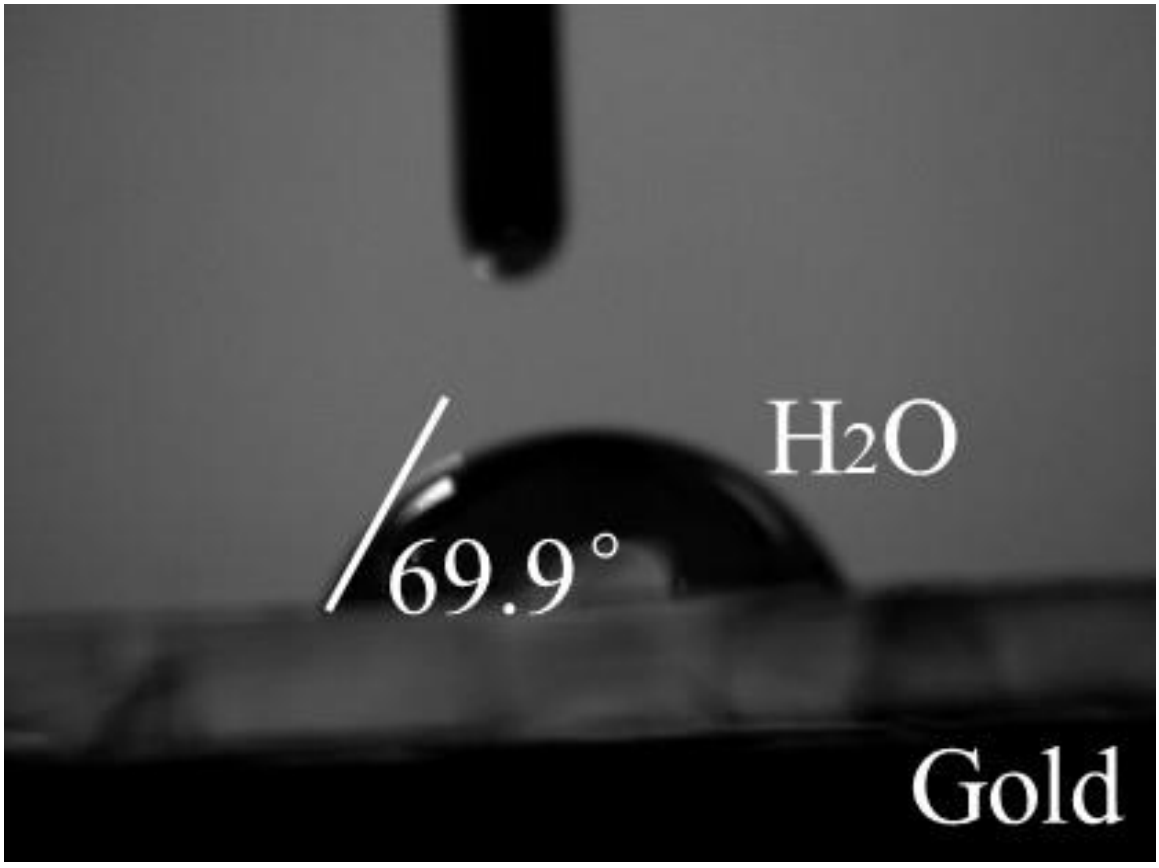

Figure 5.12 Measurement of contact angle between H_2O and Au coated glass.

Finally, another carbon fiber was pulled out of the Au coated glass after hexane evaporation (Figure 5.6e and 5.6f). With hexane pretreatment, the specific ISR on Au substrate is 3.70±1.14 μN/mm which is very close to that on the FTO glass. Apparently, the contact is dragged a little closer by the hexane pretreatment than no pretreatment since the specific ISR is a slightly higher due to the hexane evaporation. Details of spring constants, deflections, and specific ISR with hexane pretreatment are shown in the Table 5.9. Also, Figure 5.13 show un optical images before and after the debonding of individual carbon fiber out of Au coated glass with hexane pretreatment.

Table 5.9 Specific ISR between an individual carbon fiber and Au coated glass with hexane pretreatment.

Test #	Sensor #	Spring constant (N/m)	Contact length (mm)	Deflection (μm)	Debonding force (μN)	Specific ISR (μN/mm)
1	7	0.029	0.26	22	0.64	2.46
2	8	0.045	0.26	27	1.12	4.67
3	1	0.0043	0.31	305	1.45	4.67
4	1	0.0043	0.33	231	0.99	3.01
Average ± standard deviation						3.70±1.14

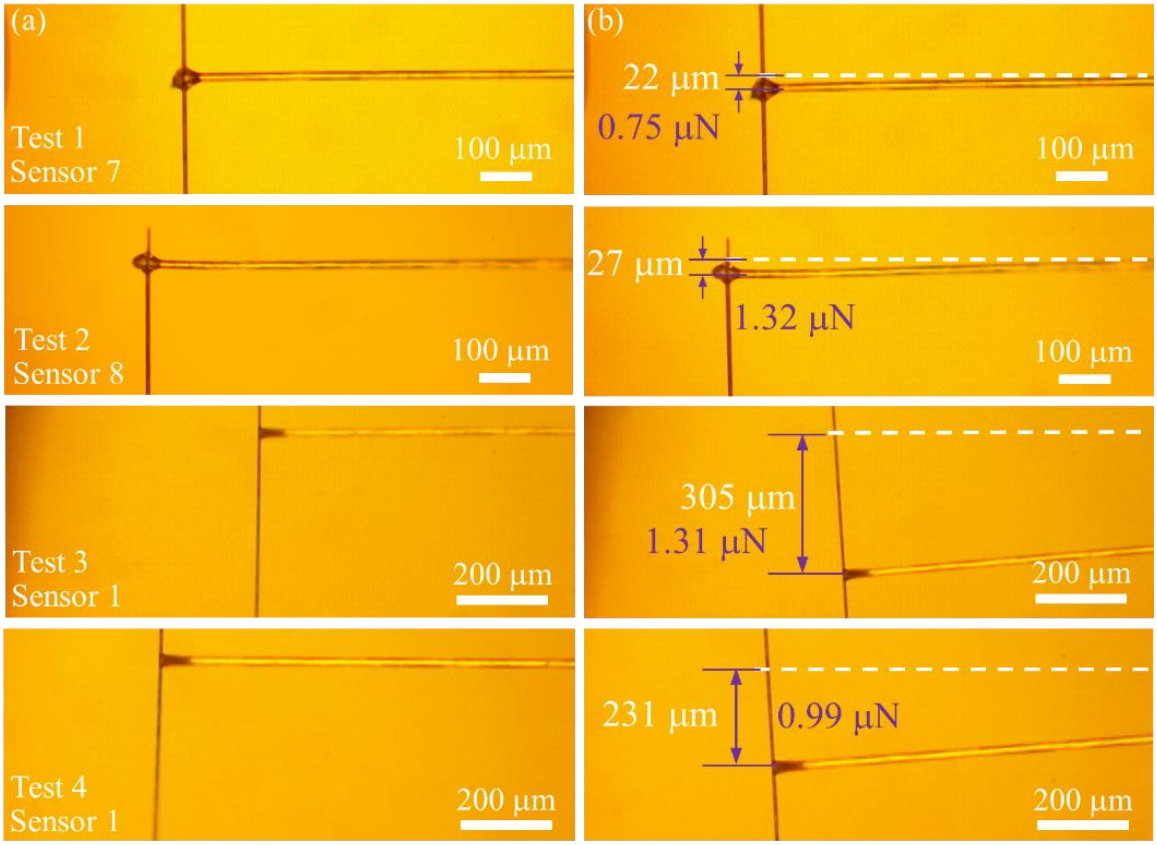

Figure 5.13 Debonding of individual carbon fiber out of Au coated glass with hexane pretreatment. Column (a) Optical image of bridged carbon fiber and aramid sensing fiber before debonding test. Column (b) Last moment before debonding the carbon fiber out of the Au with hexane pretreatment.

In summary, the weak force signals (vdW force and hydrogen bonding) which have been generally ignored in macroscopic materials systems have been measured and distinguished by an in-house nanomechanical tester. Facilitated by evaporation of polar and nonpolar medium between carbon fiber and selected substrates, the interfacial interaction has been created with either hydrogen bonding or vdW force. The specific ISR for the interface dominated by hydrogen bonding is ~60 times higher than that bridged by vdW force. The significant difference in interfacial interaction suggests that hydrogen bonding rather than vdW force has higher potential in sewing the interface if both surfaces

are supportive to form hydrogen bonds. The research would benefit the rational design and assembly of new materials together by the tunable interfacial interaction.

CHAPTER SIX

6 CONCLUSION AND RECOMMENDATION FOR FUTURE WORK

6.1 Conclusion of mechanical properties

The mechanical properties of aramid fibers and the interface mechanics between the fibers and the polymer matrix have been investigated in this study. Aramid fibers have been widely engineered into composites with various matrices to acquire their unique properties. These reinforced composites may not have a high mechanical performance attributable to the smooth and inert surface of aramid fibers. To improve the IFSS between aramid fiber and the polymer matrix, surface roughness of the aramid fibers had been increased by using the oxygen plasma treatment, the surface of the aramid fibers had been enriched with some functional groups through plasma or chemical treatments and coating the aramid fibers with some particles.

6.1.1 Applying the oxygen plasma treatment to improve the IFSS by increasing the surface roughness

The mechanical properties of aramid fibers upon plasma treatment and the interface mechanics between the fibers and the polymer matrix have been investigated in this study. The tensile strength and elastic modulus of the fibers severely decrease after 5 min of plasma treatment, while the mechanical properties rebound with extension of the treatment due to the elimination of surface defects. Unlike the decrease in tensile strength, the IFSS between the polymer matrix and the fibers with 5 min of treatment reaches the highest value of 34.91 ± 3.01 MPa which is attributed to the strong interface interlocking. By comparing the IFSS of the fibers with various degrees of treatment, surface roughness rather than functional groups dominates the interface interaction during mechanical failure. To address the stability

issue of the composites at elevated temperatures, a PDC has been used to strengthen the interface between individual aramid fibers and the polymer. The IFSS value was 26.10 ± 5.23 MPa at 100 °C, it considers high compares with that of untreated fibers tested at room temperature. Therefore, PDC may enable the aramid fiber reinforced composites to find more practical applications, especially, in a high-temperature environment.

6.1.2 Using the oxygen plasma treatment to improve the IFSS by enriching the fibers' surface with functional groups

The active period of the functional groups after plasma treatment has been carefully evaluated. After one day placement in air, the plasma-treated aramid fibers well maintained their functional groups, which can be seen from their unchanged IFSS. After a three-day placement in air, the IFSS quickly decreased 14.6%. Furthermore, no significant decrease was found in the IFSS for those fibers placed in air for 7 days or longer, indicating that all functional groups have been fully passivated at this time. As seen by the FTIR analysis, the major passivation agent is the water molecules in air. Via drying at 100 °C for 10 hours, The IFSS of the fibers aged for 7 days can be restored to 29.57±1.59 MPa, which is very similar to the result of freshly plasma-treated aramid fibers. This work will benefit engineering aramid fibers into composites, by allowing one to largely take advantage of their superior mechanical properties.

6.1.3 Coating the aramid fibers with MoO_3 to improve the IFSS.

The mechanical properties (Such as the tensile strength and the interfacial strength) of coated aramid fibers with MoO3 particles have been investigated in this study. The CVD and the PVD were used as two alternative methods to improve the IFSS and keeping the IFSS in a high performance. This method solved the issue of using plasma treatment, where the CVD and PVD methods did not generate new

defects. Also, the CVD method kept the aramid fiber with the same performance because there is no concern regarding the passivation of the functional groups on the fiber surface. By using the CVD method, the IFSS have been significantly improved from ~22 MPa to ~31 MPa. On the meantime, the tensile strength of the aramid fiber did not heavily affected. Finally, by using the CVD, the IFSS slightly increased and gave the value 25MPa.

6.1.4 Identifying van der Waals force and the hydrogen bonding between aramid fibers and silicon wafer

The weak force signals (vdW force and hydrogen bonding) which have been generally ignored in macroscopic materials systems have been measured and distinguished by an in-house nanomechanical tester. Facilitated by evaporation of polar and nonpolar medium between carbon fiber and selected substrates, the interfacial interaction has been created with either hydrogen bonding or vdW force. The specific ISR for the interface dominated by hydrogen bonding is ~60 times higher than that bridged by vdW force. The significant difference in interfacial interaction suggests that hydrogen bonding rather than vdW force has higher potential in sewing the interface if both surfaces are supportive to form hydrogen bonds.

6.2 Future Work

Although the interface interaction between aramid fibers and selected substrates have been evaluated by pull out testing and strengthened by increasing surface roughness, creating functional groups, and depositing ceramic nanoparticles, there are still more interesting and challenging scientific questions to be addressed with more effort.

6.2.1. Interface stability at higher temperature

The current progress has demonstrated that the interface interaction facilitated by PDC have a great thermal stability under temperature of ~100 °C. Once the composite is applied at higher temperature, such as temperature right below the melting point of aramid fiber or matrix, whether the interface interaction is stable is unknown. To address it, a better thermal insulation film/sheets should be used to block the heat transfer from testing area to the instrument, especially the load cells. An accompanied concern is that the system compliance at high temperature would bring error to the calculated IFSS. If all issues are well considered and resolved, the outcome from such research would be very useful.

6.2.2. Bonding between ceramic nanoparticles and aramid fibers

The ceramic particles grown by CVD would be with covalent bonding, while those deposited by PVD would be with Van der Waals force bonding. Such confirmation has not been carried out in these projects. To identify the bonding between ceramic nanoparticles and aramid fibers, XPS can be used if contaminations from the air are prevented. In addition, the bonding strength between the nanoparticles and fibers can be evaluated if an AFM probe is used to push off individual nanoparticles. Such research would help fundamentally understand the interface interaction between ceramic nanoparticles and aramid fibers.

6.2.3. Weak hydrogen bonding and van der Waals bonding

The current project was carried in air with an uncontrol on environmental condition, such as temperature, humidity level, dust in air, etc. If mechanical debonding can be carried out in an environmental SEM, all parameters can be precisely set, the weak bonding would be measured precisely. More targeted design can be carried out for specific applications and purposes. In addition to understanding the weak interaction, whether the functional groups reorientate toward the fibers or bond to water molecules can be well revealed.

6.2.4. Interface interaction between other fibers and substrates

In addition to aramid fibers, there are more commercial fibers, such as carbon fibers, glass fibers, etc. Applying the same treatment may not deliver the same results as the fibers have different compositions, chemical properties, etc. All projects included in this thesis can be benchmarks. Selected experiment can be performed to learn whether the treatment has a general significance.

REFERENCES

1. Ci, L., Suhr, J., Pushparaj, V., Zhang, X. & Ajayan, P. M. Continuous carbon nanotube reinforced composites. *Nano Lett.* **8**, 2762–2766 (2008).

2. Miracle, D. B., Donaldson, S. L. & others. Introduction to composites. *ASM Handb.* **21**, 3–17 (2001).

3. Patterson, B. A. & Sodano, H. A. Enhanced interfacial strength and UV shielding of aramid fiber composites through ZnO nanoparticle sizing. *ACS Appl. Mater. Interfaces* **8**, 33963–33971 (2016).

4. Yang, M. *et al.* Dispersions of aramid nanofibers: a new nanoscale building block. *ACS Nano* **5**, 6945–6954 (2011).

5. Goulouti, K., De Castro, J. & Keller, T. Aramid/glass fiber-reinforced thermal break--thermal and structural performance. *Compos. Struct.* **136**, 113–123 (2016).

6. Sa, R. *et al.* Surface modification of aramid fibers by bio-inspired poly (dopamine) and epoxy functionalized silane grafting. *ACS Appl. Mater. Interfaces* **6**, 21730–21738 (2014).

7. Radwan, A. S. E. M. Analysis and Material Design of Missiles Structures. (Military Technical College, 2016).

8. Mrazova, M. Advanced composite materials of the future in aerospace industry. *Incas Bull.* **5**, 139 (2013).

9. Burger, N. *et al.* Review of thermal conductivity in composites: mechanisms, parameters and theory. *Prog. Polym. Sci.* **61**, 1–28 (2016).

10. Imai, T. *et al.* Effects of nano-and micro-filler mixture on electrical insulation properties of epoxy based composites. *IEEE Trans. Dielectr. Electr. Insul.* **13**, 319–326 (2006).

11. Lv, P. *et al.* Increasing the interfacial strength in carbon fiber/epoxy composites by controlling the orientation and length of carbon nanotubes grown on the fibers. *Carbon N. Y.* **49**, 4665–4673 (2011).

12. Park, J.-M., Kong, J.-W., Kim, J.-W. & Yoon, D.-J. Interfacial evaluation of electrodeposited single carbon fiber/epoxy composites by fiber fracture source location using fragmentation test and acoustic emission. *Compos. Sci. Technol.* **64**, 983–999 (2004).

13. Rebillat, F. *et al.* Interfacial Bond Strength in SiC/C/SiC Composite Materials, As Studied by Single-Fiber Push-Out Tests. *J. Am. Ceram. Soc.* **81**, 965–978 (1998).

14. Xie, F. *et al.* Surface ammonification of the mutual-irradiated aramid fibers in 1, 4-dichlorobutane for improving interfacial properties with epoxy resin. *J. Appl. Polym. Sci.* **134**, (2017).

15. Qi, G., Zhang, B., Du, S. & Yu, Y. Estimation of aramid fiber/epoxy interfacial properties by fiber bundle tests and multiscale modeling considering the fiber skin/core structure. *Compos. Struct.* **167**, 1–10 (2017).

16. Kim, H.-I. *et al.* Effects of maleic anhydride content on mechanical properties of carbon fibers-reinforced maleic anhydride-grafted-poly-propylene matrix composites. *Carbon Lett.* **20**, 39–46 (2016).

17. Qian, D., Dickey, E. C., Andrews, R. & Rantell, T. Load transfer and deformation mechanisms in carbon nanotube-polystyrene composites. *Appl. Phys. Lett.* **76**, 2868–2870 (2000).

18. Basutkar, A. G. & Kolekar, A. A review on properties and applications of ceramic matrix composites. *IJRSI* **2**, 28 (2015).

19. Park, J.-M., Kim, D.-S. & Kim, S.-R. Improvement of interfacial adhesion and nondestructive damage evaluation for plasma-treated PBO and Kevlar fibers/epoxy composites using micromechanical techniques and surface wettability. *J. Colloid Interface Sci.* **264**, 431–445 (2003).

20. Montes-Morán, M. A., Mart\inez-Alonso, A., Tascón, J. M. D. & Young, R. J. Effects of plasma oxidation on the surface and interfacial properties of ultra-high modulus carbon fibres. *Compos. Part A Appl. Sci. Manuf.* **32**, 361–371 (2001).

21. Islam, M. S., Pickering, K. L. & Foreman, N. J. Influence of alkali treatment on the interfacial and physico-mechanical properties of industrial hemp fibre reinforced polylactic acid composites. *Compos. Part A Appl. Sci. Manuf.* **41**, 596–603 (2010).

22. Sinha, E. & Panigrahi, S. Effect of plasma treatment on structure, wettability of jute fiber and flexural strength of its composite. *J. Compos. Mater.* **43**, 1791–1802 (2009).

23. Montes-Morán, M. A., Gauthier, W., Mart\inez-Alonso, A. & Tascón, J. M. D. Mechanical properties of high-strength carbon fibres. Validation of an end-effect model for describing experimental data. *Carbon N. Y.* **42**, 1275–1278 (2004).

24. Su, M., Gu, A., Liang, G. & Yuan, L. The effect of oxygen-plasma treatment on Kevlar fibers and the properties of Kevlar fibers/bismaleimide composites. *Appl. Surf. Sci.* **257**, 3158–3167 (2011).

25. Zafar, M. T., Maiti, S. N. & Ghosh, A. K. Effect of surface treatment of jute fibers on the interfacial adhesion in poly (lactic acid)/jute fiber biocomposites. *Fibers Polym.* **17**, 266–274 (2016).

26. Shazed, M. A., Suraya, A. R., Rahmanian, S. & Salleh, M. A. M. Effect of fibre coating and geometry on the tensile properties of hybrid carbon nanotube coated carbon fibre reinforced composite. *Mater. Des.* **54**, 660–669 (2014).

27. Chen, C., Wang, X., Wang, F. & Peng, T. Preparation and Characterization of Para-Aramid Fibers with the Main Chain Containing Heterocyclic Units. *J. Macromol. Sci. Part B* **59**, 90–99 (2020).

28. Hong, S., Minary-Jolandan, M. & Naraghi, M. Controlling the wettability and adhesion of carbon fibers with polymer interfaces via grafted nanofibers. *Compos. Sci. Technol.* **117**, 130–138 (2015).

29. Gonzalez-Chi, P. I. *et al.* Influence of aramid fiber treatment and carbon nanotubes on the interfacial strength of polypropylene hierarchical composites. *Compos. Part B Eng.* **122**, 16–22 (2017).

30. Dziendzikowski Michałand Dragan, K. & Katunin, A. Localizing impact damage of composite structures with modified RAPID algorithm and non-circular PZT arrays. *Arch. Civ. Mech. Eng.* **17**, 178–187 (2017).

31. Yang, B. *et al.* Simultaneously enhancing the IFSS and monitoring the interfacial stress state of GF/epoxy composites via building in the MWCNT interface sensor. *Compos. Part A Appl. Sci. Manuf.* **112**, 161–167 (2018).

32. Lin, Y.-C. *et al.* Application of physical vapor deposition process to modify activated carbon fibers for ozone reduction. *Korean J. Chem. Eng.* **25**, 446–450 (2008).

33. Wang, J. *et al.* Improvement of aramid fiber III reinforced bismaleimide composite interfacial adhesion by oxygen plasma treatment. *Compos. Interfaces* **25**, 771–783 (2018).

34. Murakami, T., Kuroda, S. & Osawa, Z. Dynamics of polymeric solid surfaces treated with oxygen plasma: Effect of aging media after plasma treatment. *J. Colloid Interface Sci.* **202**, 37–44 (1998).

35. Ren, Y., Wang, C. & Qiu, Y. Influence of aramid fiber moisture regain during atmospheric plasma treatment on aging of treatment effects on surface wettability and bonding strength to epoxy. *Appl. Surf. Sci.* **253**, 9283–9289 (2007).

36. Canal, C., Molina, R., Bertran, E. & Erra, P. Wettability, ageing and recovery process of plasma-treated polyamide 6. *J. Adhes. Sci. Technol.* **18**, 1077–1089 (2004).

37. Chen, P. *et al.* Improvement of interfacial adhesion for plasma-treated aramid fiber-reinforced poly (phthalazinone ether sulfone ketone) composite and fiber surface aging effects. *Surf. Interface Anal. An Int. J. devoted to Dev. Appl. Tech. Anal. surfaces, interfaces thin Film.* **41**, 38–43 (2009).

38. Bright, J. D., Shetty, D. K., Griffin, C. W. & Limaye, S. Y. Interfacial Bonding and Friction in Silicon Carbide [Filament]-Reinforced Ceramic-and Glass-Matrix Composites. *J. Am. Ceram. Soc.* **72**, 1891–1898 (1989).

39. Nozaka, Y., Wang, W., Shirasu, K., Yamamoto, G. & Hashida, T. Inclined slit-based pullout method for determining interfacial strength of multi-walled carbon nanotube--alumina composites. *Carbon N. Y.* **78**, 439–445 (2014).

40. Kessman, A. J., Zhang, J., Vasudevan, S., Lou, J. & Sheldon, B. W. Carbon nanotube pullout, interfacial properties, and toughening in ceramic nanocomposites: mechanistic insights from single fiber pullout analysis. *Adv. Mater. Interfaces* **2**, 1400110 (2015).

41. Wang, H., Wang, H., Li, W., Ren, D. & Yu, Y. An improved microbond test method for determination of the interfacial shear strength between carbon fibers and epoxy resin. *Polym. Test.* **32**, 1460–1465 (2013).

42. Dhert, W. J. A. *et al.* A finite element analysis of the push-out test: Influence of test conditions. *J. Biomed. Mater. Res.* **26**, 119–130 (1992).

43. Miller, B., Muri, P. & Rebenfeld, L. A microbond method for determination of the shear strength of a fiber/resin interface. *Compos. Sci. Technol.* **28**, 17–32 (1987).

44. Folkes, M. J. & Wong, W. K. Determination of interfacial shear strength in fibre-reinforced thermoplastic composites. *Polymer (Guildf).* **28**, 1309–1314 (1987).

45. Miwa, M., Ohsawa, T. & Tahara, K. Effects of fiber length on the tensile strength of epoxy/glass fiber and polyester/glass fiber composites. *J. Appl. Polym. Sci.* **25**, 795–807 (1980).

46. Feih, S., Wonsyld, K., Minzari, D., Westermann, P. & Lilholt, H. Testing procedure for the single fiber fragmentation test. *Risoe Natl. Lab. Roskilde, Denmark* **1**, 30 (2004).

47. Barber, A. H., Cohen, S. R. & Wagner, H. D. Measurement of carbon nanotube-polymer interfacial strength. *Appl. Phys. Lett.* **82**, 4140–4142 (2003).

48. Yang, L. & Thomason, J. L. Interface strength in glass fibre--polypropylene measured using the fibre pull-out and microbond methods. *Compos. Part A Appl. Sci. Manuf.* **41**, 1077–1083 (2010).

49. Fras Zemljic?, L., Persin, Z. & Stenius, P. Improvement of chitosan adsorption onto cellulosic fabrics by plasma treatment. *Biomacromolecules* **10**, 1181–1187 (2009).

50. Takke, V., Behary, N., Perwuelz, A. & Campagne, C. Surface and adhesion properties of poly (ethylene glycol) on polyester (polyethylene terephthalate) fabric surface: Effect of air-atmospheric plasma treatment. *J. Appl. Polym. Sci.* **122**, 2621–2629 (2011).

51. Samanta, K., Jassal, M. & Agrawal, A. K. Atmospheric pressure glow discharge plasma and its applications in textile. (2006).

52. Tranchard, P., Duquesne, S., Samyn, F., Estebe, B. & Bourbigot, S. Kinetic analysis of the thermal decomposition of a carbon fibre-reinforced epoxy resin laminate. *J. Anal. Appl. Pyrolysis* **126**, 14–21 (2017).

53. Zhu, Y. *et al.* A seamless three-dimensional carbon nanotube graphene hybrid material. *Nat. Commun.* **3**, 1–7 (2012).

54. Zhang, W. *et al.* Synthesis of three-dimensional carbon nanotube/graphene hybrid materials by a two-step chemical vapor deposition process. *Carbon N. Y.* **86**, 358–362 (2015).

55. Ajayan, P. M., Schadler, L. S., Giannaris, C. & Rubio, A. Single-walled carbon nanotube-polymer composites: Strength and weakness. *Adv. Mater.* **12**, 750–753 (2000).

56. Dalton, A. B. *et al.* Super-tough carbon-nanotube fibres. *Nature* **423**, 703 (2003).

57. Yu, M.-F., Files, B. S., Arepalli, S. & Ruoff, R. S. Tensile loading of ropes of single wall carbon nanotubes and their mechanical properties. *Phys. Rev. Lett.* **84**, 5552 (2000).

58. Tao, X., Liu, J., Koley, G. & Li, X. B/SiOx nanonecklace reinforced nanocomposites by unique mechanical interlocking mechanism. *Adv. Mater.* **20**, 4091–4096 (2008).

59. Shim, J.-W., Park, S.-J. & Ryu, S.-K. Effect of modification with HNO3 and NaOH on metal adsorption by pitch-based activated carbon fibers. *Carbon N. Y.* **39**, 1635–1642 (2001).

60. Sui, C. *et al.* Aligned-SWCNT film laminated nanocomposites: Role of the film on mechanical and electrical properties. *Carbon N. Y.* **139**, 680–687 (2018).

61. Yang, Y. *et al.* Quantification and promotion of interfacial interactions between carbon nanotubes and polymer derived ceramics. *Carbon N. Y.* **95**, 964–971 (2015).

62. Chua, P. S. & Piggott, M. R. The glass fibre-polymer interface: I-theoretical consideration for single fibre pull-out tests. *Compos. Sci. Technol.* **22**, 33–42 (1985).

63. Hsueh, C.-H., Ferber, M. K. & Becher, P. F. Stress-displacement relation of fiber for fiber-reinforced ceramic composites during (indentation) loading and unloading. *J. Mater. Res.* **4**, 1529–1537 (1989).

64. Oliver, W. C. & Pharr, G. M. An improved technique for determining hardness and elastic modulus using load and displacement sensing indentation experiments. *J. Mater. Res.* **7**, 1564–1583 (1992).

65. Liu, Y.-N. *et al.* The interfacial strength and fracture characteristics of ethanol and polymer modified carbon nanotube fibers in their epoxy composites. *Carbon N. Y.* **52**, 550–558 (2013).

66. Zhang, J., Loya, P., Peng, C., Khabashesku, V. & Lou, J. Quantitative in situ mechanical characterization of the effects of chemical functionalization on individual carbon nanofibers. *Adv. Funct. Mater.* **22**, 4070–4077 (2012).

67. Joseph, K., Thomas, S. & Pavithran, C. Effect of chemical treatment on the tensile properties of short sisal fibre-reinforced polyethylene composites. *Polymer (Guildf).* **37**, 5139–5149 (1996).

68. Herrera-Franco, Pj. & Valadez-Gonzalez, A. A study of the mechanical properties of short natural-fiber reinforced composites. *Compos. Part B Eng.* **36**, 597–608 (2005).

69. Li, S., Han, K., Rong, H., Li, X. & Yu, M. Surface modification of aramid fibers via ammonia-plasma treatment. *J. Appl. Polym. Sci.* **131**, (2014).

70. Xing, L. *et al.* Enhanced interfacial properties of domestic aramid fiber-12 via high energy gamma ray irradiation. *Compos. Part B Eng.* **69**, 50–57 (2015).

71. Straub, A., Slivka, M. & Schwartz, P. A study of the effects of time and temperature on the fiber/matrix interface strength using the microbond test. *Compos. Sci. Technol.* **57**, 991–994 (1997).

72. Pegoretti, A., Fambri, L. & Migliaresi, C. Interfacial stress transfer in nylon-6/E-Glass microcomposites: Effect of temperature and strain rate. *Polym. Compos.* **21**, 466–475 (2000).

73. Gore, P. M. & Kandasubramanian, B. Functionalized aramid fibers and composites for protective applications: a review. *Ind. Eng. Chem. Res.* **57**, 16537–16563 (2018).

74. Olivito, R. S. & Zuccarello, F. A. An experimental study on the tensile strength of steel fiber reinforced concrete. *Compos. Part B Eng.* **41**, 246–255 (2010).

75. Al-Quraishi, K. K. *et al.* Strengthening the Interface between Individual Aramid Fibers and Polymer at Room and Elevated Temperatures. *Mater. Today Commun.* 101254 (2020).

76. Yang, Y. *et al.* Impact of carbon nanotube defects on fracture mechanisms in ceramic nanocomposites. *Carbon N. Y.* **115**, 402–408 (2017).

77. Singh, S., Shukla, A. & Brown, R. Pullout behavior of polypropylene fibers from cementitious matrix. *Cem. Concr. Res.* **34**, 1919–1925 (2004).

78. Zhao, D. *et al.* Comparative study of polymer containing $β$-cyclodextrin and--COOH for adsorption toward aniline, 1-naphthylamine and methylene blue. *J. Hazard. Mater.* **171**, 241–246 (2009).

79. Wang, J. *et al.* Influence of aging behavior of Armos fiber after oxygen plasma treatment on its composite interfacial properties. *Surf. Coatings Technol.* **203**, 3722–3727 (2009).

80. Kanan, S. M. & Tripp, C. P. Synthesis, FTIR studies and sensor properties of WO3 powders. *Curr. Opin. Solid State Mater. Sci.* **11**, 19–27 (2007).

81. Owusu-Nkwantabisah, S., Gammana, M. & Tripp, C. P. Dynamics of layer-by-layer growth of a polyelectrolyte multilayer studied in situ using attenuated total reflectance infrared spectroscopy. *Langmuir* **30**, 11696–11703 (2014).

82. Oh, S. Y. *et al.* Crystalline structure analysis of cellulose treated with sodium hydroxide and carbon dioxide by means of X-ray diffraction and FTIR spectroscopy. *Carbohydr. Res.* **340**, 2376–2391 (2005).

83. González-Benito, J. The nature of the structural gradient in epoxy curing at a glass fiber/epoxy matrix interface using FTIR imaging. *J. Colloid Interface Sci.* **267**, 326–332 (2003).

84. Liu, S.-H. *et al.* Improving thermal stability of polyurethane through the addition of hyperbranched polysiloxane. *Polymers (Basel).* **11**, 697 (2019).

85. Noguchi, T. & Sugiura, M. FTIR detection of water reactions during the flash-induced S-state cycle of the photosynthetic water-oxidizing complex. *Biochemistry* **41**, 15706–15712 (2002).

86. Hojabri, A., Hajakbari, F. & Meibodi, A. E. Structural and optical properties of nanocrystalline $α$-MoO 3 thin films prepared at different annealing temperatures. *J. Theor. Appl. Phys.* **9**, 67–73 (2015).

87. Wang, Q. *et al.* One-dimensional MoO 3 coated by carbon for supercapacitor with enhanced electrochemical performance. *J. Mater. Sci. Mater. Electron.* **30**, 6643–6649 (2019).

88. Chiang, T. H. & Yeh, H. C. The synthesis of $α$-MoO3 by ethylene glycol. *Materials (Basel).* **6**, 4609–4625 (2013).

89. Chithambararaj, A., Sanjini, N. S., Bose, A. C. & Velmathi, S. Flower-like hierarchical h-MoO 3: new findings of efficient visible light driven nano photocatalyst for methylene blue degradation. *Catal. Sci. Technol.* **3**, 1405–1414 (2013).

90. Yang, C. & Suo, Z. Hydrogel ionotronics. *Nat. Rev. Mater.* **3**, 125–142 (2018).

91. Hu, X., Vatankhah-Varnoosfaderani, M., Zhou, J., Li, Q. & Sheiko, S. S. Weak hydrogen bonding enables hard, strong, tough, and elastic hydrogels. *Adv. Mater.* **27**, 6899–6905 (2015).

92. Li, J., Suo, Z. & Vlassak, J. J. Stiff, strong, and tough hydrogels with good chemical stability. *J. Mater. Chem. B* **2**, 6708–6713 (2014).

93. Algara-Siller, G. *et al.* Square ice in graphene nanocapillaries. *Nature* **519**, 443–445 (2015).

94. Kühne, M. *et al.* Reversible superdense ordering of lithium between two graphene sheets. *Nature* **564**, 234–239 (2018).

95. Talebian, S. *et al.* Self-Healable Hydrogels: Self-Healing Hydrogels: The Next Paradigm Shift in Tissue Engineering?(Adv. Sci. 16/2019). *Adv. Sci.* **6**, 1970094 (2019).

96. Mead, J. L., Xie, H., Wang, S. & Huang, H. Enhanced adhesion of ZnO nanowires during in situ scanning electron microscope peeling. *Nanoscale* **10**, 3410–3420 (2018).

97. Tabor, D. & Winterton, R. S. The direct measurement of normal and retarded van der Waals forces. *Proc. R. Soc. London. A. Math. Phys. Sci.* **312**, 435–450 (1969).

98. Horn, R. G. & Israelachvili, J. N. Direct measurement of structural forces between two surfaces in a nonpolar liquid. *J. Chem. Phys.* **75**, 1400–1411 (1981).

99. Israelachvili, J. *et al.* Recent advances in the surface forces apparatus (SFA) technique. *Reports Prog. Phys.* **73**, 36601 (2010).

100. Liu, Y., Chen, X., Li, J. & Luo, J. Enhancement of friction performance enabled by a synergetic effect between graphene oxide and molybdenum disulfide. *Carbon N. Y.* **154**, 266–276 (2019).

101. Vasu, K. S. *et al.* Van der Waals pressure and its effect on trapped interlayer molecules. *Nat. Commun.* **7**, 1–6 (2016).

102. Neek-Amal, M., Peeters, F. M., Grigorieva, I. V & Geim, A. K. Commensurability effects in viscosity of nanoconfined water. *ACS Nano* **10**, 3685–3692 (2016).

103. Yang, L., Guo, Y. & Diao, D. Structure and dynamics of water confined in a graphene nanochannel under gigapascal high pressure: dependence of friction on pressure and confinement. *Phys. Chem. Chem. Phys.* **19**, 14048–14054 (2017).

104. Jinesh, K. B. & Frenken, J. W. M. Capillary condensation in atomic scale friction: how water acts like a glue. *Phys. Rev. Lett.* **96**, 166103 (2006).

105. Lee, H. *et al.* Enhancement of friction by water intercalated between graphene and mica. *J. Phys. Chem. Lett.* **8**, 3482–3487 (2017).

106. Arif, T., Yadav, S., Colas, G., Singh, C. V. & Filleter, T. Understanding the Independent and Interdependent Role of Water and Oxidation on the Tribology of Ultrathin Molybdenum Disulfide (MoS2). *Adv. Mater. Interfaces* **6**, 1901246 (2019).

107. Arif, T., Colas, G. & Filleter, T. Effect of humidity and water intercalation on the tribological behavior of graphene and graphene oxide. *ACS Appl. Mater. \& interfaces* **10**, 22537–22544 (2018).

108. Tekinalp, H. L. *et al.* Highly oriented carbon fiber--polymer composites via additive manufacturing. *Compos. Sci. Technol.* **105**, 144–150 (2014).

109. Lu, K. The future of metals. *Science (80-.).* **328**, 319–320 (2010).

110. Ritchie, R. O. The conflicts between strength and toughness. *Nat. Mater.* **10**, 817–822 (2011).

111. Ritchie, R. O. Mechanisms of fatigue crack propagation in metals, ceramics and composites: role of crack tip shielding. *Mater. Sci. Eng. A* **103**, 15–28 (1988).

112. Huang, X. Fabrication and properties of carbon fibers. *Materials (Basel).* **2**, 2369–2403 (2009).

113. Perret, R. & Ruland, W. The microstructure of PAN-base carbon fibres. *J. Appl. Crystallogr.* **3**, 525–532 (1970).

114. Johnson, W. & Watt, W. Structure of high modulus carbon fibres. *Nature* **215**, 384–386 (1967).

115. Cleveland, J. P., Manne, S., Bocek, D. & Hansma, P. K. A nondestructive method for determining the spring constant of cantilevers for scanning force microscopy. *Rev. Sci. Instrum.* **64**, 403–405 (1993).

116. Torii, A., Sasaki, M., Hane, K. & Okuma, S. A method for determining the spring constant of cantilevers for atomic force microscopy. *Meas. Sci. Technol.* **7**, 179 (1996).

117. Hamaker, H. C. The London-van der Waals attraction between spherical particles. *physica* **4**, 1058–1072 (1937).

118. Bewig, K. W. & Zisman, W. A. The wetting of gold and platinum by water. *J. Phys. Chem.* **69**, 4238–4242 (1965).

BIOGRAPHY OF THE AUTHOR

Karrar Al-Quraishi was born in Wasit, Iraq in1988. He graduated from the University of Technology in Iraq with a Bachelor of Science in Mechanical Engineering in June 2012. Before coming to the United States, he worked in an oil industry. He obtained his Master of Science degree in Mechanical Engineering from the University of Maine in Aug 2017. Karrar joined the doctoral program at the University of Maine in January 2018. He is a candidate for the Doctor of Philosophy degree in Mechanical Engineering from the University of Maine in December 2021.